The Pennsylvania State University

The Graduate School

Department of Physics

CURVATURE SCALAR DIAGNOSTICS AND PROGRESS ON A CHERN-SIMONS INITIAL VALUE FORMULATION

A Dissertation in

Physics

by

Shaun Wood

Submitted in Partial Fulfillment
of the Requirements
for the Degree of

Doctor of Philosophy

December 2009

The dissertation of Shaun Wood was reviewed and approved[1] by the following:

Abhay Ashtekar
Eberly Professor of Physics
Dissertation Advisor
Chair of Committee

Pablo Laguna
Professor of Physics (Adjunct)

Martin Bojowald
Assistant Professor of Physics

Nigel Higson
Evan Pugh Professor of Mathematics

Jayanth R. Banavar
Professor of Physics
Head of the Department of Physics

[1] Signatures on file in the Graduate School.

Abstract

In the recent past, many numerical relativity groups have gained the ability to perform fully relativistic simulations of black hole mergers. One of the key aims of these simulations is to compute gravitational waveforms. Such waveforms are interesting not only from a theoretical standpoint, but also because they are necessary for the ongoing effort to detect gravitational waves. Current numerical methods for computing gravitational waveforms depend on assumptions made about the background spacetime, typically via a choice of tetrad. Such methods require additional checks to insure the assumptions are correct.

In this dissertation, we first present the results of a project to use scalars which can be computed using only contractions of the curvature tensor as diagnostic tools in numerical relativity simulations. The scalars have been shown to contain information about the background spacetime and gravitational radiation, and are independent of any choice of tetrad, background, or coordinates. The Baker Campanelli speciality index is used to determine when the spacetime separates into background and radiation, subject to the conditions that the radiation be weak and be purely outgoing. We find that at least the second condition is not satisfied in the simulations we perform. Then, the Beetle-Burko radiation scalar is used to check the assumption that the tetrad used to compute gravitational waveforms represents the principle null directions of the background spacetime. It is essential that two vectors of the tetrad are parallel to the two principle null directions of the background in order to interpret the Newman Penrose scalar Ψ_4 as the outgoing gravitational wave. We find the tetrad passes this test whenever it can be applied in our simulations. While this does not permit us to conclude that the scalar Ψ_4 is the outgoing

gravitational wave, the test can be used in more generic simulations to catch errors in the Ψ_4 calculation.

Next, we present an attempt to write Chern-Simons modified gravity as an initial value problem. Chern-Simons modified gravity is an extension to general relativity in which a parity violating term is added to the action. One effect the modification has is to enhance or suppress the different polarizations of gravitational radiation. Therefore, there is great interest in simulating binary black hole mergers in the theory and computing the resulting gravitational radiation. We provide an incomplete set of constraints and evolution equations for the theory, and discuss difficulties of finding a complete set. Projections of the modified field equations are also provided. Once a complete initial value formulation is found and simulations are performed, gravitational wave detection can provide a strong test of Chern-Simons modified gravity.

Table of Contents

List of Figures

Acknowledgments

There is a long list of people without whom I would not have completed this thesis. I am very happy, then, to spend a few moments saying thanks. Especially, I thank my advisor Pablo Laguna for his patience and advice while I struggled down the many blind alleys and dead ends I encountered in my research. Additionally, I thank Abhay Ashtekar for his encouragement and support during my final semester at Penn State.

My friends and office mates Tanja Bode, Eloisa Bentivegna, Andrew Knapp, Jim Healy, Ian Hinder, and Frank Herrmann helped me when I needed help, and have always been handy with constructive suggestions. I am also grateful to Nico Yunes for his interest in my work, and for the many times he looked over what I had done and offered advice.

There are many more friends I would like to thank for their support: Victor Taveras, Ed Wilson-Ewing, Dave Sloan, BJ Cooley, Dan Constantino, Asher Evans, and Jeb Qualls. You guys are great. Much sincere appreciation goes to Chris Duncan, Jen O'Donnell, Julie Grier, Jeff Fraser, and Kristin Cederquist for standing by me through thick and thin. Finally, I could not have finished without my mom, dad, Erin, and Meg, who always believed I could make it.

Chapter 1

Introduction

While general relativity has made many fruitful predictions, certainly one of the most intriguing is gravitational radiation. These waves which propagate through spacetime promise another way in which GR's predictions can be tested. In addition, the waves are expected to be weakly interacting. Then, they can carry information from strongly gravitating systems which are too far away, too obscured, or too dim to be seen by other means.

Before gravitational waves could become a source of information about the universe, a great obstacle was overcome. Because of its complexity, general relativity has few known exact solutions. Instead, numerical relativity has sought, with increasing success, to generate accurate approximations to solutions of Einstein's equations. For example, stable codes can now simulate binary black holes with almost arbitrary initial linear and intrinsic angular momenta. The simulations can last for several orbits, through their merger, and indefinitely into their ring-down phase. The results of the simulations are providing a host of new predictions for general relativity. Some care, then, must be given to how gravitational radiation is computed from the results.

A direct result of the covariant formulation of general relativity is that observable quantities must be scalars. Indeed, any quantity that can be determined by a local experiment must be possible to compute as a scalar using only local information. Such is the case with gravitational radiation, which will hopefully be possible to detect with future generations of ground and space

based interferometers. While very effective methods currently exist for computing the radiation, the methods rely on additional information. The information may be a guess for the value of the background metric, or a set of vectors for projecting components of the curvature, but the result is the same. It is no longer possible to guarantee without additional checks that the computed value is the sought after gravitational radiation.

In this dissertation, we investigate a new check of the gravitational radiation computation methods used in numerical relativity. The Baker-Campanelli speciality index and the Beetle-Burko (BB) scalar are computed solely from the metric and its derivatives. The speciality index is used to determine when the spacetime separates into a background plus radiation that satisfies strict asymptotic fall off conditions. When these conditions are satisfied, the Beetle-Burko scalar is used to check that the tetrad used to compute gravitational radiation is correct up to a spin-boost transformation. Radiation cannot be computed from the BB scalar. Nor can the scalar be used to guarantee that the radiation is computed correctly. Instead, the scalar allows us to determine if the method used to compute gravitational radiation is incorrect.

In the second half of the dissertation, we present a study of Chern Simons gravity with the aim of writing the theory in a way that can be simulated numerically. Chern Simons (CS) gravity is an extension to Einstein's theory in which a parity violating term is added to the action. The term affects the amplitude of gravitational waves depending on their polarization. Given an initial value formulation of Chern-Simons gravity, simulations could be performed of binary black hole mergers, and the resulting gravitational waves could be computed. The results of such simulations would provide new tests for the theory.

The dissertation is organized as follows: In chapter 2 we will review the 3+1 decomposition of Einstein's equations. This is a method by which Einstein's equations are rewritten

as a system of evolution equations for constrained, time varying tensors in a three dimensional space. The resulting form is especially useful to numerical relativity, where it is used to simulate astrophysically interesting solutions of general relativity. In chapter 3 and appendix A we will discuss the Newman-Penrose (NP) scalars. The scalars are a popular tool for extracting information from numerical simulations. We will also discuss an ambiguity present in the choice of the tetrad when computing the NP scalars, and ways in which the ambiguity is typically removed. In chapter 4, we present work we did using the Beetle-Burko scalar. We give a method for computing the scalar numerically. Then, we use the scalar as a check of the validity of one of the popular methods of calculating the NP scalars. Next, we attempt to write an initial value formulation of Chern-Simons modified gravity in chapter 5. We demonstrate the difficulties associated with trying to produce a form of the full theory which can be simulated numerically. Finally, in chapter 6, we summarize the work and discuss open questions.

1.1 Conventions

The spacetime metric will always have the signature $(-+++)$. Geometrized units, in which $G = c = 1$ are used unless otherwise specified. Greek indices α through ω are used to label tensor components in a four dimensional spacetime basis, and have values of 0,1,2, or 3. Latin indices *a* through *z* label tensor components in a three dimensional spatial basis, and have values of 1, 2, or 3. Indices that are repeated are summed over.

When it is ambiguous whether a quantity is computed from a 4 dimensional metric or a 3 dimensional metric, the former are prefixed by a ${}^{(4)}$.

Tensor densities are denoted $\widetilde{f}$ where f is a tensor density of weight 0.

Parentheses surrounding indices indicate tensor symmetries. For example, $f_{(ab)} = \frac{1}{2}(f_{ab} + f_{ba})$. Square brackets surrounding indices indicate tensor anti-symmetries, $f_{[ab]} = \frac{1}{2}(f_{ab} - f_{ba})$.

The partial derivative of the tensor f with respect to the coordinate x^α is written as $\partial_\alpha f$ or $f_{,\alpha}$. The Lie derivative of the tensor f along a vector field v^α is denoted $\mathcal{L}_v f$. Time derivatives of the tensor may be written $\partial_t f$ or $\dot{f}$.

The determinant of the spacetime metric is written g. The determinant of the spatial metric is written γ. Otherwise, when a tensor of rank 2 is written without indices, the trace of that tensor is indicated. For example, $K = g^{\alpha\beta}K_{\alpha\beta}$.

Chapter 2

The Formulation of Numerical Relativity.

2.1 Einstein's Equations

Rather than being a fixed background quantity, the spacetime metric of general relativity is a variable. In the resulting theory, a spacetime's geometry is intricately coupled to its energy and momentum content. With the addition of general covariance, the coordinates in which solutions are described lose all physical meaning. However, as profound and productive as this result is, coordinates play an important role in finding solutions to Einstein's equations. In particular, great strides in finding solutions have been made by choosing a time coordinate and reinterpreting the theory as one governing the evolution of spatial quantities.

In full general relativity, the value of the metric is governed by Einstein's equations. These 10 partial differential equations are written in a covariant form as follows: The Christoffel connection ${}^{(4)}\Gamma^{\alpha}_{\beta\gamma}$ is computed from the metric $g_{\alpha\beta}$ and its inverse $g^{\alpha\beta}$ via

$$ {}^{(4)}\Gamma^{\alpha}_{\beta\gamma} = \frac{1}{2} g^{\alpha\delta}(\partial_{\gamma} g_{\beta\delta} + \partial_{\beta} g_{\gamma\delta} - \partial_{\delta} g_{\beta\gamma}). \tag{2.1} $$

The significance of the Christoffel connection is that defines a unique torsion free, metric compatible covariant derivative ∇_{α}. The Riemann curvature tensor ${}^{(4)}R^{\alpha}{}_{\beta\gamma\delta}$ is given by

$$ {}^{(4)}R^{\alpha}{}_{\beta\gamma\delta} = \partial_{\gamma}{}^{(4)}\Gamma^{\alpha}_{\beta\delta} - \partial_{\delta}{}^{(4)}\Gamma^{\alpha}_{\beta\gamma} + {}^{(4)}\Gamma^{\alpha}_{\gamma\varepsilon}\,{}^{(4)}\Gamma^{\varepsilon}_{\beta\delta} - {}^{(4)}\Gamma^{\alpha}_{\delta\varepsilon}\,{}^{(4)}\Gamma^{\varepsilon}_{\beta\gamma}. \tag{2.2} $$

The Riemann curvature tensor is a measure of the failure of vectors to be parallel transported around a closed loop into themselves. Thus, a spacetime for which ${}^{(4)}R^{\alpha}{}_{\beta\gamma\delta} = 0$ is flat, Minkowski space. The Ricci tensor ${}^{(4)}R_{\alpha\beta}$, the Ricci scalar ${}^{(4)}R$, and the Einstein tensor ${}^{(4)}G_{\alpha\beta}$ are given by

$$ {}^{(4)}R_{\beta\delta} = {}^{(4)}R^{\alpha}{}_{\beta\alpha\delta}, \tag{2.3} $$

$$ {}^{(4)}R = g^{\beta\delta}{}^{(4)}R_{\beta\delta}, \tag{2.4} $$

and

$$ {}^{(4)}G_{\alpha\beta} = {}^{(4)}R_{\alpha\beta} - \frac{1}{2} g_{\alpha\beta}{}^{(4)}R \tag{2.5} $$

Then, Einstein's equations are

$$ {}^{(4)}G_{\alpha\beta} = 8\pi T_{\alpha\beta}. \tag{2.6} $$

The stress energy tensor $T_{\alpha\beta}$ is a symmetric, divergenceless tensor which generally depends on the metric, and is related to the matter fields in the spacetime.

In spite of the elegance of (2.6), the steps of the previous paragraph demonstrate that it in general represents ten distinct, second order, non-linear, coupled PDEs for the components of the metric. A solution is completely infeasible without some simplification. Thus, the first step in obtaining a solution to (2.6) is to make assumptions about the symmetry of the spacetime and the stress energy which constrain the form of $g_{\alpha\beta}$ and $T_{\alpha\beta}$. Then, Einstein's equations are computed in coordinates adapted to the symmetries. (2.6) will reduce to PDEs for the remaining unknown components of the metric. Solutions obtained in this fashion include the Schwarzschild and Kerr metrics. For example, by assuming spherical symmetry and vacuum, the number of independent components of the Schwarzschild metric can be reduced to two. However, the

required assumptions for exact solutions are too strong, and more general solutions are desired. The spacetime of two black holes in orbit around each other, for instance, lacks enough symmetry to offer much hope for finding an exact solution for the metric.

2.2 The 3+1 Decomposition

Numerical relativists overcome the great difficulty of solving Einstein's equations by first 3+1 decomposing them. The spacetime is foliated by three dimensional space-like surfaces. On any given surface, there are both gauge and dynamical quantities which define a solution. Passage between two surfaces is reinterpreted as evolution in time. Then, either (2.6) or the Einstein-Hilbert action,

$$I_{EH} = \frac{1}{8\pi}\int d^4x\sqrt{-g}^{(4)}R, \tag{2.7}$$

can be used to find constraint and evolution equations for the quantities. Numerical relativists then use computational methods to approximate solutions. The power of this method lies in the fact that solutions can be found without making assumptions about the spacetime symmetry.

To foliate a spacetime is to split the spacetime into non-intersecting 3 dimensional hypersurfaces. Specifically, a continuous time function t is defined on the spacetime so that any surface on which $t = \tau$ is constant is a three dimensional space-like hypersurface. From t are defined a unit time-like normal to the space-like surface,

$$n_\alpha \equiv -\frac{\nabla_\alpha t}{|\nabla_\alpha t|}, \tag{2.8}$$

and a tensor which projects quantities onto the surface,

$$\gamma^{\alpha}{}_{\beta} \equiv g^{\alpha}{}_{\beta} + n^{\alpha} n_{\beta} \tag{2.9}$$

A time vector field t^{α} is constructed to satisfy the equation

$$t^{\alpha} \nabla_{\alpha} t = 1. \tag{2.10}$$

The choices of t and the spacetime coordinates are in no way unique. They will affect the values of t^{α}, n_{α}, and $\gamma^{\alpha}{}_{\beta}$. The freedom of choosing coordinates results in gauge quantities called the lapse (α) and the shift (β^{α}). The lapse and shift are related to t^{α} and n_{α} in the following way:

$$\alpha \equiv -n_{\alpha} t^{\alpha} \tag{2.11}$$

$$\beta^{\alpha} \equiv \gamma^{\alpha}{}_{\beta} t^{\beta} \tag{2.12}$$

$$t^{\alpha} = \alpha n^{\alpha} + \beta^{\alpha}. \tag{2.13}$$

They specify the way the coordinate system on a surface $\Sigma_{\tau 1}$ at a generic time $\tau 1$ evolves onto a surface $\Sigma_{\tau 2}$ at another time $\tau 2$. A coordinate stationary observer is transported along an integral curve of t^{α} from one surface to the other (Fig 2.1).

To simplify matters, we will choose the spacetime coordinate system so that contravariant (upper) spatial tensor indices have value 1, 2, or 3. This is equivalent to choosing $x^0 = t$. Then,

$$t^{\alpha} = (1, 0, 0, 0), \tag{2.14}$$

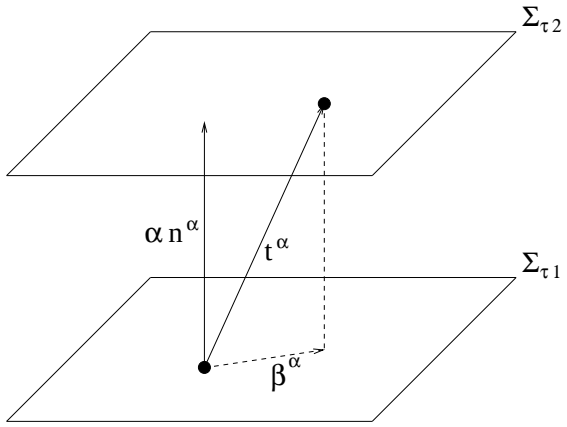

Fig. 2.1. A spatial coordinate point evolves from one surface $\Sigma_{\tau 1}$ to another surface $\Sigma_{\tau 2}$ along integral curves of the vector t^{α}

and

$$n^{\alpha} = \frac{1}{\alpha}(1, -\beta^1, -\beta^2, -\beta^3) \tag{2.15}$$

$$n_{\alpha} = -\alpha(1,0,0,0). \tag{2.16}$$

Now, the rate of change of a tensor along an integral curve of t^{α}, which is the same as the rate of change of the field with respect to t, can be expressed as the partial derivative of the field with respect to t.

$$\mathcal{L}_t f^{\alpha\beta\ldots}{}_{\gamma\delta\ldots} = \partial_t f^{\alpha\beta\ldots}{}_{\gamma\delta\ldots} \tag{2.17}$$

Because of (2.15), the time derivative of a spatial tensor with covariant (lowered) indices is

$$\partial_t f_{\alpha\beta\ldots} = \alpha \mathcal{L}_n f_{\alpha\beta\ldots} + \mathcal{L}_{\beta} f_{\alpha\beta\ldots}. \tag{2.18}$$

A spatially covariant derivative is defined by projecting all free indices of the spacetime covariant derivative of a tensor,

$$D_\alpha f^{\beta\gamma\ldots}{}_{\rho\sigma\ldots} \equiv \gamma^\mu{}_\alpha \gamma^\beta{}_\nu \gamma^\gamma{}_\delta \gamma^\varepsilon{}_\rho \gamma^\phi{}_\sigma \ldots \nabla_\mu f^{\nu\delta\ldots}{}_{\varepsilon\phi\ldots} \tag{2.19}$$

The derivative D_α is compatible with the spatial metric and torsion free. The connection is given by

$$\Gamma^\alpha_{\beta\gamma} = \frac{1}{2}\gamma^{\alpha\delta}(\partial_\beta \gamma_{\gamma\delta} + \partial_\gamma \gamma_{\beta\delta} - \partial_\delta \gamma_{\beta\gamma}) \tag{2.20}$$

and a spatial Riemann tensor is defined analogous to (2.2).

Finally, the extrinsic curvature ($K_{\alpha\beta}$) is a spatial tensor related to the rate of change of the spatial metric.

$$K_{\alpha\beta} = -\frac{1}{2}\mathcal{L}_n \gamma_{\alpha\beta}, \tag{2.21}$$

or, equivalently,

$$\partial_t \gamma_{\alpha\beta} = -2\alpha K_{\alpha\beta} + \mathcal{L}_\beta \gamma_{\alpha\beta}. \tag{2.22}$$

Hence, unless otherwise specified, we will treat $K_{\alpha\beta}$ as an explicit function of $\partial_t \gamma_{\alpha\beta}$ in all derivations. The 3-metric, extrinsic curvature, lapse, and shift are the variables in which general relativity is cast in the 3+1 decomposition.

2.3 The ADM equations

The first step, then, is to rewrite the Riemann curvature tensor in terms of α, β^α, $\gamma_{\alpha\beta}$, and $K_{\alpha\beta}$. The projection of the Riemann tensor with $\gamma^\alpha{}_\beta$ on all four indices is given by Gauss's

equation. Projecting three indices with $\gamma^{\alpha}{}_{\beta}$ and one with n^{α} gives Codazzi's equation. And, projecting two indices with $\gamma^{\alpha}{}_{\beta}$ and two with n^{α} gives Ricci's equation. The results are conveniently summarized as

$$\begin{aligned} {}^{(4)}R^{\alpha}{}_{\beta\rho\sigma} &= (R^{\alpha}{}_{\beta\rho\sigma} + K^{\alpha}_{\rho}K_{\beta\sigma} - K^{\alpha}_{\sigma}K_{\beta\rho}) - 2n^{\alpha}D_{[\rho}K_{\sigma]\beta} \\ &\quad -2n_{\beta}(D_{[\sigma}K^{\alpha}_{\rho]}) - 2(D^{\alpha}K_{\beta[\sigma} - D_{\beta}K^{\alpha}_{[\sigma})n_{\rho]} \\ &\quad +2n^{\alpha}n_{[\rho}(\mathcal{L}_n K_{\sigma]\mu}\gamma^{\mu}_{\beta} + \frac{1}{\alpha}D_{\sigma]}D_{\beta}\alpha + K^{\mu}_{\sigma]}K_{\beta\mu}) \\ &\quad +2n_{\beta}n_{[\sigma}(\mathcal{L}_n K_{\rho]\mu}\gamma^{\mu\alpha} + \frac{1}{\alpha}D_{\rho]}D^{\alpha}\alpha + K_{\rho]\mu}K^{\mu\alpha}). \end{aligned} \tag{2.23}$$

The expression can be substituted anywhere the four dimensional Riemann tensor appears, resulting in an expression in terms of the spatial quantities and their derivatives. In particular, the Einstein-Hilbert action (2.7) is

$$\begin{aligned} I_{EH} &= \frac{1}{8\pi}\int d^4x\alpha\sqrt{\gamma}\Big(R + K^2 - K^{\alpha\beta}K_{\alpha\beta} - 2(\gamma^{\alpha\beta}\mathcal{L}_n K_{\alpha\beta} + \frac{1}{\alpha}D^{\beta}D_{\beta}\alpha \\ &\quad + K^{\alpha\beta}K_{\alpha\beta})\Big) \\ &= \frac{1}{8\pi}\int dt\int d^3x\alpha\sqrt{\gamma}\Big(R + K^{\alpha\beta}K_{\alpha\beta} - K^2 - 2\nabla_{\alpha}(n^{\alpha}K + a^{\alpha})\Big) \\ &= \frac{1}{8\pi}\int d^4x\mathscr{L}, \end{aligned} \tag{2.24}$$

where $a^{\alpha} = n^{\beta}\nabla_{\beta}n^{\alpha}$ and $\mathscr{L}$ is the Lagrangian for Einstein's gravity. The divergence term in the Lagrangian is hereafter dropped, since we will require the variation of the fields in the theory to be zero on the boundary of the spacetime. Recalling the coordinate choices from before (2.14, 2.15), the Lagrangian can be re-interpreted as a functional of time evolving fields (α, β^a, γ_{ab}, and K_{ab}) on a 3 dimensional space, with equations of motion given by the Euler Lagrange equations

for the Lagrangian

$$\mathscr{L} = \alpha\sqrt{\gamma}(R + K^{ab}K_{ab} - K^2). \tag{2.25}$$

Here, K_{ab} is a function of $\dot{\gamma}_{ab}$, γ_{ab}, α, and β^a given by (2.22).

The Euler Lagrange (EL) equation of motion for a generic field ϕ in the Lagrangian $\mathscr{L}$ is

$$0 = \frac{\partial\mathscr{L}}{\partial\phi} - \partial_a\frac{\partial\mathscr{L}}{\partial(\partial_a\phi)} + \partial_a\partial_b\frac{\partial\mathscr{L}}{\partial(\partial_a\partial_b\phi)} - \partial_t\frac{\partial\mathscr{L}}{\partial(\partial_t\phi)} \tag{2.26}$$

So, the EL equation for α is

$$0 = \sqrt{\gamma}(R + K^2 - K^{ab}K_{ab}). \tag{2.27}$$

This equation is known as the Hamiltonian constraint. A similar equation, called the momentum constraint, follows from the Euler Lagrange equations for β^a.

$$0 = 2\sqrt{\gamma}(-D^bK_{ab} + D_aK). \tag{2.28}$$

These two equations provide conditions which γ_{ab} and K_{ab} must satisfy at every instant in time.

The evolution equation for K_{ab} follows from the Euler Lagrange equation for γ_{ab}. Without much difficulty, the time derivative of K_{ab} can be solved for,

$$\begin{aligned}\partial_tK_{ab} = {} & -D_aD_b\alpha + \alpha(R_{ab} + K_{ab}K - 2K_{ac}K^c{}_b) + \beta^cD_cK_{ab} \\ & + K_{ac}D_b\beta^c + K_{bc}D_a\beta^c.\end{aligned} \tag{2.29}$$

It is also straightforward to show that (2.27) and (2.28) are preserved under evolution. Then, equations (2.27 , 2.28 , 2.22, and 2.29) are a complete set of constraints and evolution equations. Together, they are known as the ADM equations [8], and are equivalent to Einstein's field equations. However, instead of a spacetime covariant theory, we now have a theory of constrained, time evolving fields (γ_{ab} and K_{ab}) on a 3 dimensional space with four gauge degrees of freedom (α and β^a).

2.4 ADM Mass and Angular Momentum

In special cases, spacetimes can be characterized in an intuitive way by their asymptotic behavior. If the spacetimes are asymptotically flat, then there are coordinates in which the metric differs from the Minkowski metric by terms of order $O(1/r)$. Then, the ADM mass, momentum and angular momentum of the spacetime are defined in terms of integrals of the extrinsic curvature and spatial metric on a sphere in the limit $r \to \infty$ as follows. To define the ADM quantities for a conformally flat spacetime, the metric and extrinsic curvature are conformally decomposed first.

$$\gamma_{ab} = \psi^4 f_{ab} \tag{2.30}$$

$$K_{ab} = \psi^{-2} \bar{K}_{ab} \tag{2.31}$$

Here, f_{ab} is the flat metric. Because the spacetime is asymptotically flat, the conformal factor ψ is a scalar function that approaches 1 in the limit of large distance from the origin, $\psi = 1 + O(1/r)$.

The ADM mass, linear momentum, and angular momentum integrals are is given by [50, 21, 62]

$$M = -\frac{1}{2\pi} \oint_\infty \bar{D}_a \psi d^2 S^a. \tag{2.32}$$

The covariant derivative $\bar{D}_a$ is compatible with the flat metric, and d^2S^a is the area element of the sphere in the limit $r \to \infty$. The ADM linear momentum is

$$P^a = \frac{1}{8\pi} \oint_\infty \bar{K}^a_b d^2S^b, \tag{2.33}$$

and the ADM angular momentum is

$$J^a = \frac{1}{8\pi} \varepsilon^{abc} \oint_\infty x_b \bar{K}_{cd} d^2S^d. \tag{2.34}$$

2.5 Bowen York Initial Data

The initial data are solutions of the Hamiltonian and momentum constraints. The solutions are constructed so that they represent astrophysically interesting scenarios such as two black holes in orbit around each other. To solve the constraints, simplifying assumptions are typically made. For instance, Bowen-York initial data [21, 20, 63] are found by setting

$$K = 0 \tag{2.35}$$

$$\gamma_{ab} = \psi^4 f_{ab}, \tag{2.36}$$

Here, ψ is called the conformal factor, and f_{ab} is the flat spatial metric. To solve the momentum constraint, it helps to further decompose the extrinsic curvature

$$K_{ab} = \psi^{-2}(\bar{A}^{TT}_{ab} + \bar{A}^{L}_{ab}). \tag{2.37}$$

$\bar{A}^{TT}_{ab}$ is the transverse traceless component of the extrinsic curvature, and $\bar{A}^{L}_{ab}$ is the longitudinal component. They satisfy the constraints

$$\bar{D}^a \bar{A}^{TT}_{ab} = 0 \tag{2.38}$$

$$\bar{A}^{L}_{ab} = \bar{D}_a W_b + \bar{D}_b W_a - \frac{2}{3}\bar{\gamma}_{ab}\bar{D}^c W_c, \tag{2.39}$$

where $\bar{D}_a$ is the covariant derivative compatible with the flat metric f_{ab}. With the extrinsic curvature decomposed this way, (2.28) takes the form

$$f^{bc}\bar{D}_b\bar{D}_c W_a + \frac{1}{3} f^{bc}\bar{D}_a\bar{D}_b W_c = 0 \tag{2.40}$$

By specializing to Cartesian coordinates, and making the substitution

$$W_a = V_a + \partial_a U \tag{2.41}$$

$$\partial^a\partial_a U = -\frac{1}{4}\partial^a V_a, \tag{2.42}$$

the momentum constraint is now

$$\partial^b\partial_b V_a = 0. \tag{2.43}$$

Equations (2.42, 2.43) are four separate Poisson equations which can be solved analytically. Solutions for U and V_a are used to construct W_a using (2.41) and $\bar{A}^{L}_{ab}$ using (2.39). Because $\bar{A}^{TT}_{ab}$ is arbitrary so long as it satisfies (2.38), it will be set to zero. Then, K_{ab} is known up to the conformal factor.

We are interested in solutions of (2.43) and (2.42) which give spacetimes with known ADM mass, momentum, and angular momentum. One solution is

$$V_a = -\frac{2}{r}P_a, \tag{2.44}$$

$$U = \frac{1}{4r}P_a x^a \tag{2.45}$$

where P_a is a constant, $r^2 = x^a x_a$. The traceless conformal extrinsic curvature is

$$\bar{A}^L_{ab} = \frac{3}{2r^3}\left(P_a x_b + P_b x_a + P_c x^c(-f_{ab} + x_a x_b r^{-2})\right). \tag{2.46}$$

The result is the extrinsic curvature for initial data representing a black hole with ADM momentum P_a, located at the origin. However, the solution can be translated to any point. In addition, since the momentum constraint (2.40) is linear, multiple solutions (2.46) can be added together to make new solutions.

A second interesting solution to (2.43) and (2.42) is

$$V_a = -\varepsilon_{abc}J^b x^c r^{-3} \tag{2.47}$$

$$U = 0. \tag{2.48}$$

Then, the traceless conformal extrinsic curvature is

$$\bar{A}^L_{ab} = \frac{3}{r^5}(\varepsilon_{acd}J^c x^d x_b + \varepsilon_{bcd}J^c x^d x_a) \tag{2.49}$$

This is the extrinsic curvature for the initial data of a black hole with intrinsic angular momentum J_a, located at the origin. Again, the result can be translated away from the origin, and added to other solutions to make initial data with multiple black holes, or black holes with both linear momentum and intrinsic angular momentum.

Under the Bowen York assumptions, the Hamiltonian constraint (2.27) takes the form

$$\bar{D}^2\psi = -\frac{1}{8}\psi^5 K_{ab}K^{ab}. \tag{2.50}$$

Equation (2.50) is an elliptic equation for ψ, which can be solved numerically with a high degree of accuracy. Though numerical solutions can be very accurate, the assumption of conformal flatness has interesting consequences. On account of the assumption, the initial data contain a pulse of gravitational radiation which does not generally correspond to the desired initial scenario. However, this pulse radiates away quickly and without much effect [18].

Singularities pose additional problems to solving (2.27). Specifically, near the singularities ψ diverges as one over the distance to the singularity. The diverging behavior of ψ continues during the evolution. A popular method for overcoming this difficulty is the puncture method [22]. The method is based around rewriting the conformal factor in terms of an initial function u. The properties of the function u are that for large distance r to the singularities, $u \sim 1/r$, and that u and its first and second derivatives exist everywhere. For initial data for N black holes with bare masses m_i and coordinate locations $X^a_{(i)}$, write ψ as

$$\psi = 1 + \sum_{i=1}^{N} \frac{m_i}{|x^a - X^a_{(i)}|} + u. \tag{2.51}$$

The Hamiltonian constraint is now a constraint for u

$$\bar{D}^2 u = -\frac{1}{8}\left(1 + \sum_{i=1}^{N} \frac{m_i}{|x^a - X^a_{(i)}|} + u\right)^5 K_{ab}K^{ab}. \tag{2.52}$$

The boundary conditions on u are the properties of u given above. The solution is computed numerically using a spectral code for solving quasi-linear elliptic equations. The code used at PSU was written by Marcus Ansorg [7], and is specialized to producing initial data for binary black hole simulations in vacuum. In order to solve (2.52) and to perform the simulation, the singularity points must be removed from the domain. This is achieved simply by having singularities initially located at coordinates that do not correspond to the numerical grid points. The singularities will move during the simulation, but will never fall exactly on grid points. This technique, known as the moving puncture technique, has lead to stable black hole evolutions without complicated gauge or boundary conditions near the black hole [13, 27, 23].

2.6 BSSN Equations

While the ADM equations are in a form which can be integrated numerically, they are susceptible to rapid growth of numerical errors. A much more stable scheme for solving Einstein's equations numerically was formulated in 1998 by Baumgarte and Shapiro [14, 56]. This scheme, known as the BSSN system, is a hyperbolic formulation which preserves the gauge freedoms of general relativity (see [15] for a review). In the system, the metric and extrinsic curvature are conformally decomposed, and the extrinsic curvature is divided into its trace and its trace free part.

$$\phi \equiv \frac{1}{12}\ln\gamma \tag{2.53}$$

$$\gamma_{ab} = e^{4\phi}\bar{\gamma}_{ab} \tag{2.54}$$

$$K_{ab} = e^{4\phi}\bar{A}_{ab} + \frac{1}{3}e^{4\phi}\bar{\gamma}_{ab}K \tag{2.55}$$

Because we choose $\bar{\gamma} = 1$, $e^{4\phi}$ is a scalar density with weight $\frac{2}{3}$. In addition, the trace of the conformal Christoffel connection is made a dynamic variable,

$$\bar{\Gamma}^a \equiv \bar{\gamma}^{bc}\bar{\Gamma}^a_{bc} = -\bar{\gamma}^{ab}_{,b}. \tag{2.56}$$

The definition of $\bar{\Gamma}^a$ functions as a new constraint. Then, the new set of dynamical quantities is ϕ, K, $\bar{\gamma}_{ab}$, $\bar{A}_{ab}$, and $\bar{\Gamma}^a$. The evolution equations follow from the ADM equations and (2.56) [4]:

$$\partial_t\phi = -\frac{1}{6}\alpha K + \beta^a\partial_a\phi + \frac{1}{6}\partial_a\beta^a, \tag{2.57}$$

$$\partial_t K = -D^a D_a\alpha + \alpha(\bar{A}_{ab}\bar{A}^{ab} + \frac{1}{3}K^2) + \beta^a\partial_a K, \tag{2.58}$$

$$\partial_t\bar{\gamma}_{ab} = -2\alpha\bar{A}_{ab} + \beta^c\partial_c\bar{\gamma}_{ab} + \bar{\gamma}_{ac}\partial_b\beta^c + \bar{\gamma}_{bc}\partial_a\beta^c - \frac{2}{3}\bar{\gamma}_{ab}\partial_c\beta^c, \tag{2.59}$$

$$\begin{aligned}\partial_t\bar{A}_{ab} \;=\; & e^{-4\phi}\Big(-D_aD_b\alpha + \alpha R_{ab} - \frac{1}{3}\gamma_{ab}(D^cD_c\alpha + \alpha R)\Big) \\ & +\alpha(K\bar{A}_{ab} - 2\bar{A}_{ac}\bar{A}^c_b) + \beta^c\partial_c\bar{A}_{ab} + \bar{A}_{ac}\partial_b\beta^c + \bar{A}_{bc}\partial_a\beta^c \\ & -\frac{2}{3}\bar{A}_{ab}\partial_c\beta^c\end{aligned} \tag{2.60}$$

$$\begin{aligned}
\partial_t \bar{\Gamma}^a &= -\partial_b \partial_t \bar{\gamma}^{ab} \\
&= -\partial_b (2\alpha \bar{A}^{ab} + \beta^c \partial_c \bar{\gamma}^{ab} - \bar{\gamma}^{ac} \partial_c \beta^b - \bar{\gamma}^{bc} \partial_c \beta^a + \frac{2}{3} \bar{\gamma}^{ab} \partial_c \beta^c) \\
&= -2\bar{A}^{ab} \partial_b \alpha + 2\alpha (\bar{\Gamma}^a_{bc} \bar{A}^{bc} - \frac{2}{3} \bar{\gamma}^{ab} \partial_b K + 6\bar{A}^{ab} \partial_b \phi) + \beta^b \partial_b \bar{\Gamma}^a \\
&\quad -\bar{\Gamma}^b \partial_b \beta^a + \frac{2}{3} \bar{\Gamma}^a \partial_b \beta^b + \frac{1}{3} \bar{\gamma}^{ab} \partial_b \partial_c \beta^c + \bar{\gamma}^{bc} \partial_b \partial_c \beta^a
\end{aligned} \tag{2.61}$$

In the last step of deriving equation (2.61), the momentum constraint is used to eliminate the divergence of $\bar{A}_{ab}$, and (2.56) is used to replace divergences of $\bar{\gamma}_{ab}$ with $\bar{\Gamma}^a$. The reasons for the enhanced stability of the BSSN system are not fully understood. However, there is evidence that by using the momentum constraint to eliminate the divergence of $\bar{A}_{ab}$ in (2.61), the system of equations is made strongly hyperbolic, and constraint violating errors propagate out of the domain of the simulation [57, 61, 35, 54, 55]. In the ADM system, momentum constraint violating errors do not propagate, and can grow as a result of the non-linearity of the evolution equations [14, 3].

2.7 Gauge Conditions

The final step in preparing Einstein's equations for numerical integration is to choose the lapse and shift. These choices must be made carefully, since poorly chosen coordinates will develop coordinate singularities. While these singularities are non-physical, they will still ruin simulations. One popular and successful choice for the lapse is called the "1 plus log" slicing condition,

$$\partial_t \alpha = -2\alpha K + C_1 \beta^a \partial_a \alpha. \tag{2.62}$$

The choice is very simple and easily calculable. In addition, it possesses a property known as singularity avoidance. Less proper time elapses on the surface for points nearer to singularities, resulting in more stable evolution [19]. The term proportional to the constant C_1 is known as the lapse advection, and is included to further reduce instability in the simulations.

A common choice of shift is to use the "Gamma driver" condition. The choice attempts to minimize distortion (u_{ab}), which is related to the time derivative of the conformal 3 metric,

$$u_{ab} \equiv e^{4\phi}\partial_t \bar{\gamma}_{ab}. \tag{2.63}$$

To minimize the distortion, its divergence is set to zero, yielding an elliptic equation for β^a. Because of the difficulty posed by solving an elliptic equation at every time step in a simulation, the condition is approximated by

$$\begin{aligned} 0 &= \partial_b \partial_t \bar{\gamma}^{ab} \\ &= \partial_t \bar{\Gamma}^a. \end{aligned} \tag{2.64}$$

Then, the condition is further approximated by

$$\partial_t \beta^a = \frac{3}{4}\alpha^{C_2} B^a + \mu \beta^b \partial_b \beta^a \tag{2.65}$$

$$\partial_t B^a = \partial_t \bar{\Gamma}^a - \eta B^a - \zeta \beta^a \partial_a \bar{\Gamma}^a + \mu \beta^a \partial_a B^a. \tag{2.66}$$

The constants C_2, μ, η, and ζ are chosen from experience to maximize the stability of the simulation. The choices used in the simulations in this dissertation are $C_1 = 1$, $C_2 = 0$, $\eta = 2$, $\mu = 1$, $\zeta = 1$, and are collectively known as the moving puncture gauge. While the gauge conditions

approximate ideal coordinate choices such as maximal slicing and minimal distortion, they are as valid as any other choice of α and β^a. That is, α and β^a, being gauge quantities, must have no effect on observable quantities, and can be chosen in any fashion. These choices are made on account of their relative simplicity and the fact that they lead to stable evolutions [4].

2.8 Numerical Methods

To perform the simulations, we use the Cactus code [1]. Cactus provides an open source framework for parallel computing specifically geared towards science and engineering problems. The code is divided into two parts, known as the flesh and the thorns. A thorn is a module, typically designed to perform a specific task such as a calculation or an I/O function. The flesh is responsible for initializing the thorns and scheduling the the tasks they perform. Unlike the flesh, thorns can be easily written or modified to add functionality to the code. To further simplify the coding of tensor equations for Cactus thorns, we use Kranc. Kranc is a set of Mathematica scripts which can convert tensor equations directly into Cactus thorns. The scripts were written by Sascha Husa, Ian Hinder, and Christiane Lechner for handling complicated systems of equations [38].

A numerical relativity simulation must first divide the space-like surface Σ into a set of points called the grid. The functions on the surface are represented by their values on the grid points. Derivatives are then approximated by finite differences. Higher grid resolution is needed near singularities. For this, we use multiple grids with different grid spacings. Grids with higher resolution represent smaller spatial regions close to the singularities. This grid refinement technique is managed by the Carpet thorn [2]. Initial data are calculated using the Bowen-York method. Then, they are evolved using the BSSN equations. As the code is running, additional

computations can be performed. For example, the location of the black hole horizons or the approximate location of the singularities themselves can be tracked. Or, gravitational radiation can be computed from the solution. Code for binary black hole inspirals typically requires tens of CPUs and tens of gigabytes of memory to run successfully. By further increasing the number of CPUs and amount of memory for runs, increasingly accurate simulations are being performed.

Chapter 3

Newman Penrose Scalars and Gravitational Radiation

3.1 Linear gravitational waves

An important prediction of Einstein's theory is that waves in the curvature can propagate through the spacetime. Though never observed directly, this gravitational radiation plays an integral role in highly energetic dynamics. For example, a system of closely orbiting compact objects will lose angular momentum due to gravitational radiation. The process will continue until the objects merge. The radiation, if measured with sufficient accuracy, would give information about the masses and other properties of the orbiting objects. In addition, the gravitational radiation could possibly be used to constrain alternative theories of gravity.

Gravitational radiation is modeled as a linear perturbation of the spacetime metric which obeys a wave equation. Consider, as an analytic example, a linear perturbation of a flat spacetime metric ($\eta_{\alpha\beta}$),

$$g_{\alpha\beta} = \eta_{\alpha\beta} + h_{\alpha\beta} \tag{3.1}$$

with $|h_{\alpha\beta}| \ll 1$. Then, all terms proportional to $|h_{\alpha\beta}|^2$ will be ignored in the following calculations. An infinitesimal coordinate transformation $x_\alpha \rightarrow x_\alpha + \xi_\alpha$, $|\xi^\alpha| \ll 1$, will not affect the background metric. Hence, there is a gauge freedom in $h_{\alpha\beta}$ associated with ξ_α,

$$h_{\alpha\beta} \rightarrow h_{\alpha\beta} + \partial_\alpha \xi_\beta + \partial_\beta \xi_\alpha. \tag{3.2}$$

The gauge freedom can be used to fix the radiation gauge in vacuum ($T_{\alpha\beta} = 0$).

$$\partial^{\alpha} h_{\alpha\beta} = 0 \tag{3.3}$$

$$\eta^{\alpha\beta} h_{\alpha\beta} = 0 \tag{3.4}$$

$$h_{0\alpha} = 0 \tag{3.5}$$

Then, Einstein's equations to first order in $h_{\alpha\beta}$ are

$$\partial^{\gamma}\partial_{\gamma} h_{\alpha\beta} = 0 \tag{3.6}$$

A solution to (3.6) which also satisfies (3.3-3.5) is the plane wave

$$h_{\alpha\beta} = H_{\alpha\beta} \exp(i k_{\mu} x^{\mu}). \tag{3.7}$$

The radiation gauge and Einstein's equations constrain the values of $H_{\alpha\beta}$ and k_{μ}, so that k_{μ} is null, and orthogonal to $H_{\alpha\beta}$. There are eight independent constraints on the value of $H_{\alpha\beta}$ from the gauge conditions, leaving two independent solutions. These two solutions are interpreted as the two polarization states of the radiation.

Waves such as the plane wave in the radiation gauge have non-zero curvature, indicating they generate real physical effects. One effect of gravitational radiation is to create strain in the directions transverse to the wave vector. The magnitude of the strain is very small, and related to the mass quadrupole (Q_{ab}) and distance (r) of the sources. For non-relativistic sources that are

small compared to the wavelength and do not self gravitate

$$Q_{ab} = \int T_{00} x_a x_b d^3x \tag{3.8}$$

$$h_{ab} = \frac{2}{r} \frac{d^2 Q_{ab}}{dt^2}. \tag{3.9}$$

The amplitude of waves produced by two solar mass black holes in a circular orbit of radius ten times their Schwarzschild radius, at a distance of 100 Mpc is expected to be on the order of 10^{-22}. The amplitude of the perturbation is proportional the fractional change in distance between two freely moving test masses that are initially stationary relative to each other. Thus, the strain induced by gravitational radiation is an actual measurable quantity given a sufficiently sensitive detector.

In addition to ripples in curvature, systems which emit gravitational waves also radiate energy, momentum, and angular momentum. For example, the effective stress-energy carried by the waves (in the radiation gauge) is given by [39]

$$T_{\mu\nu} \equiv \frac{1}{32\pi} \left\langle h_{\alpha\beta,\mu} h^{\alpha\beta}{}_{,\nu} \right\rangle, \tag{3.10}$$

where the angled brackets $\langle ... \rangle$ indicate that the quantity enclosed is averaged over a scale larger than the wavelength of the gravitational radiation. Then, equation (3.10) indicates that we can compute quantities like the momentum flux and energy flux if we know the value of the gravitational radiation $h_{\alpha\beta}$.

3.2 Newman Penrose scalars

The Newman Penrose scalars are a set of five complex scalars specially suited to the computation of gravitational radiation [49, 28]. The NP scalars are projections of the Weyl tensor $C_{\alpha\beta\gamma\delta}$,

$$C_{\alpha\beta\gamma\delta} = R_{\alpha\beta\gamma\delta} - g_{\alpha[\gamma}R_{\delta]\beta} + g_{\beta[\gamma}R_{\delta]\alpha} + \frac{1}{3}g_{\alpha[\gamma}g_{\delta]\beta}R, \tag{3.11}$$

using a null tetrad ($\mathfrak{l}^\alpha$, $\mathfrak{n}^\alpha$, $\mathfrak{m}^\alpha$, $\bar{\mathfrak{m}}^\alpha$). The vectors $\mathfrak{l}^\alpha$ and $\mathfrak{n}^\alpha$ are real, while $\mathfrak{m}^\alpha$ and $\bar{\mathfrak{m}}^\alpha$ are complex and conjugate to each other. The tetrad vectors satisfy the following orthonormality conditions:

$$\begin{gathered} \mathfrak{l}_\alpha\mathfrak{l}^\alpha = \mathfrak{m}_\alpha\mathfrak{m}^\alpha = \bar{\mathfrak{m}}_\alpha\bar{\mathfrak{m}}^\alpha = \mathfrak{n}_\alpha\mathfrak{n}^\alpha = 0, \\ \mathfrak{l}_\alpha\mathfrak{n}^\alpha = -\mathfrak{m}_\alpha\bar{\mathfrak{m}}^\alpha = -1, \\ \mathfrak{l}_\alpha\mathfrak{m}^\alpha = \mathfrak{l}_\alpha\bar{\mathfrak{m}}^\alpha = \mathfrak{n}_\alpha\mathfrak{m}^\alpha = \mathfrak{n}_\alpha\bar{\mathfrak{m}}^\alpha = 0 \end{gathered} \tag{3.12}$$

The NP scalars are, then,

$$\Psi_0 = C_{\alpha\beta\gamma\delta}\mathfrak{l}^\alpha\mathfrak{m}^\beta\mathfrak{l}^\gamma\mathfrak{m}^\delta \tag{3.13}$$

$$\Psi_1 = C_{\alpha\beta\gamma\delta}\mathfrak{l}^\alpha\mathfrak{n}^\beta\mathfrak{l}^\gamma\mathfrak{m}^\delta \tag{3.14}$$

$$\Psi_2 = C_{\alpha\beta\gamma\delta}\mathfrak{l}^\alpha\mathfrak{m}^\beta\bar{\mathfrak{m}}^\gamma\mathfrak{n}^\delta \tag{3.15}$$

$$\Psi_3 = C_{\alpha\beta\gamma\delta}\mathfrak{l}^\alpha\mathfrak{n}^\beta\bar{\mathfrak{m}}^\gamma\mathfrak{n}^\delta \tag{3.16}$$

$$\Psi_4 = C_{\alpha\beta\gamma\delta}\bar{\mathfrak{m}}^\alpha\mathfrak{n}^\beta\bar{\mathfrak{m}}^\gamma\mathfrak{n}^\delta \tag{3.17}$$

Because the Weyl tensor is the trace free curvature tensor, waves in the metric which are purely coordinate effects will not influence the tensor's value. In addition, if the tetrad is chosen to

reflect the background symmetries of the spacetime, the NP scalars Ψ_0 and Ψ_4 will isolate information about the gravitational radiation.

3.3 Petrov classification

The Weyl tensor also provides a natural method for classifying the spacetime. There are at most four linearly independent bivectors $\Sigma_{\alpha\beta}$ that are eigenvectors of the Weyl tensor

$$C^{\alpha\beta}{}_{\mu\nu}\Sigma_{\alpha\beta} = \lambda\Sigma_{\mu\nu}. \tag{3.18}$$

The multiplicity of the eigenvectors $\Sigma_{\alpha\beta}$ can be used to classify spacetimes as algebraically special or not [52]. This multiplicity is also closely related to the degeneracy of principle null directions of the spacetime. The principle null directions (PND) are represented by vectors v^α for which [49]

$$R_{\alpha\beta\gamma[\delta}v_{\varepsilon]}v^\beta v^\gamma = 0. \tag{3.19}$$

Again, there are at most four linearly independent PND. More intuitively, the principle null directions are the directions along which radiation travels with minimum distortion [51, 36].

3.3.1 Petrov type D spacetimes

The classifications of most importance to this work are Petrov type D, and Petrov type I. The set of type D spacetimes includes the Kerr and Schwarzschild metrics and is defined by having two distinct eigen-bivectors, both being degenerate. The two distinct PND are also degenerate. The type D spacetimes contain no gravitational radiation. However, they serve as suitable background metrics for vacuum spacetimes that contain gravitational radiation.

The Kerr metric in Boyer-Lindquist coordinates (t, r, θ, ϕ) is given by the line element

$$\begin{aligned} ds^2 &= -\frac{1}{\Sigma}(\Delta - a^2\sin^2\theta)dt^2 - \frac{1}{\Sigma}2a\sin^2\theta(r^2+a^2-\Delta)dtd\phi \\ &\quad + \frac{\Sigma}{\Delta}dr^2 + \Sigma d\theta^2 + \frac{1}{\Sigma}((r^2+a^2)^2 - \Delta a^2\sin^2\theta)d\phi^2 \end{aligned} \tag{3.20}$$

where

$$\Sigma = r^2 + a^2\cos^2\theta, \tag{3.21}$$

$$\Delta = r^2 + a^2 - 2Mr. \tag{3.22}$$

This solution to Einstein's equations has the properties of being stationary and axisymmetric, with ADM mass M and angular momentum aM. The Schwarzschild metric can be recovered by letting $a = 0$. The repeated PNDs of the spacetime are

$$v1^a = \frac{1}{\Delta}(r^2+a^2, \Delta, 0, a) \tag{3.23}$$

and

$$v2^a = \frac{1}{\Delta}(r^2+a^2, -\Delta, 0, a). \tag{3.24}$$

For the Kerr metric, these PND are also tangent to outgoing and ingoing future directed geodesics respectively.

For the type D spacetime if the real tetrad vectors $\mathfrak{l}^\alpha$ and $\mathfrak{n}^\alpha$ are proportional to the principal null vectors, then all of the NP scalars except Ψ_2 are zero. These choices and the orthonormality conditions (3.12) eliminate all but two of the degrees of freedom of the tetrad. The remaining two correspond to a scaling of $\mathfrak{l}^\alpha$ and $\mathfrak{n}^\alpha$, and a phase for $\mathfrak{m}^\alpha$ and $\bar{\mathfrak{m}}^\alpha$. To fix these

degrees of freedom, additional scalars known as the spin coefficients are introduced. These are

$$\begin{aligned}
\kappa &= \mathfrak{m}^{\mu}\mathfrak{l}^{\nu}\nabla_{\nu}\mathfrak{l}_{\mu} && (3.25)\\
\lambda &= -\bar{\mathfrak{m}}^{\mu}\bar{\mathfrak{m}}^{\nu}\nabla_{\nu}\mathfrak{n}_{\mu} && (3.26)\\
\sigma &= \mathfrak{m}^{\mu}\mathfrak{m}^{\nu}\nabla_{\nu}\mathfrak{l}_{\mu} && (3.27)\\
\nu &= \bar{\mathfrak{m}}^{\mu}\mathfrak{n}^{\nu}\nabla_{\nu}\mathfrak{n}_{\mu} && (3.28)\\
\varepsilon &= \frac{1}{2}(\mathfrak{n}^{\mu}\mathfrak{l}^{\nu}\nabla_{\nu}\mathfrak{l}_{\mu} - \bar{\mathfrak{m}}^{\mu}\mathfrak{l}^{\nu}\nabla_{\nu}\mathfrak{m}_{\mu}) && (3.29)
\end{aligned}$$

By setting $\mathfrak{l}^{\alpha}$ and $\mathfrak{n}^{\alpha}$ proportional to the PND, the Bianchi identities [49] show that $\kappa = \lambda = \sigma = \nu = 0$.

The Kinnersley tetrad is defined for type D spacetimes by choosing $\varepsilon = 0$ and $\mathfrak{l}^{\alpha}(r)_{\alpha} \to 1$ as $r \to \infty$ [42]. The resulting tetrad is

$$\begin{aligned}
\mathfrak{l}^{\alpha} &= v1^{\alpha}\\
\mathfrak{n}^{\alpha} &= \tfrac{\Delta}{2\Sigma}v2^{\alpha}\\
\mathfrak{m}^{\alpha} &= \tfrac{1}{\sqrt{2}(r+ia\cos\theta)}(ia\sin\theta, 0, 1, i\csc\theta)\\
\bar{\mathfrak{m}}^{\alpha} &= \tfrac{1}{\sqrt{2}(r-ia\cos\theta)}(-ia\sin\theta, 0, 1, -i\csc\theta)
\end{aligned} \qquad (3.30)$$

The only non-zero NP scalar is Ψ_2, with value [59]

$$\Psi_2 = -\frac{M}{(r-ia\cos\theta)^3}. \qquad (3.31)$$

3.3.2 Petrov type I spacetimes

A Petrov type I spacetime is not algebraically special. The Weyl tensor of a type I spacetime possesses four independent eigen-bivectors and four distinct principle null directions. In general, spacetimes studied in numerical relativity are of this type. However, if the gravitating bodies are isolated to one region of the spacetime, then far from that region the spacetime can be approximated by a type D spacetime plus a linear perturbation. When this is the case, the tetrad can be set to the Kinnersly tetrad of the background spacetime. The resulting NP scalars have the following interpretation. The scalars Ψ_0 and Ψ_4 represent ingoing and outgoing gravitational radiation respectively. The scalars Ψ_1 and Ψ_3 represent longitudinal, gauge dependent degrees of freedom in the curvature tensor. And, the scalar Ψ_2 represents the static (Coulombic) curvature of the spacetime due to the mass and angular momentum of the background Kerr black hole [58].

In the case of a linear perturbation, the metric can be written

$$g_{\alpha\beta} = g_{\alpha\beta}{}^{A} + h_{\alpha\beta}{}^{B} \tag{3.32}$$

where $g_{\alpha\beta}{}^{A}$ is the Kerr metric (3.20), and the perturbation $h_{\alpha\beta}{}^{B}$ is small enough to be neglected at quadratic and higher orders. The superscript A will be used to identify quantities that are zeroth order in $h_{\alpha\beta}{}^{B}$ while B will be used for quantities that are first order in the perturbation. Then, if the tetrad is chosen to be the Kinnersley tetrad of the background spacetime (3.30),

$$\begin{aligned} &\Psi_0{}^{A} = \Psi_1{}^{A} = \Psi_3{}^{A} = \Psi_4{}^{A} = 0, \\ &\kappa^{A} = \sigma^{A} = \nu^{A} = \lambda^{A} = \varepsilon^{A} = 0. \end{aligned} \tag{3.33}$$

Furthermore, in the limit $r \to \infty$ [59],

$$\Psi_4^B = \partial_t^2 h_{\theta\theta}^B + i\partial_t^2 h_{\theta\phi}^B. \tag{3.34}$$

The values $h_{\theta\theta}^B$ and $h_{\theta\phi}^B$, which represent the transverse traceless components of the metric perturbation, can be recovered from Ψ_4^B, and physical quantities such as the stress energy of the gravitational waves (3.10) can be computed.

The Teukolsky equation [59] shows that for large r, $\Psi_0 = O(r^{-5})$ along a null geodesic whose tangent is l^α whenever the radiation in a spacetime is purely outgoing. Then, the Peeling theorem [49] guarantees that the asymptotic behavior of the NP scalars in the Kinnersley tetrad of the background metric is $\Psi_1 = O(r^{-4})$, $\Psi_2 = O(r^{-3})$, $\Psi_3 = O(r^{-2})$, and $\Psi_4 = O(r^{-1})$. In contrast, if the radiation is purely ingoing, $\Psi_4 = O(r^{-5})$, $\Psi_3 = O(r^{-4})$, $\Psi_2 = O(r^{-3})$, $\Psi_1 = O(r^{-2})$, and $\Psi_0 = O(r^{-1})$. Furthermore, the Teukolsky equation is separable, and the angular equation has as eigenfunctions the spin-weighted spherical harmonics [48, 31, 60]. In particular, the scalar Ψ_0 has spin-weight $s = 2$ and the scalar Ψ_4 has $s = -2$. For this reason, when we report the value of Ψ_0 and Ψ_4 expanded in terms of spherical harmonics, they will always be spherical harmonics of the appropriate spin-weight.

The scalars Ψ_0^B and Ψ_4^B are invariant under infinitesimal rotations of the coordinates and the tetrad. Because the Kinnersly conditions (3.33) rely on splitting the metric into background and perturbation and are difficult to solve, there is interest in finding a choice of tetrad which will produce the same results as the Kinnersly tetrad (3.34), with a simpler set of conditions. Specifically, we desire conditions which only require knowledge of spatial quantities, and which

do not require the solution of differential equations. There are two popular tetrad choices meeting these criteria which we will discuss.

3.4 Fiducial tetrad

The first choice, outlined in [11] is highly suited to numerical simulation. Starting with three spatial vectors,

$$v_1^a = (-y, x, 0) \tag{3.35}$$

$$v_2^a = (x, y, z) \tag{3.36}$$

$$v_3^a = \sqrt{\gamma}\gamma^{ab}\varepsilon_{bcd}v_1^c v_2^d \tag{3.37}$$

and a time-like unit vector n^α, the spatial vectors are orthonormalized via the Graham-Schmidt procedure in the order they are indexed. Then, the resulting set of orthonormal vectors are used to construct unit vectors in the $\hat{\phi}$, $\hat{r}$, and $\hat{\theta}$ directions respectively.

$$\begin{aligned} \hat{r}^0 = 0, \quad \hat{\theta}^0 = 0, \quad \hat{\phi}^0 = 0 \\ \hat{r}^a = v_2^a, \quad \hat{\theta}^a = v_3^a, \quad \hat{\phi}^a = v_1^a. \end{aligned} \tag{3.38}$$

Finally, the null tetrad is formed using the time-like unit vector and the three orthonormal spatial vectors. The real vectors $\mathfrak{l}^\alpha$ and $\mathfrak{n}^\alpha$ are chosen so that their spatial projection lies solely in the $\hat{r}^\alpha$

direction.

$$\begin{aligned} \mathfrak{l}^\alpha &= \frac{1}{\sqrt{2}}(n^\alpha + \hat{r}^\alpha), \\ \mathfrak{n}^\alpha &= \frac{1}{\sqrt{2}}(n^\alpha - \hat{r}^\alpha), \\ \mathfrak{m}^\alpha &= \frac{1}{\sqrt{2}}(\hat{\theta}^\alpha + i\hat{\phi}^\alpha). \end{aligned} \tag{3.39}$$

It is easily seen that in regions where the spacetime metric has the form of a perturbed Minkowski metric, the tetrad will approach the Kinnersly tetrad modified by a type III tetrad rotation (A.5), with $\Lambda = \frac{1}{\sqrt{2}}$, $\theta = 0$. However, since the PND are not found, there is no guarantee that the vectors $\mathfrak{n}^\alpha$ and $\mathfrak{l}^\alpha$ agree closely enough with the PND of the background spacetime to be used to extract radiation. Instead, this is assumed at the outset and tested after the gravitational wave amplitudes are computed. Such tests might include comparing the radiated quantities like energy and momentum to the initial and final ADM energy and momentum.

3.5 Transverse quasi-Kinnersly tetrad

The second popular choice is known as the transverse frame - also known as the quasi-Kinnersly (qK) frame. The tetrad is referred to as a frame because two degrees of freedom corresponding to a type III (spin-boost) tetrad rotation remain unfixed. The frame is transverse in the sense that $\Psi_1 = \Psi_3 = 0$. The motivation of searching for the qK frame is that in the limit that the spacetime is nearly Petrov type D, a tetrad from the qK frame will differ from the Kinnersly tetrad by an infinitesimal null rotation of the tetrad vectors. Such rotations leave Ψ_0 and Ψ_4 unchanged to lowest order in the perturbation. Hence, computing Ψ_4 in the transverse

quasi-Kinnersly frame will be equivalent to computing it in the Kinnersly frame so long as an appropriate method for fixing the spin-boost freedom of the tetrad is used.

The quality that a spacetime is nearly Petrov type D is measured by the Baker-Campanelli speciality index S [9]. The scalar is defined in terms of the quadratic and cubic curvature invariants I and J,

$$I = \Psi_4\Psi_0 - 4\Psi_3\Psi_1 + 3\Psi_2^2 \tag{3.40}$$

$$J = \det\begin{vmatrix} \Psi_4 & \Psi_3 & \Psi_2 \\ \Psi_3 & \Psi_2 & \Psi_1 \\ \Psi_2 & \Psi_1 & \Psi_0 \end{vmatrix}, \tag{3.41}$$

$$S \equiv 27\frac{J^2}{I^3}. \tag{3.42}$$

The speciality index has already been investigated (see [11, 10] for examples) and has the property that its value is 1 whenever the spacetime is algebraically special (Petrov type D). Furthermore, when the spacetime is representable as a Kerr background with a small perturbation, there exists a Kinnersley frame associated with the background metric, and S can be written

$$S = 1 - 3\frac{\Psi_0^B\Psi_4^B}{(\Psi_2^A)^2} \tag{3.43}$$

to lowest order in the perturbation. In the limit $S \to 1$, the PND coincide in pairs, and the qK tetrad differs from the Kinnersley tetrad by an infinitesimal null rotation which leaves the unchanged the leading order values of Ψ_0 and Ψ_4 [44].

The recipe for computing the qK frame from γ_{ab} and K_{ab} is given in [16], and we will outline it briefly here. First, the spatial metric and extrinsic curvature are used to compute the electric and magnetic components of the Weyl tensor, E_{ab} and B_{ab}.

$$E_{ab} = (\gamma_a{}^c\gamma_b{}^d - \frac{1}{3}\gamma_{ab}\gamma^{cd})(R_{cd} + KK_{cd} - K_{ce}K^e{}_d - 4\pi S_{cd}), \tag{3.44}$$

where $S_{\alpha\beta} = \gamma_\alpha{}^\mu\gamma_\beta{}^\nu T_{\mu\nu}$ is the stress energy tensor with indices projected.

$$B_{ab} = \frac{1}{2}(\gamma_a{}^c\gamma_b{}^d + \gamma_b{}^c\gamma_a{}^d)\varepsilon_c{}^{ef}\nabla_f K_{de}. \tag{3.45}$$

From these tensors, construct the 3×3 tensor $C^a{}_b$,

$$C^a{}_b = E^a{}_b - iB^a{}_b. \tag{3.46}$$

The tensor will have three eigenvectors (degenerate cases are treated separately, in the reference [16]). The eigenvector corresponding the the eigenvalue with greatest norm will correspond to the qK frame [44] and is labeled $\hat{\sigma}^a$. Separate $\hat{\sigma}^a$ into real and imaginary parts,

$$\hat{\sigma}^a = x^a + iy^a \tag{3.47}$$

Then, find the vectors $\hat{\lambda}^a$, $\hat{\nu}^a$ and $\hat{\mu}^a$,

$$\hat{\lambda}^a = (\varepsilon^{abc}x_b y_c - x^a)\|x\|^{-2}, \tag{3.48}$$

$$\hat{\nu}^a = (\varepsilon^{abc}x_b y_c + x^a)\|x\|^{-2}, \tag{3.49}$$

and

$$\hat{\mu}^a = (1+\hat{\lambda}^b\hat{v}_b)^{-1}(\hat{\lambda}^a+\hat{v}^a+i\varepsilon^{abc}\hat{\lambda}_b\hat{v}_c). \tag{3.50}$$

One tetrad from the transverse qK frame is

$$\mathfrak{l}^\alpha = \frac{1}{\sqrt{1-\hat{\lambda}^b\hat{v}_b}}(n^\alpha+\hat{\lambda}^\alpha) \tag{3.51}$$

$$\mathfrak{n}^\alpha = \frac{1}{\sqrt{1-\hat{\lambda}^b\hat{v}_b}}(n^\alpha+\hat{v}^\alpha) \tag{3.52}$$

$$\mathfrak{m}^\alpha = \frac{\sqrt{1+\hat{\lambda}^b\hat{v}_b}}{\sqrt{2}\sqrt{1-\hat{\lambda}^c\hat{v}_c}}(n^\alpha+\hat{\mu}^\alpha) \tag{3.53}$$

The procedure for finding the tetrad is entirely algebraic. Also, the tetrad can be found for each point on the spatial slice without information from any other point. Thus, the procedure can be easily used in a numerical simulation. However, the scale of $\mathfrak{l}^\alpha$ and $\mathfrak{n}^\alpha$ and the phase of $\mathfrak{m}^\alpha$ and $\bar{\mathfrak{m}}^\alpha$ remain unfixed.

There is no generic way of fixing the spin-boost degrees of freedom. In [26], Campanelli *et al.* fix the spin-boost freedom by relating the tetrad that results from the above recipe when applied to the Kerr spacetime to the Kinnersley tetrad. Burko [24] uses additional spin coefficients to fix the tetrad in stages. The coefficients used have special behavior under the spin-boost rotation,

$$\rho = -\mathfrak{m}^\mu\bar{\mathfrak{m}}^\nu\nabla_\nu\mathfrak{l}_\mu, \tag{3.54}$$

$$\tau = -\mathfrak{m}^\mu\mathfrak{n}^\nu\nabla_\nu\mathfrak{l}_\mu, \tag{3.55}$$

$$\varpi = \bar{\mathfrak{m}}^\mu\mathfrak{l}^\nu\nabla_\nu\mathfrak{n}_\mu. \tag{3.56}$$

Then, under a type III rotation, $\rho \to \Lambda\rho$ while $\tau \to e^{i\theta}\tau$ and $\varpi \to e^{-i\theta}\varpi$. These relationships can be used to fix ρ, τ, and ϖ to desired values. For example, for the Kerr black hole and Kinnersly tetrad, $\rho^3 = \Psi_2/M$. However, this method has several setbacks. The ADM mass of the background spacetime is used along with ρ to fix Λ. However, in numerical simulations, only the approximate ADM mass is available, since the computation of the ADM mass should be performed by integrating over a sphere at spatial infinity. Furthermore, the method described for fixing the spin freedom may fail for spacetimes in which the magnetic components of the Weyl tensor are non-zero. For these reasons, this particular method is not used in numerical simulation.

A newer method for fixing the spin boost freedom up to an overall constant is described by Nerozzi and Elbracht [47]. The method relies on rewriting the Kinnersley condition $\varepsilon = 0$ as an equation for the spin boost in terms of other scalar invariants. A method in which the scalar Ψ_4 is determined uniquely by other scalar invariants would be ideal, since the gravitational wave amplitude would be calculable using only local, coordinate independent information. Presently, no such expression exists.

3.6 The Bowen York spinning black hole: an example

We provide now, as an example, the two tetrad choices for Bowen-York spinning black hole initial data [21]. The initial data represent a black hole at the origin with angular momentum L. In spherical polar coordinates ($f_{ab} = \mathrm{diag}\{1, r^2, r^2\sin^2\theta\}$), the solution of the momentum constraint (2.46) is

$$\bar{A}_{r\phi} = 3Lr^{-2}\sin^2\theta, \tag{3.57}$$

with all other components equal to 0. The Hamiltonian constraint then takes the form

$$f^{ab}\partial_a\partial_b\psi = -\frac{9}{4}\psi^{-7}r^{-6}\sin^2\theta \tag{3.58}$$

The equation is quasi-linear, and would normally require a numerical method for a solution. For a black hole of mass M, an approximate solution can be constructed for small L/M^2. Then, expanding ψ to fourth order in powers of L/M^2,

$$\begin{aligned}\psi &= 1+\frac{M}{2r}+\frac{L^2}{M^4}\left(F_{20}P_0(\cos\theta)+F_{22}P_2(\cos\theta)\right) \\ &\quad +\frac{L^4}{M^8}\left(F_{40}P_0(\cos\theta)+F_{42}P_2(\cos\theta)+F_{44}P_4(\cos\theta)\right)\end{aligned} \tag{3.59}$$

where P_n is the Legendre polynomial of order n. The Hamiltonian constraint can then be written as a set of linear, separable differential equations for F_{ab}, which depend solely on r. Then, the solution is

$$F_{20} = -\frac{M^4}{5r(M+2r)^5}\left(20r^2+8Mr+M^2\right), \tag{3.60}$$

$$F_{22} = -\frac{M^3}{10r^3}, \tag{3.61}$$

$$\begin{aligned}F_{40} &= \frac{M^7}{825r(M+2r)^{11}}\left(-65M^5-1158M^4r-8476M^3r^2\right. \\ &\quad \left.-28040M^2r^3-3420Mr^4+8448r^5\right)\end{aligned} \tag{3.62}$$

$$\begin{aligned}F_{42} &= \frac{2M^7}{825r^3(M+2r)^{11}}\left(M^7+22M^6r+220M^5r^2+1320M^4r^3\right. \\ &\quad \left.+5280M^3r^4+12112M^2r^5+7744Mr^6-17600r^7\right),\end{aligned} \tag{3.63}$$

and

$$F_{44} = -\frac{256M^5r^4}{275(M+2r)^{11}}\left(M^2+22Mr+4r^2\right). \tag{3.64}$$

This result extends the derivation of [25]. In particular, the values of F_{40}, F_{42} and F_{44} are necessary since otherwise $\mathfrak{m}^\alpha$ cannot be computed to lowest order in L. For simplicity, we choose the geodesic gauge for the computations in the following two sections,

$$\alpha = 1, \tag{3.65}$$

$$\beta^a = 0. \tag{3.66}$$

3.6.1 The fiducial tetrad

Using the above initial data and equations (3.39), it is straightforward to compute the value of the tetrad.

$$\mathfrak{l}^\alpha = \frac{1}{\sqrt{2}}(1,\psi^{-2},0,0) \tag{3.67}$$

$$\mathfrak{n}^\alpha = \frac{1}{\sqrt{2}}(1,-\psi^{-2},0,0) \tag{3.68}$$

$$\mathfrak{m}^\alpha = \frac{1}{\psi^2\sqrt{2}}(0,0,\frac{1}{r},\frac{i}{r\sin\theta}) \tag{3.69}$$

3.6.2 The qK tetrad

Using the above initial data, and following the prescribed method for finding the quasi-Kinnersly frame to order L^2 (see Appendix B),

$$\sqrt{1-\hat{\lambda}^a\hat{\nu}_a} = \frac{1}{\sqrt{2}} + \frac{4\sqrt{2}(M-2r)^2r^2\sin^2\theta}{M^2(M+2r)^6}L^2, \tag{3.70}$$

$$\frac{\sqrt{1+\hat{\lambda}^b\hat{\mathrm{v}}_b}}{\sqrt{1-\hat{\lambda}^c\hat{\mathrm{v}}_c}} = -4\frac{(M-2r)r\sin\theta}{M(M+2r)^3}L. \tag{3.71}$$

Finally, the resulting tetrad, to order L^2, is

$$\mathfrak{l}^0 = \frac{1}{\sqrt{2}} + \frac{4\sqrt{2}(M-2r)^2r^2\sin^2\theta}{M^2(M+2r)^6}L^2 \tag{3.72}$$

$$\mathfrak{l}^1 = -\frac{2\sqrt{2}r^2}{(M+2r)^2} - 8\sqrt{2}r^2\frac{M^3+8M^2r+20Mr^2+4r^3+12r^3\cos(2\theta)}{5M(M+2r)^8}L^2 \tag{3.73}$$

$$\mathfrak{l}^2 = \frac{176\sqrt{2}(M-2r)r^3\sin(2\theta)}{5M^2(M+2r)^7}L^2 \tag{3.74}$$

$$\mathfrak{l}^3 = -\frac{8\sqrt{2}(M-2r)r^2}{M(M+2r)^5}L \tag{3.75}$$

for $\mathfrak{l}^\alpha$,

$$\mathfrak{n}^0 = \frac{1}{\sqrt{2}} + \frac{4\sqrt{2}(M-2r)^2r^2\sin^2\theta}{M^2(M+2r)^6}L^2 \tag{3.76}$$

$$\mathfrak{n}^1 = 2\sqrt{2}\frac{r^2}{(M+2r)^2} + \frac{8\sqrt{2}r^2(M^3+8M^2r+20Mr^2+4r^3+12r^3\cos(2\theta))}{5M(M+2r)^8}L^2 \tag{3.77}$$

$$\mathfrak{n}^2 = -\frac{176\sqrt{2}(M-2r)r^3\sin(2\theta)}{5M^2(M+2r)^7}L^2 \tag{3.78}$$

$$\mathfrak{n}^3 = -\frac{8(M-2r)r^2}{M(M+2r)^5}L \tag{3.79}$$

for $\mathfrak{n}^\alpha$, and

$$\mathfrak{m}^0 = -2\sqrt{2}\frac{(M-2r)r\sin\theta}{M(M+2r)^3}L. \tag{3.80}$$

$$\mathfrak{m}^1 = \frac{176\sqrt{2}i(M-2r)r^4\sin(2\theta)}{5M^2(M+2r)^7}L^2 \tag{3.81}$$

$$\begin{aligned}\mathfrak{m}^2 &= 2\sqrt{2}ir(M+2r)^{-2} \\ &\quad + \frac{8\sqrt{2}ir(M^3+8M^2r+20Mr^2+4r^3+12r^3\cos(2\theta))}{5M(M+2r)^8}L^2\end{aligned} \tag{3.82}$$

$$\begin{aligned}\mathfrak{m}^3 &= 2\sqrt{2}r\csc\theta(M+2r)^{-2} \\ &\quad + \frac{8\sqrt{2}r\csc\theta}{5M^2(M+2r)^8}(M^4+8M^3r+25M^2r^2-16Mr^3+20r^4 \\ &\quad -r^2(5M^2-32Mr+20r^2)\cos(2\theta))L^2\end{aligned} \tag{3.83}$$

for $\mathfrak{m}^\alpha$. While this tetrad is clearly different from the fiducial tetrad choice (3.39), there are two remaining degrees of freedom corresponding to a type III tetrad rotation that can be applied to the vectors above. The degrees of freedom can not be used to make the two tetrads equal to order L^2, however. Hence, by actually computing the qK frame , we can check that the fiducial tetrad is not in the qK frame. The NP scalars Ψ_0 and Ψ_4 will both be of order L^2 in the quasi-Kinnersley frame, and so the result of computing them using the fiducial tetrad will differ from the result of computing them using a tetrad in the qK frame.

This result illustrates the motivation for searching for a tetrad independent expression for gravitational wave amplitudes. While Ψ_0 and Ψ_4 can be related to gravitational wave amplitudes, this can only be done when the tetrad is specially chosen to reflect the symmetries of the background spacetime. Since numerical simulations do not separate the background metric from the perturbation, it is not feasible to construct a tetrad in this way. Instead, a fiducial tetrad

is used, and the extracted radiation is checked for expected behavior at large distances from the final black hole. A scalar, tetrad independent expression would require no such checks.

Unfortunately, such an expression for gravitational wave amplitude has proven very difficult to find. The transverse frame is a fruitful starting point for such a search. This is because the transverse frame requires no split of the metric into background and perturbation to find. Instead Ψ_1 and Ψ_3 are set to zero, which results in an algebraic expression which uniquely determines the tetrad up to a spin-boost transformation. However, from a numerical point of view, no method for fixing the spin-boost parameter that is also preferable to using the fiducial tetrad has yet been found. This is because the fiducial tetrad has been successful historically at producing convergent waves for a variety of simulations [30]. In addition, the transverse qK tetrad appears to require the solution of a non algebraic constraint ($\varepsilon = 0$). The search for an algebraic condition which fixes the spin-boost freedom is the subject of ongoing research [47].

Chapter 4

The Beetle-Burko scalar

4.1 The definition

Computing the NP scalar Ψ_4 is currently one of the most popular methods for determining the gravitational wave content of numerically simulated spacetimes. However, the scalar relies on the choice of tetrad used to compute it (3.17). The relation of the scalar to the gravitational radiation (3.34) requires that the tetrad be sufficiently close to the Kinnersley tetrad of the background spacetime. However, solving the Kinnersley tetrad conditions (3.33) represents a significant hurdle. In particular, the spacetime must be separated into background and perturbation, then differential equations for the tetrad vector components must be integrated. In numerical simulations, a fiducial tetrad such as (3.39) is used instead. The tetrad is assumed to be sufficiently close to the Kinnersley tetrad to allow the desired interpretation of Ψ_4.

To avoid the assumptions made when using the fiducial tetrad, a tetrad independent scalar quantity from which we can compute the metric perturbation is required. Much current research [16, 44, 46, 26, 45, 24, 47] has focused on the value of the NP scalars in the transverse qK frame (Section 3.5) due to the fact that the tetrad conditions are algebraic and the tetrad is closely related to the Kinnersley tetrad. The qK frame does not uniquely fix the value of Ψ_4. Instead, tetrads in the frame are related by a spin-boost rotation (A.6). While the search for an algebraic method for fixing the spin boost freedom is ongoing, an interesting alternative is to construct a scalar that is related to Ψ_4, and that is invariant under the spin boost rotation. One such scalar

has been proposed by Beetle and Burko [17]. The BB scalar (ξ) has the value of $\Psi_0\Psi_4$ in the qK frame. Though Ψ_0 and Ψ_4 do not have a unique value in the frame, their product does. The uniqueness of ξ is further illustrated by the fact that it can be defined entirely in terms of other scalar invariants.

$$I \equiv \frac{1}{16}\left(C_{\alpha\beta}{}^{\gamma\delta}C_{\gamma\delta}{}^{\alpha\beta} - iC_{\alpha\beta}{}^{\gamma\delta}\,{}^{*}C_{\gamma\delta}{}^{\alpha\beta}\right) \tag{4.1}$$

$$J \equiv \frac{1}{96}\left(C_{\alpha\beta}{}^{\gamma\delta}C_{\gamma\delta}{}^{\mu\nu}C_{\mu\nu}{}^{\alpha\beta} - iC_{\alpha\beta}{}^{\gamma\delta}C_{\gamma\delta}{}^{\mu\nu}\,{}^{*}C_{\mu\nu}{}^{\alpha\beta}\right), \tag{4.2}$$

where ${}^{*}C_{\alpha\beta}{}^{\gamma\delta} = \frac{1}{2}\varepsilon_{\alpha\beta}{}^{\mu\nu}C_{\mu\nu}{}^{\gamma\delta}$. Then, using (3.42) to construct S,

$$W \equiv 2S - 1 + 2\sqrt{S^2 - S} \tag{4.3}$$

$$\xi = \frac{I}{4}\left(2 - W^{\frac{1}{3}} - W^{-\frac{1}{3}}\right). \tag{4.4}$$

From the definition of the BB scalar, we can see that its value will be non-zero in physically interesting spacetimes which contain gravitational radiation. However, because it is a product of Ψ_0 and Ψ_4, there is no generic way to extract metric perturbations from it. Also, though the value of the BB scalar is associated with the values of the NP scalars in the qK frame, it is not necessary to compute the BB scalar in order to identify the qK frame [16]. The scalar does give us a check of whether the tetrad used to calculate the NP scalars is in the qK frame, since then $\xi - \Psi_0\Psi_4$ will vanish. In addition, we can use the BB scalar to check that we are close to the qK frame in the sense that the ratio $|\xi - \Psi_0\Psi_4| \ll 1$. Such information is useful because then, the tetrad differs by an infinitesimal rotation from one in the qK frame. Because as $S \to 1$ the tetrads in the qK frame are related to the Kinnersley tetrad by two infinitesimal null

rotations and one non-infinitesimal spin boost transformation, we can check if the tetrad we use to calculate the NP scalars differs at most by these transformations from the Kinnersley tetrad.

Put more quantitatively, if $S \to 1$, then we expect the spacetime to separate into background and perturbation. There will be a Kinnersley tetrad associated with the background for which equations (3.33) hold. Additionally, as long as the radiation is purely ingoing or purely outgoing, the Peeling theorem (section 3.3.2) will hold. Assume the radiation is purely outgoing, which will be the case for regions far from the origin whenever the sources are localized near the origin. The null rotations which take a Kinnersley tetrad to a qK tetrad are given by a type I rotation with $\bar{d} = -\frac{\Psi_3^B}{3\Psi_2^A}$ and a type II rotation with $\bar{e} = -\frac{\Psi_1^B}{3\Psi_2^A}$ (see equations A.1 and A.3). Then,

$$\xi - \Psi_0^B \Psi_4^B = 4\bar{d}\Psi_0^B \Psi_3^B + 4\bar{e}\Psi_1^B \Psi_4^B \tag{4.5}$$

to lowest order in the perturbation. Computing the values of all NP scalars in order to find $\bar{d}$ and $\bar{e}$ constitutes more work than most numerical relativists are going to go through in order to check their tetrad. Instead, notice that each term in equation (4.5) is $O(r^{-6})$. In addition, it is required that the perturbation of the Kerr background be small, and so $\Psi_3^B r^{-1} \ll \Psi_2^A$ and $\Psi_1^B r \ll \Psi_2^A$. Then, if the tetrad we are using satisfies the Kinnersley conditions, we expect

$$|\xi - \Psi_0^B \Psi_4^B| r^6 \ll 1. \tag{4.6}$$

If we replace Ψ_0^B and Ψ_4^B with Ψ_0 and Ψ_4 computed using the fiducial tetrad, the condition must still hold. Otherwise, the fiducial tetrad is not sufficiently close to the Kinnersley tetrad.

However, if the condition is satisfied, it is still not necessarily the case that the fiducial tetrad is the Kinnersley tetrad.

4.2 An analytic example: the Bowen York boosted black hole

It is clear, analytically, that the fiducial tetrad (3.39) is not in the qK frame for Bowen-York initial data for spinning black holes. This is additionally true for boosted black hole initial data. As we derive in appendix C, for a Bowen York black hole of ADM mass M at the origin with ADM linear momentum $P^a = P(\partial_z)^a$,

$$\begin{aligned}\Psi_0(P) &= -\frac{12\sin^2\theta}{5(M+2r)^{12}}\Big(2r(21M^7+273M^6r+1498M^5r^2+4466M^4r^3 \\ &\quad +7712M^3r^4+7504M^2r^5+3552Mr^6+1440r^7) \\ &\quad +21M(M+2r)^7\ln\left(\frac{M}{M+2r}\right)\Big)P^2 \\ &= \Psi_4(P),\end{aligned} \tag{4.7}$$

to order P^2 for the fiducial tetrad choice, while

$$\begin{aligned}\xi(P) &= \frac{144\sin^4\theta}{25M^2(M+2r)^{24}}\Big(2r(21M^8+273M^7r+1498M^6r^2+4466M^5r^3 \\ &\quad +7712M^4r^4+7504M^3r^5+3552M^2r^6+1440Mr^7-1280r^8) \\ &\quad +21M^2(M+2r)^7\ln\left(\frac{M}{M+2r}\right)\Big)^2P^4.\end{aligned} \tag{4.8}$$

Hence, the first tetrad is not in the qK frame. In fact, for very large r, $\Psi_0(P)\Psi_4(P) = O(r^{-8})$ for the fiducial tetrad, while $\Psi_0\Psi_4 = O(r^{-6})$ for a tetrad in the qK frame. All this information could be obtained without actually computing the qK frame.

In a numerical simulation, it is still possible that the gauge choices made by evolution schemes will cause the fiducial tetrad to belong to the qK frame. In fact, this appears to be the case, since gravitational radiation computed with the fiducial tetrad has always satisfied the properties expected of gravitational radiation. In particular, some of the quantities computed with Ψ_4 are the radiated energy, momentum, and angular momentum. Other quantities such as the initial and final ADM energy, momentum, and angular momentum are computed using the spatial metric and its derivatives. These two groups of quantities can be compared to each other as a check of Ψ_4. Results of such comparisons seem to give very good agreement. Waveforms calculated using different evolution schemes and extraction methods have been compared to each other by Hannam *et al.* [37], and different methods are found to produce waves with amplitude and phase that agree to within their estimated uncertainty.

The BB scalar provides an additional tool for checking that the tetrad belongs to the qK frame. The benefit that the BB scalar possesses over other checks is that the BB scalar computation is completely gauge invariant. For instance, no assumptions are made about the tetrad or the coordinates when computing the scalar. The BB scalar also provides information about the accuracy of tetrad vectors $\mathfrak{l}^\alpha$ and $\mathfrak{n}^\alpha$, as shown below.

If the tetrad fails to belong to a qK frame, it must also fail to be related to the Kinnersley frame by an infinitesimal null-rotation and a spin-boost transformation. Hence, if the difference $|\xi - \Psi_0\Psi_4|$ is large and $S \to 1$, we can conclude that the tetrad we are using fails for the purpose of extracting gravitational radiation. A reason for the failure could be that the tetrad differs from the Kinnersley tetrad by a null rotation that is both not a spin boost and not infinitesimal. This assumes the existence of a Kinnersley tetrad for the spacetime. The existence of a Kinnersley tetrad cannot be proven with the BB scalar (for examples, see [25]), but is expected for binary

black hole spacetimes at large r. If the difference of ξ and $\Psi_0\Psi_4$ is small, it is still not guaranteed that the NP scalars represent ingoing and outgoing radiation. A small difference only guarantees that the tetrad used is in the transverse qK frame.

4.3 Numerical implementation

The method we use for computing the BB scalar using numerical data (γ_{ab} and K_{ab} at an instant in time) is as follows: First, compute the NP scalars using the fiducial tetrad (3.39). The PSU group's method follows [11] and uses a thorn written by Tanja Bode and Ian Hinder [18]. Second, we calculate the scalars I and J using (3.40) and (3.41). While expressed in terms of NP scalars which depend on the tetrad, I and J are independent of the choice of tetrad, as is clear from their alternate expressions (4.1) and (4.2). Third, use equations (3.42), (4.3), and (4.4) to compute W and ξ. To do this numerically, it is necessary to split all quantities into real and imaginary parts. Also, since the square and cube root are multivalued, it is necessary to choose how to divide up their ranges into single valued functions on Riemann sheets joined along branch cuts.

When coding the computation of ξ, we chose the branch cuts for both the square root function and the cube root function to be along the positive real axis. We divide S into real and imaginary parts,

$$S_r \equiv Re[S] \tag{4.9}$$

$$S_i \equiv Im[S]. \tag{4.10}$$

The formula for W, then, is

$$\begin{aligned} W &= \Big(2S_r - 1 + \big(2\big[(S_r^2 - S_r - S_i^2)^2 + (2S_rS_i - S_i)^2\big]^{\frac{1}{2}} + 2(S_r^2 - S_r \\ &\quad -S_i^2)\big)^{\frac{1}{2}}\ \mathrm{sign}(2S_rS_i - S_i)\Big) + i\Big(2S_i + \big(2\big[(S_r^2 - S_r - S_i^2)^2 \\ &\quad +(2S_rS_i - S_i)^2\big]^{\frac{1}{2}} - 2(S_r^2 - S_r - S_i^2)\big)^{\frac{1}{2}}\Big), \end{aligned} \tag{4.11}$$

where $\mathrm{sign}(x)$ is similar to the *signum* function.

$$\mathrm{sign}(x) \equiv \begin{cases} -1 & : x < 0 \\ 1 & : x \geq 0 \end{cases} \tag{4.12}$$

As a result of this choice, there are two branch cuts for both W and ξ. The first is along the ray $S_i = 0$ and $S_r < 0$, and the second is along the ray $S_i = 0$, $S_r > 1$.

In the vicinity of the first branch cut ($S_i = 0$, $S_r < 0$), let $S = S_r + i\varepsilon$, where S_r and ε are both real. Then, to first order in ε,

$$W \approx 2S_r - 1 - 2\,\mathrm{sign}(\varepsilon)(S_r^2 - S_r)^{\frac{1}{2}} + 2i\Big(\varepsilon + |\varepsilon|\Big(S_r^2 - S_r\Big)^{-\frac{1}{2}}\Big(S_r^2 - S_r + \frac{1}{4}\Big)^{\frac{1}{2}}\Big). \tag{4.13}$$

The computation of ξ requires three Riemann sheets, which we label sheet (I), sheet (II) and sheet (III). The sheets are distinguished by the value of the cube root on each. To compute the cube root, we define θ_W as the angle of W on the complex plane, measured counter-clockwise

from the positive real axis. Then, the values of ξ on each sheet are

$$\xi_I = \frac{I}{4}\Big(2-|W|^{\frac{1}{3}}\exp(\frac{1}{3}i\theta_W)-|W|^{-\frac{1}{3}}\exp(-\frac{1}{3}i\theta_W)\Big), \tag{4.14}$$

$$\xi_{II} = \frac{I}{4}\Big(2-|W|^{\frac{1}{3}}\exp(\frac{1}{3}i(\theta_W+2\pi))-|W|^{-\frac{1}{3}}\exp(-\frac{1}{3}i(\theta_W+2\pi))\Big), \tag{4.15}$$

$$\xi_{III} = \frac{I}{4}\Big(2-|W|^{\frac{1}{3}}\exp(\frac{1}{3}i(\theta_W+4\pi))-|W|^{-\frac{1}{3}}\exp(-\frac{1}{3}i(\theta_W+4\pi))\Big). \tag{4.16}$$

For simplicity, we make the definition

$$W_1 \equiv 2S_r - 1 + 2\sqrt{S_r^2 - S_r}. \tag{4.17}$$

Along the first branch cut ($S_i = 0$, $S_r < 0$), $\theta_W \approx \pi$ regardless of ε, so

$$\xi_I \approx \frac{I}{4}\Big(2-\frac{1}{2}\Big[|W_1|^{\frac{1}{3}}+|W_1|^{-\frac{1}{3}}\Big]+i\frac{\sqrt{3}}{2}\,\mathrm{sign}(\varepsilon)*\Big[|W_1|^{\frac{1}{3}} -|W_1|^{-\frac{1}{3}}\Big]\Big) \tag{4.18}$$

$$\xi_{II} \approx \frac{I}{4}\Big(2+|W_1|^{\frac{1}{3}}+|W_1|^{-\frac{1}{3}}\Big) \tag{4.19}$$

$$\xi_{III} \approx \frac{I}{4}\Big(2-\frac{1}{2}\Big[|W_1|^{\frac{1}{3}}+|W_1|^{-\frac{1}{3}}\Big]-i\frac{\sqrt{3}}{2}\,\mathrm{sign}(\varepsilon)*\Big[|W_1|^{\frac{1}{3}} -|W_1|^{-\frac{1}{3}}\Big]\Big). \tag{4.20}$$

The same check in the vicinity of the branch cut along $S_i = 0$, $S_r > 1$ gives

$$W \approx 2S_r - 1 + 2\,\mathrm{sign}(\varepsilon)(S_r^2 - S_r)^{\frac{1}{2}} + 2i\Big(\varepsilon + |\varepsilon|\Big(S_r^2 - S_r\Big)^{-\frac{1}{2}}\Big(S_r^2 - S_r + \frac{1}{4}\Big)^{\frac{1}{2}}\Big). \tag{4.21}$$

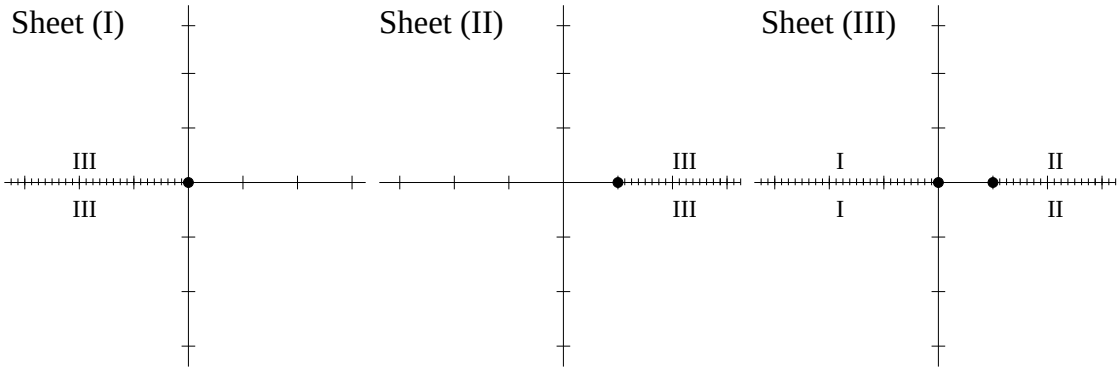

Fig. 4.1. The three values of ξ are associated with three Riemann sheets, connected along branch cuts as illustrated.

Then, $\theta_W = 0$ regardless of ε, so

$$\xi_I \approx \frac{I}{4}\left(2-(W_1)^{\frac{1}{3}}-(W_1)^{-\frac{1}{3}}\right) \tag{4.22}$$

$$\xi_{II} \approx \frac{I}{4}\left(2+\frac{1}{2}\left[(W_1)^{\frac{1}{3}}+(W_1)^{-\frac{1}{3}}\right]-i\frac{\sqrt{3}}{2}\,\mathrm{sign}(\varepsilon)*\left[(W_1)^{\frac{1}{3}}-(W_1)^{-\frac{1}{3}}\right]\right) \tag{4.23}$$

$$\xi_{III} \approx \frac{I}{4}\left(2+\frac{1}{2}\left[(W_1)^{\frac{1}{3}}+(W_1)^{-\frac{1}{3}}\right]+i\frac{\sqrt{3}}{2}\,\mathrm{sign}(\varepsilon)*\left[(W_1)^{\frac{1}{3}}-(W_1)^{-\frac{1}{3}}\right]\right) \tag{4.24}$$

From these equations, it is clear how to connect the Riemann sheets using the branch cuts, as illustrated in Fig. 4.1. For example, sheet (I) is connected to sheet (III) along the ray $S_i = 0$, $S_r < 0$.

To calculate ξ at an instant in time in a simulation, start at the outer boundary of a space-time and use equation (4.14). Traverse the grid along a line of adjacent grid points, continuing to use (4.14) until the value of S crosses the branch cut $S_i = 0$ and $S_r < 0$. From that point onward,

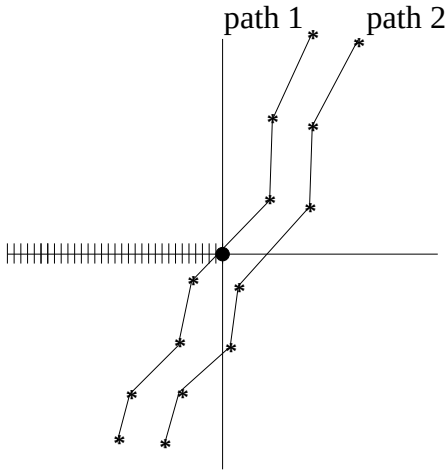

Fig. 4.2. The value of S along two adjacent paths through the grid points is plotted. If the value of S starts in the first quadrant of sheet (I), path 1 will end in the third quadrant of sheet (III) while path 2 will end in the third quadrant of sheet (I).

use (4.16) until S crosses another branch cut. Keep track of which sheet S is on and use the appropriate equation (4.14 - 4.16) to compute ξ.

There is still ambiguity over which equation to use when the line connecting two adjacent values of S passes very close to the either point $S = 0$ or $S = 1$. In such a situation, if the branch cut is crossed (or not crossed) in error, it is possible that the values of ξ on two adjacent grid points will be calculated using two different equations from (4.14 - 4.16), even though the line connecting the values of S on the two grid points does not cross a branch cut (see Fig. 4.2). This means that the resulting ξ will be discontinuous. In the figure, we expect that in the continuum limit path 1 does not cross the branch cut. However, we would not know this in a simulation, and can only guess by looking at points in the neighborhood of these ambiguities if a path such as path 1 crosses the branch cut.

Another simpler approach to calculating ξ is to use (4.14) for all grid points. Then, there is no longer the guarantee that ξ is continuous, or that it equals $\Psi_0\Psi_4$ in the qK frame. However, since we only care about the value of ξ in regions of the space time where we expect to be able to extract gravitational radiation, this approach is fine so long as S only crosses the branch cuts outside of these regions. In the following simulations, we always use (4.14) to compute ξ.

4.4 Numerical computation of ξ on initial data slices

In this section we describe simulations we performed which only produced initial data and the corresponding values for the NP scalars and the BB scalar. The goal of the simulations was to check that the method used for computing ξ gave values in agreement with [25] for spinning black hole initial data and with (4.8) for boosted black hole initial data. Both simulations were performed using approximate solutions of the Bowen-York method for computing initial data. Once the initial data were calculated, the NP scalars were calculated using the fiducial tetrad. Then, ξ was calculated using the method outlined in Section 4.3. The results indicate that the code which computes the BB scalar functions correctly. In addition, the results illustrate a need for very high resolution when calculating the BB scalar. Finally, the fact that the fiducial tetrad does not belong to the transverse qK frame is illustrated by comparing $\Psi_0\Psi_4$ to ξ for the initial data. All simulations were performed on desktops belonging to the Penn State Gravity department.

4.4.1 Spinning black hole initial data

The approximate initial data for a black hole with ADM mass M and angular momentum L are given by (3.57, 3.59) along with definitions for conformally related quantities (Section

2.5). For these data, the conformal factor ψ is approximated as a power series in L, and the assumption that $L/M^2 \ll 1$ was made when solving the Hamiltonian constraint. Analytically, to lowest order in L/M^2, the value of the NP scalars Ψ_0 and Ψ_4 are given in [26] and the value of the BB scalar is given in [25].

$$\Psi_0(L) = \Psi_4(L) = \frac{1536L^2r^5}{5M(M+2r)^{12}}(4r^2+64rM+M^2)\sin^2\theta \tag{4.25}$$

$$\xi(L) = \frac{3^2 2^{22} L^4 r^{10}}{25M^2(M+2r)^{24}}(4r^2-21rM+M^2)^2\sin^4\theta \tag{4.26}$$

For the initial data runs, we used a grid of side length 48 with grid spacing of 1.6. The ADM mass of the spacetime is fixed to $M = 1$ In Figure 4.3, we plot the numerically computed BB scalar along with the predicted value to lowest order in L/M^2 for $L = 0.05M^2$. Because the axes are log scaled, only rough agreement can be deduced from the plot. Any agreement is only for large r, since close to the black hole, the numerically computed ξ_I grows to approximately 20 orders of magnitude greater than the analytically computed value. More important is the value of the difference $|\xi(L) - \xi_I|$. For the same initial data, Figure 4.4 is a plot of the difference of the numerically computed and the analytically approximated values of ξ as a function of r. The approximated value $\xi(L)$ is included as a reference. We can see that the difference has a greater asymptotic fall off rate than the scalar itself. As a result, the difference is smaller than two orders of magnitude smaller than the BB scalar itself for $r > 20M$.

More generally, the error in the numerically computed value of ξ will depend on the grid spacing Δx and the angular momentum L. In Figure 4.5, we plot the scaled differences $|\xi_I - \xi(L)|/(\Delta x)^4/L^4$ for several values of L and Δx. It is then clear that the difference scales as

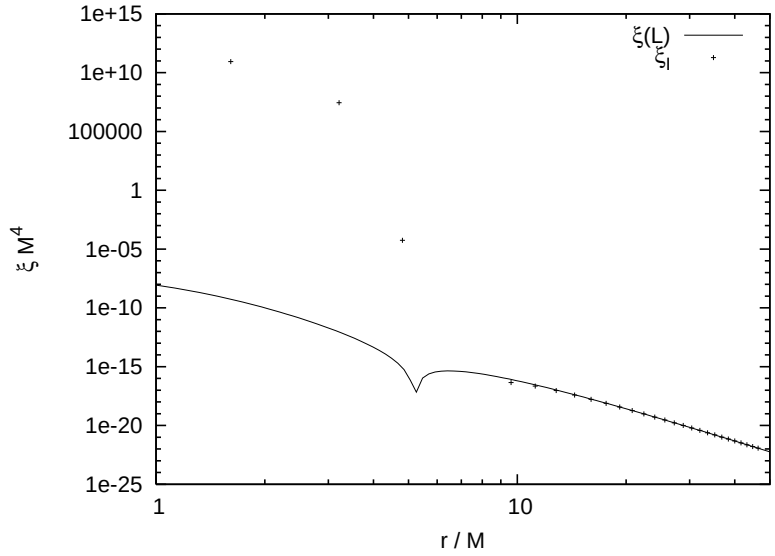

Fig. 4.3. Numerically computed and analytically approximated values of ξM^4 for Bowen York spinning black hole initial data.

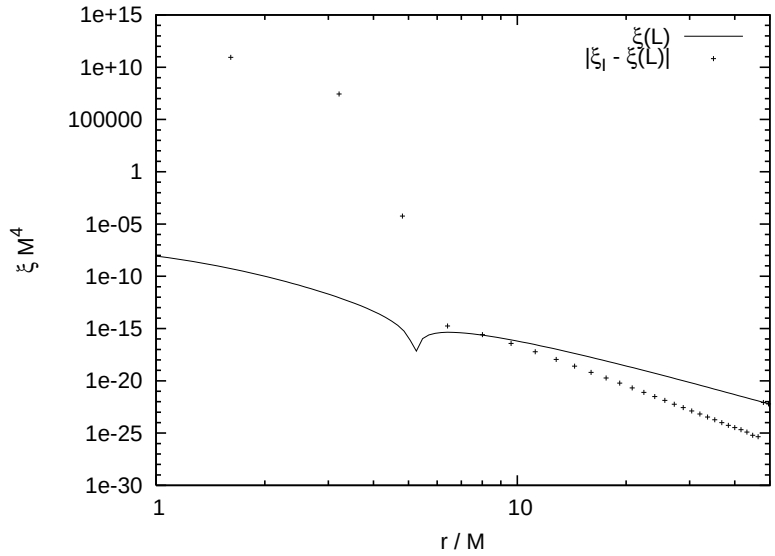

Fig. 4.4. The difference $|\xi_I - \xi(L)|M^4$ for the Bowen York spinning black hole initial data.

(Δx^4) and L^4. From the formula for $\xi(L)$, (4.26), we expect the difference to be of higher order in L. However, the error represented by $|\xi_I - \xi(L)|$ is likely a result of the truncation of the finite difference series used to calculate the partial derivative. The derivative is used to compute the Riemann curvature tensor, used when computing the NP scalars and the BB scalar. Hence, the grid spacing plays a significant role in the accuracy of the numerical BB scalar calculation.

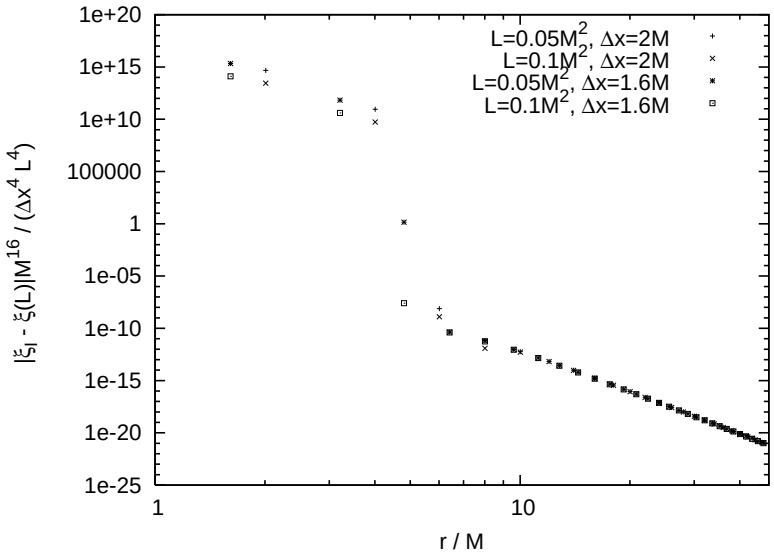

Fig. 4.5. The scaled difference $|\xi_I - \xi(L)|M^{16}/(\Delta x)^4/L^4$ for various values of L and Δx

Finally, the values of ξ_I and $\Psi_0\Psi_4$ are plotted in Figure 4.6. Analytically, we expect $\Psi_0\Psi_4 = \frac{1}{16}\xi$ for very large r. This is, of course, what is seen in the simulation. Thus, $\Psi_0\Psi_4$ is not equal to ξ in any limit. From this, we can conclude that the tetrad used to compute the NP scalars is not a qK tetrad in the limit of large r. Then, the tetrad differs from the Kinnersley tetrad by a null rotation of type I or II (see Appendix A). Thus, the value of Ψ_4 does not correspond

to the gravitational wave amplitude via (3.34). This was determined previously by computing the qK tetrad (3.6). However, using the BB scalar to achieve the same goal is straightforward in numerical simulations.

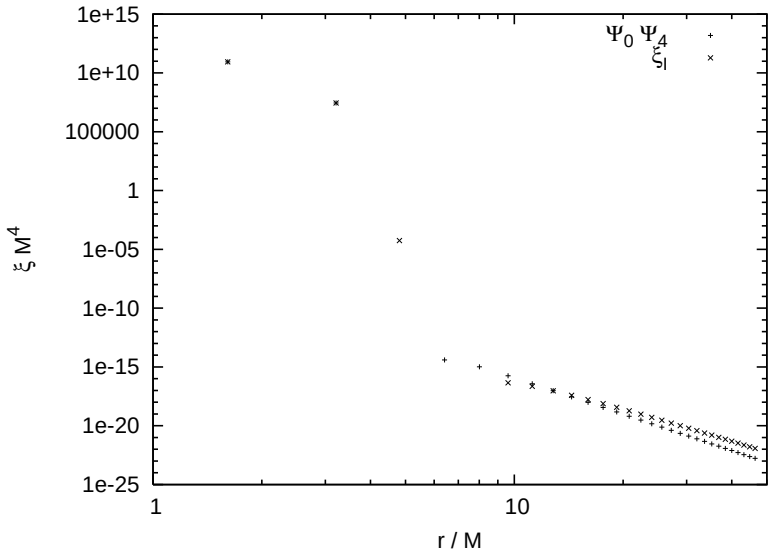

Fig. 4.6. The values of $\xi_I M^4$ and $\Psi_0 \Psi_4 M^4$ for Bowen York spinning black hole initial data.

I have also used the BB scalar to show that the fiducial tetrad fails to be a qK tetrad for the Bowen York boosted black hole initial data (section 4.2). These results do not, however, indicate that the fiducial tetrad is not suitable for computing Ψ_4 in numerical simulations. It may happen that during the course of a simulation, the gauge conditions cause the solution to take a form so that the fiducial tetrad is sufficiently close to the Kinnersley tetrad to be used to compute the gravitational radiation.

4.4.2 Boosted black hole initial data

The approximate initial data for a black hole with ADM mass M and linear momentum $P^a = P(\partial_z)^a$ is given by (C.1), (C.4) along with the definitions for conformally related quantities (Section 2.5). The conformal factor is approximated as a power series in P, and the assumption $P/M \ll 1$ is used to solve the Hamiltonian constraint. The resulting NP scalars $\Psi_0(P)$ and $\Psi_4(P)$ and BB scalar $\xi(P)$ are given by (4.7) and (4.8).

The grid setup we used is the same as for the the spinning black hole initial data. A single grid with side length of 48, (Δx) of 1.6, was used, with initial data for a boosted black hole with ADM mass M fixed to 1. For a black hole with momentum $P = 0.05M$, Figure 4.7 is a plot of the difference $|\xi_I - \xi(P)|$. The value of $\xi(P)$ is included for reference. The values agree only when r is sufficiently large. However, for large r the difference appears to have the same radial dependence as $\xi(P)$, indicating that the difference is dominated by terms higher order in P, and not dependent on the resolution. This result is more clearly illustrated in Figure 4.8, in which the scaled difference $|\xi_I - \xi(P)|/P^6$ is plotted for various resolutions and momenta. It is clear that for large r, the difference is independent of Δx and has order P^6 dependence on the momentum. Interestingly, it can be seen that closer to the origin, the difference does depend on Δx as well as r. For $4M < r < 10M$, the difference scales as $(\Delta x)^4 P^4$ (Fig. 4.9). Again, the grid spacing plays an important role in the accuracy of the BB scalar calculation, since the order P^4 error in the calculation is also order $(\Delta x)^4$.

Finally, we compare the value of ξ_I to $\Psi_0\Psi_4$ in Fig. 4.10. As expected from the results of section 4.2, ξ_I not only differs from $\Psi_0\Psi_4$, but has a different rate of decrease with increasing r. That is, for very large r, $\xi_I = O(r^{-6})$ while $\Psi_0\Psi_4 = O(r^{-8})$. As with the spinning black

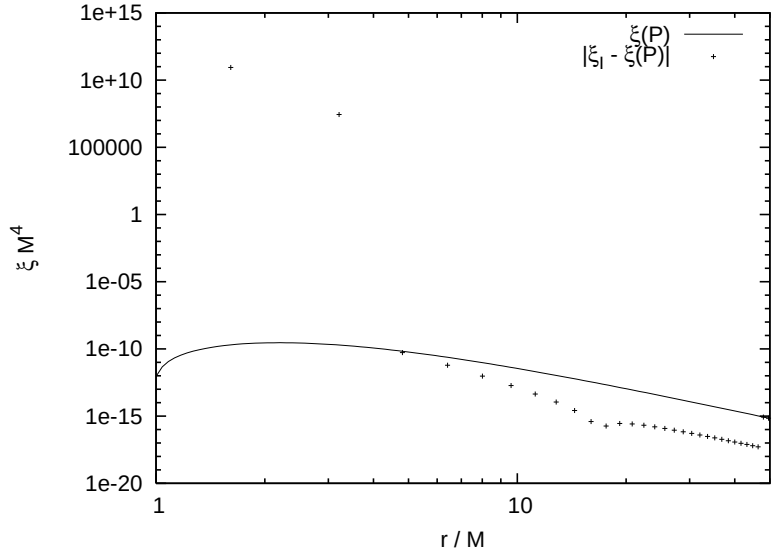

Fig. 4.7. The difference $|\xi_I - \xi(P)|M^4$ for Bowen York boosted black hole initial data.

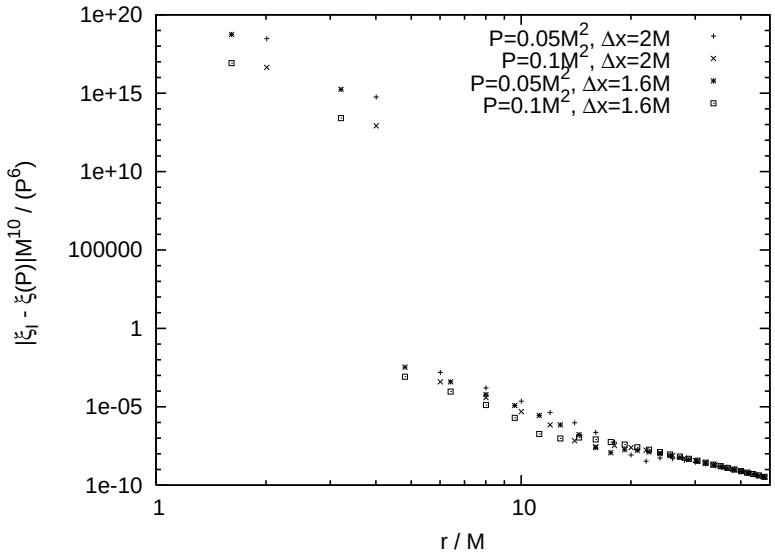

Fig. 4.8. The scaled difference $|\xi_I - \xi(P)|M^{10}/P^6$ for Bowen York boosted black hole initial data for various values of P and Δx.

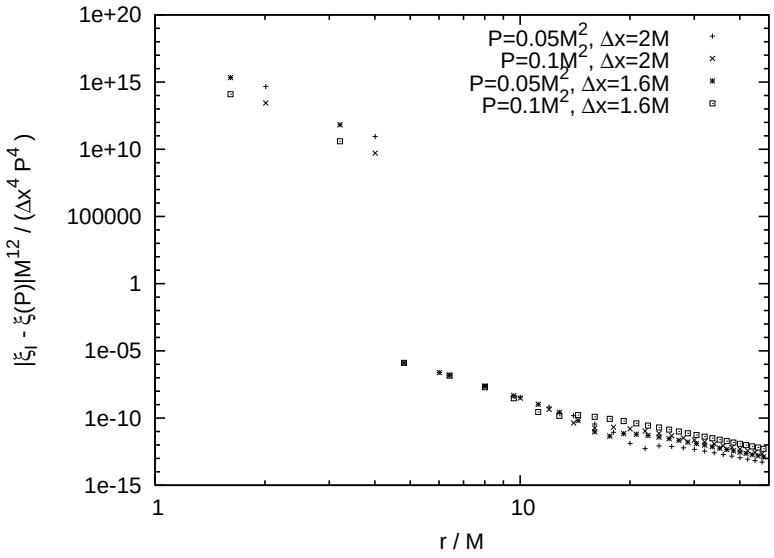

Fig. 4.9. The scaled difference $|\xi_I - \xi(P)|M^{12}/(\Delta x)^4/P^4$ for various values of (Δx) and P for Bowen York boosted black hole initial data.

hole initial data, we can conclude that the tetrad is insufficient for using Ψ_4 to compute the gravitational wave amplitude via (3.34) on the initial leaf. It is still possible that at later times the tetrad is sufficient. However, I do not test this possibility.

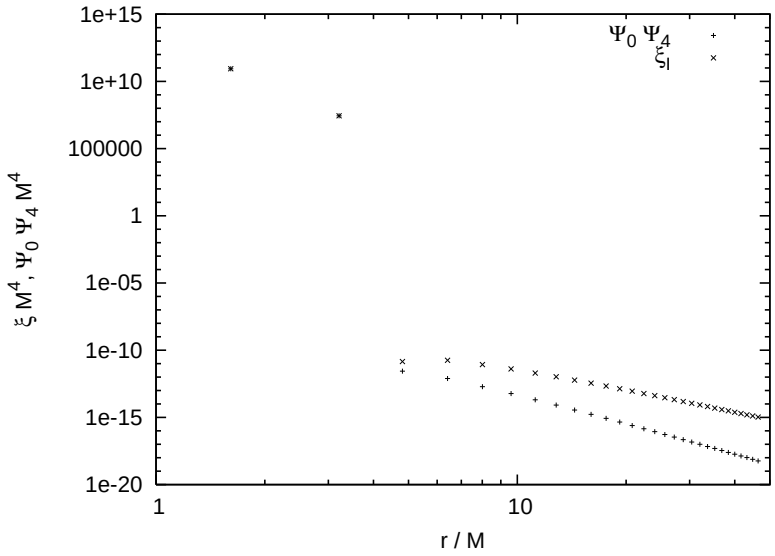

Fig. 4.10. The values of $\xi_I M^4$ and $\Psi_0\Psi_4 M^4$ for Bowen York boosted black hole initial data.

4.5 The R1 solution

In this section we give the results of computing the BB scalar in a full numerical relativity simulation. The purpose of the computation was to use the BB scalar as a check of the tetrad used to compute Ψ_4. The initial data is is the R1 initial data [12]. That is, the initial data represents Bowen York initial data for two equal mass black holes in quasi-circular orbit. In terms of the initial conformal metric in Cartesian coordinates (2.5), the locations of the black

hole singularities are at $(0, 3.257, 0)$ and $(0, -3.257, 0)$ respectively. The initial ADM mass of the spacetime is $M_i = 0.996$. The momentum of the black hole at $(0, 3.257, 0)$ is $P^a = (-1.33, 0, 0)$ while the momentum of the second black hole is $P^a = (1.33, 0, 0)$.

The properties of the R1 run are that the singularities spiral in towards the origin. A common horizon forms before two complete orbits, or approximately at coordinate time $t = 160M$. The resulting black hole is initially strongly perturbed, and sheds its perturbation by radiating gravitational waves. For large t, the black hole is a Kerr black hole with ADM mass $M_f = 0.962$ and Kerr parameter $a \approx 0.69 M_f$.

I performed the runs using a grid with opposite corners at $(-320, -320, 0)$ and $(320, 320, 320)$. Since the initial data possesses the symmetry of being invariant under reflection across the $z = 0$ plane, values of functions on gridpoints with $z < 0$ were computed via exploiting this symmetry. The grid spacing used was $\Delta x = 10$, resulting in $4(32^3)$ grid points There were 8 additional refinement levels, the coarsest 3 containing $4(32^3)$ grid points, and the finest 5 containing $4(16^3)$ grid points. The grid spacing is reduced by a factor of 2 for each refinement, resulting in a grid spacing of $\Delta x = 1/25.6$ for the finest grid.

In Figure 4.11 we plot the magnitude of the $l = 2$, $m = 2$ (spin-weight -2) mode of Ψ_4 versus t for a detector located at $r = 50$. The pulse from the Bowen- York initial data reaches the detector shortly after $t = 50$. The pulse is immediately followed by radiation from the inspiral phase of the black hole orbit. Finally, radiation from the merger reaches the detector at $t \approx 220$, followed by the quasi-normal ringdown phase. In Figure 4.12 we plot the $l = 0$, $m = 0$ mode of S versus t for a detector located at $r = 50$. If $S = 1$, $S^{0,0} = 2\sqrt{\pi} \approx 3.54$. The purpose of the plot is to illustrate that S differs from 1 by a very large amount at time $t > 30$ and $t < 510$ for this detector. Since we only require that $\xi = \Psi_0 \Psi_4$ when $S \approx 1$, ξ is not a useful check of the tetrad

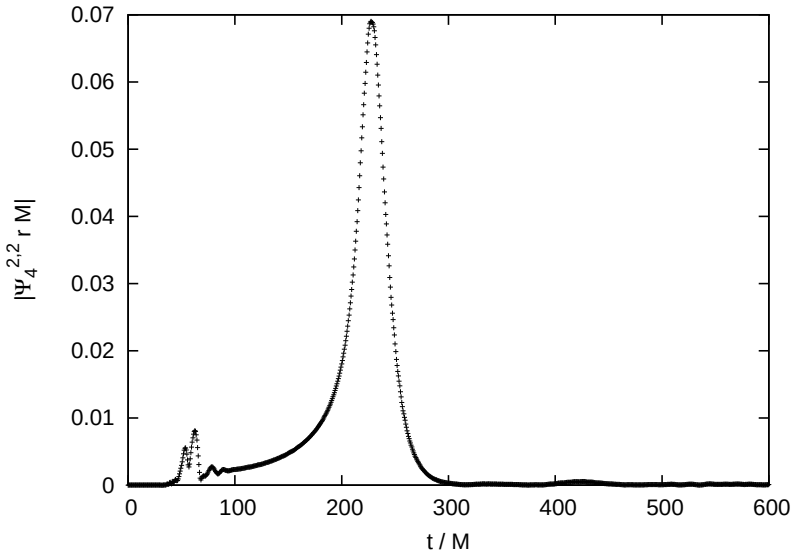

Fig. 4.11. The magnitude of the $l = 2$, $m = 2$ mode of Ψ_4 ($|\Psi_4^{2,2}|Mr$) for an R1 run, measured with a detector at $r = 50$.

in the regions in which $|S-1|$ is not very small. However, these regions correspond exactly to those regions for which there is radiation passing by the detector. This is very unfortunate from

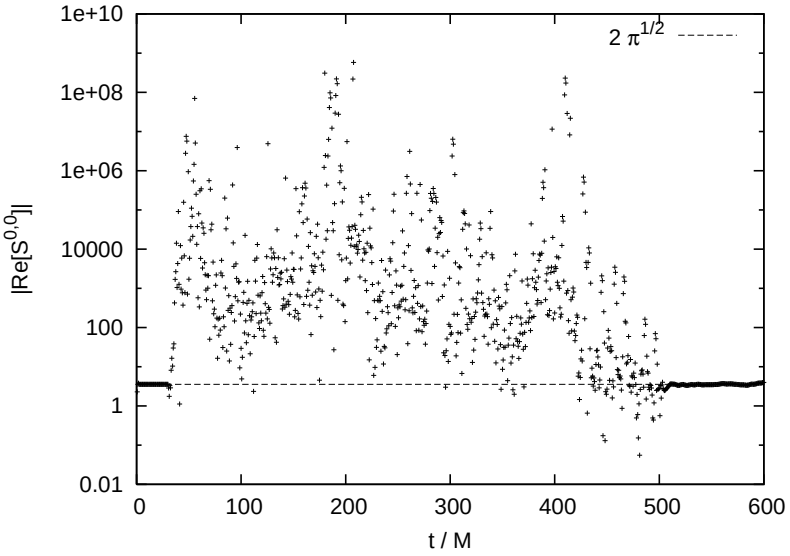

Fig. 4.12. $S^{0,0}$ versus t for an R1 run, measured by a detector at $r = 50$.

the viewpoint of desiring to use the BB scalar as a tetrad check. $S \to 1$ is expected whenever the NP scalars display peeling behavior. The peeling behavior for Ψ_4 is illustrated in Figure 4.13. We plot the quantity $Re[\Psi_4^{2,2}]r$ for detectors at $r = 50, 60, 70$, versus $t-r$. The values at each $t-r$ are nearly equal, indicating that on the null lines $u = t-r = constant$, $\Psi_4 = O(r^{-1})$, as expected. However, the Peeling theorem also predicts that for outgoing radiation, $\Psi_0 = O(r^{-5})$. This is generally not the case for this simulation, and at several points in the evolution Ψ_0 displays the peeling behavior of ingoing radiation. That is, $\Psi_0 = O(r^{-1})$ on the null lines $u' = t+r = constant$. For instance, Figure 4.14 shows $Re[\Psi_0^{2,2}]r$ for detectors at $r = 50, 60, 70$ versus $t+r$.

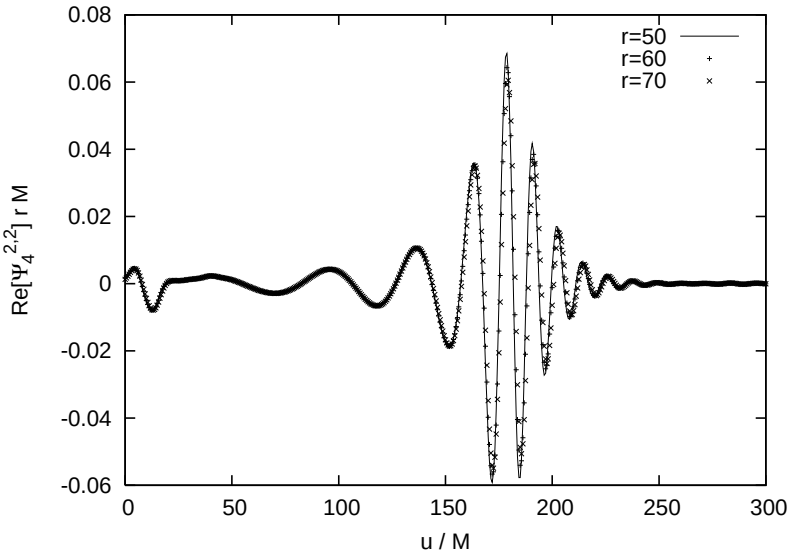

Fig. 4.13. $Re[\Psi_4^{2,2}]rM$ versus u for detectors at $r = 50, 60, 70$, for R1 binary black hole initial data.

Figure 4.11 shows the Bowen York pulse reaches the detector at $r = 50$ at $t = 50$, and drops in magnitude before $t = 100$. The grid boundary nearest the detectors and also enclosing them is a cube with opposite corners at $(-80,-80,-80)$ and $(80,80,80)$. The pulse will begin reflecting from this boundary at $t = 80$ and finish before $t = 190$. From the figure, we can see that $\Psi_0 = O(r^{-1})$ as expected for ingoing radiation for values of $u' = t + r$ between 160 and 270.

We can still use ξ to investigate the tetrad on null lines for which $S \approx 1$. For example, these correspond to the times $t < 30$ and $t > 510$ for the $r = 50$ detector. The null lines are approximated by constant u surfaces, with $u = t - r$. Figure 4.15 is a plot of the value of $|Re[S^{0,0}] - 2\sqrt{\pi}|$ on the null line $u = -30$. We can see that $|Re[S^{0,0}] - 2\sqrt{\pi}| < 0.1$ for $r \leq 80$. At $r = 90$, the value jumps 5 orders of magnitude. While we have no explanation for the sudden jump at present, it coincides closely with the failure of Ψ_0 to decrease proportionally to r^{-5} along the same line (see figure 4.16). It is possible that the large value of S is the result of spurious radiation from grid boundaries and other numerical effects, rather than physical effects such as a failure of the spacetime to be separable into a Kerr background plus perturbation. For the same null line we plot $|\xi^{2,0} - (\Psi_0\Psi_4)^{2,0}|r^6$ in figure 4.17. The value of the difference remains less than 10^{-3} in the same region where $|Re[S^{0,0}] - 2\sqrt{\pi}| < 0.1$. While the smallness of $\xi - \Psi_0\Psi_4$ does not verify that the fiducial tetrad is the correct tetrad for computing the NP scalars, it also does not indicate any problems in the tetrad. The value is only a qualitative measure of the "correctness" of the $\mathfrak{l}^\alpha$ and $\mathfrak{n}^\alpha$ vectors, since placing limits on the null rotation parameters would require additional information. However, no other gauge invariant checks of the tetrad are performed in general.

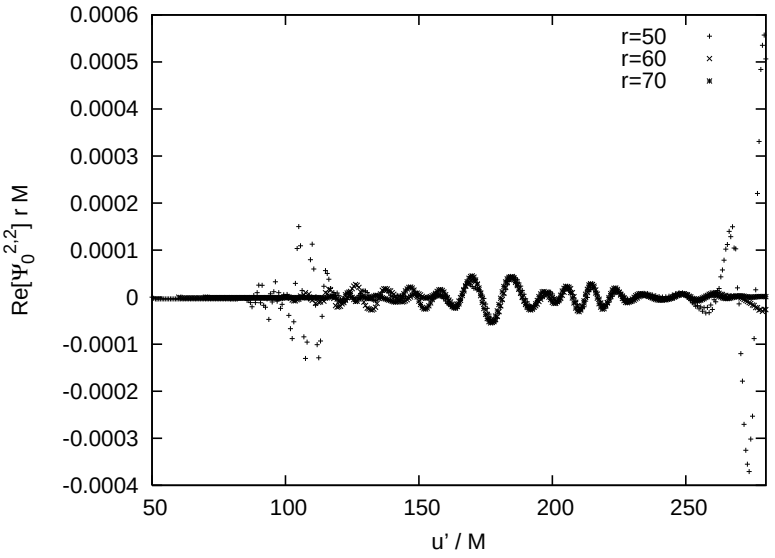

Fig. 4.14. $Re[\Psi_0^{2,2}]rM$ versus u' measured by detectors at $r = 50, 60, 70$,for R1 binary black hole initial data.

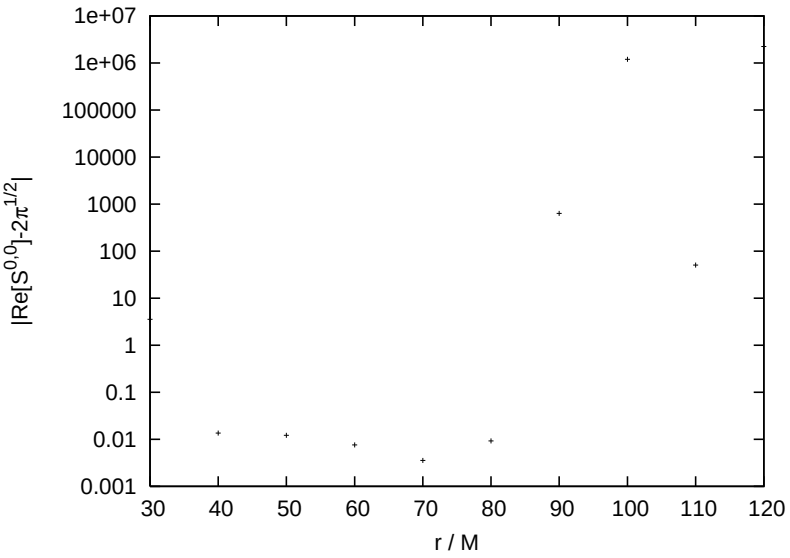

Fig. 4.15. The difference $|Re[S^{0,0}] - 2\sqrt{\pi}|$ on the null line $u = -30$ for R1 initial data.

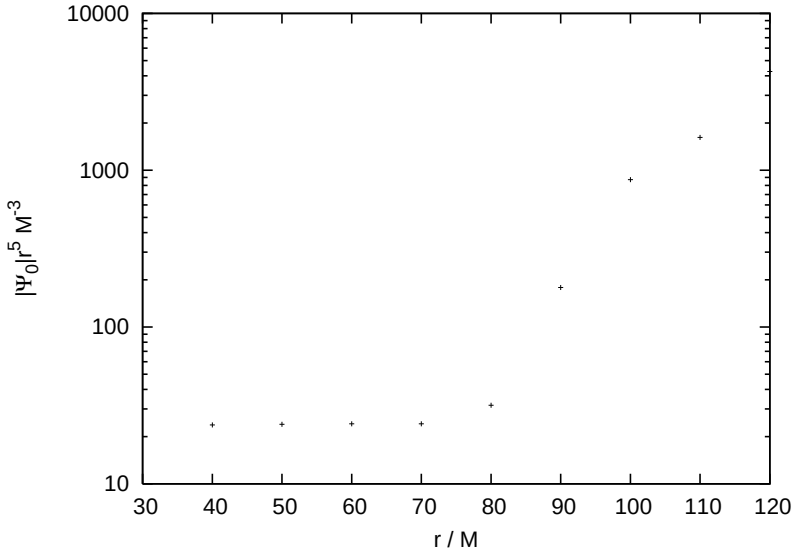

Fig. 4.16. $\Psi_0 r^5 M^{-3}$ versus r on the null line $u = -30$ for R1 initial data.

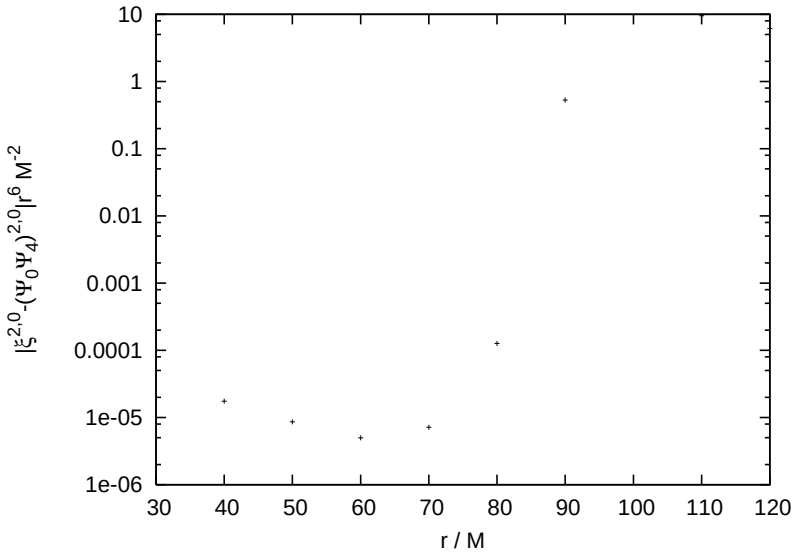

Fig. 4.17. The difference $|\xi^{2,0} - (\Psi_0\Psi_4)^{2,0}|r^6 M^{-2}$ versus r on the null line $u = -30$ for R1 initial data.

4.6 Conclusions

In the course of this study, we performed two analytic checks of the tetrad commonly used by numerical relativists for computing gravitational radiation. The first check was to compute the quasi-Kinnersley tetrad frame for approximate Bowen-York spinning black hole initial data. Using the frame, it was possible to show that the fiducial tetrad does not belong to the qK frame on the initial leaf. From this, it is possible to conclude that Ψ_4 computed using the fiducial tetrad does not represent the outgoing gravitational wave amplitude on the initial leaf. In the second check we bypass the computation of the qK tetrad frame by computing the BB scalar instead. We compare the value of the BB scalar to the value $\Psi_0\Psi_4$ for approximate Bowen-York boosted black hole initial data. Again, the fiducial tetrad does not belong to the qK frame, and the value of Ψ_4 does not represent the outgoing gravitational wave amplitude on the initial leaf.

In order to compute the BB scalar during numerical simulations, we wrote a thorn for the Cactus framework implementing the calculation outlined in section 4.3. The thorn was tested using the Bowen-York spinning black hole and boosted black hole examples given above. The earlier result that the fiducial tetrad failed to belong to the qK frame for the Bowen-York initial data was confirmed numerically using the thorn. Additionally, 4th order finite differencing error was observed in the BB scalar calculation for both examples.

Finally, we used the BB scalar as a check of the tetrad for a full numerical relativity simulation. The R1 initial data for equal mass binary black holes in quasi-circular orbit was chosen for the simulation. Because the BB scalar is only a valid check of the tetrad when the speciality index S is approximately 1, the BB scalar could not be used as a check for most of the solution. The cause of the discrepancy between the expected value of S and the result from

the simulation was investigated. We found that the value of Ψ_0 along ingoing null geodesics for some detectors indicated that radiation was reflecting off of grid boundaries. Additionally, the points for which S differed greatly from 1 correspond closely to the points for which Ψ_0 behaved unlike how we expect Ψ_0 to behave for an outgoing wave. The correspondence indicates that the behavior of Ψ_0 is not the result of a bad choice of tetrad or a gauge effect, since S would not differ greatly from 1 for either of these cases. What is not known at this time is whether the effect is purely the result of numerical effects such as radiation reflected from the grid boundaries.

We then compute the difference $|\xi - \Psi_0\Psi_4|r^6$ for the R1 solution on a null line for which $S \approx 1$. The difference is a lower bound on the sum of the two null rotation parameters which take the fiducial tetrad to a qK tetrad. Thus, while no conclusions can be drawn if the difference is small, we can conclude that the tetrad is unfit for computing gravitational radiation if the difference is large. We found the difference to be small in the case of the R1 run whenever $S \approx 1$ Thus, the study was inconclusive. However, computing the difference has the potential to catch errors in the tetrad in more general numerical simulations.

An interesting additional investigation would be to run a simulation for which the detectors remain causally disconnected from the grid boundaries through late times, and for which S is computed. Specifically, the investigation would have the detectors uncontaminated by unphysical radiation from grid boundaries while seeing radiation from the merger and ringdown of the simulated spacetime. Then, we expect $S \approx 1$ for detectors far enough from the gravitating bodies. Large grid simulations are presently being run with the desired grid and detector setup by Resswig *et al.* [53]

Chapter 5

Chern-Simons Gravity

5.1 Background

Chern-Simons gravity is an alternative theory of gravity currently being studied. Like general relativity, the theory is a classical metric theory of gravity. The action for the theory is related to the Einstein-Hilbert action (2.7) by the addition of a parity violating term [40],

$$I_{CS} = \frac{\varepsilon_1}{4}\int d^4x\sqrt{-g}\theta\,{}^*RR \tag{5.1}$$

The quantity ${}^*RR$ is the Pontryagin density, and is the contraction of the four dimensional Riemann tensor with its dual,

$${}^*RR \equiv {}^{*(4)}R^{\alpha\beta}{}_{\gamma\delta}\,{}^{(4)}R^{\gamma\delta}{}_{\beta\alpha} \tag{5.2}$$

$${}^{*(4)}R^{\alpha\beta}{}_{\gamma\delta} \equiv \frac{1}{2}\varepsilon^{\mu\nu}{}_{\gamma\delta}\,{}^{(4)}R^{\alpha\beta}{}_{\mu\nu}. \tag{5.3}$$

The Pontryagin density is equal to the divergence of the Chern-Simons topological current K^α,

$$K^\alpha = 2\varepsilon^{\alpha\beta\gamma\delta}\Big(\frac{1}{2}\,{}^{(4)}\Gamma^\sigma_{\beta\tau}\partial_\gamma\,{}^{(4)}\Gamma^\tau_{\delta\sigma} + \frac{1}{3}\,{}^{(4)}\Gamma^\sigma_{\beta\tau}\,{}^{(4)}\Gamma^\tau_{\gamma\eta}\,{}^{(4)}\Gamma^\eta_{\delta\sigma}\Big). \tag{5.4}$$

For this reason, if the scalar θ is a constant, the CS contribution to the action (5.1) is a surface term. Also added to the total action is a kinetic term for the field θ

$$I_\theta = -\frac{\varepsilon_2}{2}\int d^4x\sqrt{-g}\Big[g^{\alpha\beta}(\nabla_\alpha\theta)(\nabla_\beta\theta)+2V(\theta)\Big]. \tag{5.5}$$

The resulting action is the action for dynamical Chern-Simons modified gravity [6].

$$I_{tot} = I_{EH} + I_{CS} + I_\theta \tag{5.6}$$

The constants ε_1 and ε_2 are dimensionful, and can be chosen so that ε_1 has units $length^2$ and ε_2 has units $length^0$, for example. Then, θ is dimensionless. This choice will have no effect on the following discussion, though. The value of the coupling constants will be treated as unknown, though some of the theories that motivate CS gravity give them specific values. In the original formulation of CS modified GR, ε_2 was fixed to 0. In the resulting equations of motion, there was no difference between treating θ as a freely specifiable parameter of the theory or as a field variable. Arguments against this "non-dynamical" form of CS gravity (summarized in [6]) have led to the reformulation of CS gravity in which the dynamics of the θ field are specified. This dynamical CS gravity is theory we will investigate below.

Varying the action with respect to θ give the equation of motion for θ

$$\varepsilon_2\Box\theta = \varepsilon_2\frac{dV}{d\theta} - \frac{\varepsilon_1}{4}{}^*RR. \tag{5.7}$$

The dynamics of θ are sourced not only by the potential V, but also the Pontryagin density. The equations of motion for the metric are found by varying the action with respect to $g_{\alpha\beta}$

$$ {}^{(4)}G_{\alpha\beta} + 8\pi\varepsilon_1 C_{\alpha\beta} = 8\pi T^{\theta}_{\alpha\beta}. \tag{5.8} $$

The stress energy term on the RHS results from varying the term I_θ with respect to $g_{\alpha\beta}$

$$ T^{\theta}_{\alpha\beta} = \frac{1}{2}\varepsilon_2\Big((\nabla_\alpha\theta)(\nabla_\beta\theta) - \frac{1}{2}g_{\alpha\beta}(\nabla^\gamma\theta)(\nabla_\gamma\theta) - g_{\alpha\beta}V(\theta)\Big). \tag{5.9} $$

The C-tensor $C_{\alpha\beta}$ is given by

$$ C_{\alpha\beta} = \gamma_{\mu(\alpha}\gamma_{\beta)\nu}(v_\sigma\varepsilon^{\sigma\rho\tau\mu}\nabla_\tau {}^{(4)}R^{\nu}{}_{\rho} + v_{\sigma\tau}\,{}^{*(4)}R^{\tau\mu\nu\sigma}) \tag{5.10} $$

The covariant derivatives of the CS coupling field θ are abbreviated as $v_\alpha = \nabla_\alpha\theta$ and $v_{\alpha\beta} = \nabla_\beta v_\alpha$. The equations of motion for $g_{\alpha\beta}$ are third order in derivatives of the metric. The covariant derivative of the C-tensor gives the Pontryagin density

$$ \nabla^\alpha C_{\alpha\beta} = -\frac{1}{8}v_\beta\,{}^{*}RR. \tag{5.11} $$

There are several interesting results following from the additional terms in the action. Some spacetimes, such as the Schwarzschild and the Friedmann Robertson Walker spacetimes, persevere in CS modified GR [40, 34]. Others, like a full stationary axisymmetric-symmetric solution have proven too difficult to find to date [33]. Slow rotation and weak coupling assumptions

have led to an approximate spinning black hole solution [64]. A form of gravitational wave birefringence for which radiation still travels along null geodesics, but wave amplitude is suppressed or enhanced depending on polarization is shown to be a consequence of the CS modification. Also in the weak field, a PPN expansion of the field equations has revealed a modification to frame dragging and gyroscopic precession [5].

Jackiw and Pi first proposed the the action $I_{EH} + I_{CS}$ as a deformation of the Einstein Hilbert action by a Chern-Simons term. The purpose of their study was to generalize the Chern-Simons topological current to 4 dimensions, and to investigate the effect of a parity violating action in GR. The term has physical motivation in that it appears in 4 dimensional compactifications of string theory, where it is was shown by Green and Schwarz to be necessary for canceling gravitational anomalies [32]. More recently, it has appeared in the effective action resulting from modifying the Holst action by promoting the Barbero-Immirzi parameter to a scalar field, and coupling the theory to fermions [43].

5.2 3+1 decomposition

In this section, we write the Lagrangian for CS modified gravity in terms of spacial quantities. Then, we compute the Euler-Lagrange equations for these spacial quantities. Finally, we show that the key difficulty in arriving at an initial value formulation for CS modified gravity lies in finding an expression for $\partial_t^2 K_{ab}$.

Using the expression for the Riemann tensor with indices projected using n^α and $\gamma^\alpha{}_\beta$ (2.23), the CS modified Lagrangian is

$$\begin{aligned}\mathscr{L} &= \alpha\sqrt{\gamma}\Big(R + K_{ab}K^{ab} - K^2 + 8\pi\varepsilon_1\theta\varepsilon^{abc}\Big[\big(R^{de}{}_{bc} + 2K^d{}_b K^e{}_c\big)D_e K_{ad} \\ &\quad + \frac{2}{\alpha}D_b K^d{}_c\big(\dot{K}_{ad} - \beta^e D_e K_{ad} - K_{ae}D_d\beta^e - K_{de}D_a\beta^e + D_a D_d\alpha \\ &\quad + \alpha K_{ae}K^e{}_d\big)\Big] + 4\pi\varepsilon_2\Big[(\mathcal{L}_n\theta)^2 - (D_a\theta)(D^a\theta) - 2V\Big]\Big)\end{aligned} \tag{5.12}$$

By using the symmetry of the ε_1 terms, we can simplify the Lagrangian as

$$\begin{aligned}\mathscr{L} &= \alpha\sqrt{\gamma}\Big(R + K_{ab}K^{ab} - K^2 + 16\pi\varepsilon_1\theta\varepsilon^{abc}D_a K^d{}_b\Big[R_{cd} + \frac{1}{\alpha}D_c D_d\alpha \\ &\quad + K_{cd}K + \frac{1}{\alpha}(\dot{K}_{cd} - \beta^e D_e K_{cd} - K_{ce}D_d\beta^e - K_{de}D_c\beta^e)\Big] \\ &\quad + 4\pi\varepsilon_2\Big[(\mathcal{L}_n\theta)^2 - (D_a\theta)(D^a\theta) - 2V\Big]\Big)\end{aligned} \tag{5.13}$$

Note that the Lagrangian has second time derivatives of the spacial metric and time derivatives of the lapse and shift in the $\dot{K}_{ab}$ term. These issues can be remedied by promoting K_{ab} to the status of a new variable (L_{ab}) with the addition of a constraint. Additionally, introducing yet another new variable $M_{ab} \equiv \mathcal{L}_n(K_{ab})$ will help to isolate $\mathcal{L}_n(K_{ab})$ in the resulting equations of motion. Note that we perform these substitutions only for simplification. They will not modify

the equations of motion.

$$\begin{aligned}\mathscr{L} &= \alpha\sqrt{\gamma}\Big(R + L_{ab}L^{ab} - L^2 + 16\pi\varepsilon_1\theta\varepsilon^{abc}D_aL^d{}_b\Big[M_{cd} + \frac{1}{\alpha}D_cD_d\alpha \\ &\quad + R_{cd} + L_{cd}L\Big] + 4\pi\varepsilon_2\Big[(\mathcal{L}_n\theta)^2 - (D_a\theta)(D^a\theta) - 2V\Big] \\ &\quad + \lambda^{ab}[L_{ab} + \frac{1}{2\alpha}(\dot{\gamma}_{ab} - D_a\beta_b - D_b\beta_a)] + \mu^{ab}[M_{ab} + \frac{1}{\alpha}(-\dot{L}_{ab} \\ &\quad + \beta^cD_cL_{ab} + L_{ac}D_b\beta^c + L_{bc}D_a\beta^c)]\Big)\end{aligned} \tag{5.14}$$

Here, λ^{ab} and μ_{ab} are Lagrange multipliers. With this Lagrangian, we proceed to finding the Euler-Lagrange equations of motion. The expectation is to find that γ_{ab}, L_{ab}, M_{ab} λ^{ab}, μ^{ab}, and $\mathcal{L}_n\theta$ are spacial quantities with associated constraint and evolution equations. Additionally, α and β^a will remain gauge quantities.

The α equation of motion, given by $\frac{\partial\mathscr{L}}{\partial\alpha} = 0$, is simply

$$\begin{aligned}0 &= \sqrt{\gamma}\Big(R + L_{ab}L^{ab} - L^2 + 16\pi\varepsilon_1\varepsilon^{abc}\big[\theta D_aL^d{}_b(M_{cd} + R_{cd} + L_{cd}L) \\ &\quad + D_dD_c(\theta D_aL^d{}_b)\big] + 8\pi\varepsilon_2\big[-\frac{1}{2}(\mathcal{L}_n\theta)^2 - \frac{1}{2}(D_a\theta)(D^a\theta) - V\big] \\ &\quad + \lambda^{ab}L_{ab} + \mu^{ab}M_{ab}\Big)\end{aligned} \tag{5.15}$$

The derivation of the equation follows that of the Hamiltonian constraint from the Einstein Hilbert action. However, the new equation is modified with terms proportional to θ and its spacial and time derivatives. This equation is also a constraint, since it lacks time derivatives of spacial variables.

I proceed with the β^a equation of motion, $\frac{\partial \mathscr{L}}{\partial \beta^a} = 0$

$$0 = \sqrt{\gamma}\Big(-8\pi\varepsilon_2(\mathcal{L}_n\theta)D_a\theta + D^b\lambda_{ab} + \mu^{bc}D_aL_{bc} - 2D_b(\mu^{bc}L_{ac})\Big) \tag{5.16}$$

The equation constrains the divergence of λ^{ab} much as the momentum constraint constrains the divergence of K_{ab}.

The final primary constraint is the equation of motion for M_{ab}, $\frac{\partial \mathscr{L}}{\partial M_{ab}} = 0$,

$$0 = \sqrt{\gamma}(\mu^{ab} + 16\pi\varepsilon_1\theta\varepsilon^{cd(a}D_cL^{b)}{}_d). \tag{5.17}$$

From the constraint, we can see that μ^{ab} is entirely dependent on γ_{ab}, L_{ab}, and θ. We can use this equation of motion to eliminate μ^{ab} from the other equations of motion.

The rest of the equations of motion represent evolution equations for $\mathcal{L}_n\theta$, γ_{ab}, L_{ab}, μ^{ab}, and λ^{ab}. For example, the θ equation of motion is given by $\partial_t(\frac{1}{\alpha}\frac{\partial \mathscr{L}}{\partial \mathcal{L}_n\theta}) - D_c(\frac{1}{\alpha}\beta^c\frac{\partial \mathscr{L}}{\partial \mathcal{L}_n\theta}) - \frac{\partial \mathscr{L}}{\partial \theta} = 0$,

$$\begin{aligned} 0 = {} & 8\pi\sqrt{\gamma}\Big[\varepsilon_2\Big(\partial_t(\mathcal{L}_n\theta) + \mathcal{L}_n\theta(-\alpha K + D^c\beta_c) - D_c(\beta^c\mathcal{L}_n\theta) \\ & - D_a(\alpha D^a\theta) + \alpha\frac{\partial V}{\partial \theta}\Big) - 2\alpha\varepsilon_1\varepsilon^{abc}D_aL^d{}_b\Big(M_{cd} + \frac{1}{\alpha}D_cD_d\alpha \\ & + R_{cd} + L_{cd}L\Big)\Big]. \end{aligned} \tag{5.18}$$

This is the evolution equation for $\mathcal{L}_n\theta$. It is identical to eq. (5.7). The equation of motion for λ^{ab} recovers the definition for L_{ab}, which is an evolution equation for γ_{ab},

$$\dot{\gamma}_{ab} = \mathcal{L}_\beta\gamma_{ab} - 2\alpha L_{ab}. \tag{5.19}$$

I will use this equation to eliminate all occurrences of $\dot{\gamma}_{ab}$ in all of the following equations. The equation of motion for L_{ab} gives an evolution equation for μ^{ab}

$$\begin{aligned}\dot{\mu}^{ab} &= \mathcal{L}_\beta \mu^{ab} + \alpha\big(L\mu^{ab} + 2L\gamma^{ab} - 2L^{ab} \\ &\quad + 16\pi\varepsilon_1 \varepsilon^{cd(a}\gamma^{b)e}\big[-\frac{1}{\alpha}D_c(\theta(\alpha M_{de} + D_d D_e \alpha \\ &\quad + \alpha R_{de} + L_{de}L)) - L\theta D_c L_{de}\big] + \gamma^{ab}L_{cd}\mu^{cd} - \lambda^{ab}\big).\end{aligned} \tag{5.20}$$

Because μ^{ab} is constrained to be a function of other spacial variables, we will see later that this equation is actually a constraint on λ^{ab}. The equation of motion for M^{ab} gives the evolution equation for L_{ab},

$$\dot{L}_{ab} = \mathcal{L}_\beta L_{ab} + \alpha M_{ab} \tag{5.21}$$

Finally, varying γ_{ab} will give an evolution equation for λ^{ab},

$$\begin{aligned}
\dot{\lambda}^{ab} &= \mathcal{L}_\beta \lambda^{ab} + \alpha\Big(L\lambda^{ab} + \gamma^{ab}(R + L_{cd}L^{cd} - L^2) - 2R^{ab} - 4L^{ac}L^b{}_c \\
&\quad + 4LL^{ab} + \frac{2}{\alpha}(D^aD^b\alpha - \gamma^{ab}D^cD_c\alpha)\Big) \\
&\quad + 16\pi\varepsilon_1\varepsilon^{cde}\gamma^{f(a}\gamma^{b)g}\Big[2\alpha\theta D_c L_{df}(-M_{eg} - \frac{1}{\alpha}D_eD_g\alpha - R_{eg} - L_{eg}L) \\
&\quad + D_c(\alpha\theta L_{df}[M_{eg} + \frac{1}{\alpha}D_eD_g\alpha + R_{eg} + L_{eg}L]) \\
&\quad + D^h(\alpha\theta L_{df}\gamma_{cg}[M_{eh} + \frac{1}{\alpha}D_eD_h\alpha + R_{eh} + L_{eh}L]) \\
&\quad - D^h(\alpha\theta L_{dh}\gamma_{cf}[M_{eg} + \frac{1}{\alpha}D_eD_g\alpha + R_{eg} + L_{eg}L]) \\
&\quad + D_e(\theta D_c L_{df}D_g\alpha) + D^h(\theta D_c L_{dh}\gamma_{ef}D_g\alpha) - D^h(\theta D_c L_{df}\gamma_{eg}D_h\alpha) \\
&\quad + \gamma_{ef}D_hD_g(\alpha\theta D_c L^h{}_d) + D_eD_f(\alpha\theta D_c L_{dg}) - \gamma_{ef}D^hD_h(\alpha\theta D_c L_{dg}) \\
&\quad - 2\gamma_{fg}D_eD_h(\alpha\theta D_c L^h{}_d) - 2\alpha\theta D_c L^h{}_d L_{eh}L_{fg}\Big] \\
&\quad + 8\pi\varepsilon_2\alpha\Big[\frac{1}{2}\gamma^{ab}((\mathcal{L}_n\theta)^2 - (D^a\theta)(D_a\theta) - 2V) + 2(D^a\theta)(D^b\theta)\Big]
\end{aligned} \tag{5.22}$$

We have now performed variations with respect to all of the field variables. At this stage, there are evolution equations for θ, γ_{ab}, L_{ab}, μ^{ab}, and λ^{ab}. In addition, there is one scalar constraint, a constraint which fixes the value of μ^{ab}, and a vector constraint. Below, we will replace M_{ab} with $M'_{ab} \equiv M_{ab} + \frac{1}{\alpha}D_aD_b\alpha + R_{ab} + L_{ab}L$, and $-16\pi\varepsilon_1\theta\varepsilon^{cd(a}D_cL^{b)}{}_d$ with μ^{ab}. In summary, the set of equations of motion is:

$$\begin{aligned}
0 &= R + L_{ab}L^{ab} - L^2 - D_aD_b\mu^{ab} - \mu^{ab}(R_{ab} + L_{ab}L) \\
&\quad + 4\pi\varepsilon_2[-(\mathcal{L}_n\theta)^2 - (D^a\theta)(D_a\theta) - 2V]
\end{aligned} \tag{5.23}$$

$$0 = D^b\lambda_{ab} + \mu^{bc}D_aL_{bc} - 2D_b(\mu^{bc}L_{ab}) - 8\pi\varepsilon_2(\mathcal{L}_n\theta)D_a\theta \tag{5.24}$$

$$0 = \mu^{ab} + 16\pi\varepsilon_1\theta\varepsilon^{cd(a}D_cL^{b)}{}_d \tag{5.25}$$

$$\dot{\gamma}_{ab} = \mathcal{L}_\beta\gamma_{ab} - 2\alpha L_{ab} \tag{5.26}$$

$$\partial_t(\mathcal{L}_n\theta) = \mathcal{L}_\beta(\mathcal{L}_n\theta) + \alpha L(\mathcal{L}_n\theta) + D_a(\alpha D^a\theta) - \alpha\frac{\partial V}{\partial\theta} - \alpha\frac{1}{8\pi\theta\varepsilon_2}\mu^{ab}M'_{ab} \tag{5.27}$$

$$\dot{L}_{ab} = \mathcal{L}_\beta L_{ab} + \alpha M'_{ab} - D_aD_b\alpha - \alpha R_{ab} - L_{ab}L \tag{5.28}$$

$$\begin{aligned}\dot{\mu}^{ab} &= \mathcal{L}_\beta\mu^{ab} + \alpha\Big(2L\mu^{ab} + 2L\gamma^{ab} - 2L^{ab} - \lambda^{ab} + \gamma^{ab}L_{cd}\mu^{cd}\Big) \\ &\quad -16\pi\varepsilon_1\varepsilon^{cd(a}\gamma^{b)f}D_c(\alpha\theta M'_{df})\end{aligned} \tag{5.29}$$

$$\begin{aligned}\dot{\lambda^{ab}} &= \mathcal{L}_\beta\lambda^{ab} + \alpha\Big(L\lambda^{ab} + \gamma^{ab}(R + L_{cd}L^{cd} - L^2) - 2R^{ab} \\ &\quad -4L^{ac}L^b{}_c + 4LL^{ab}\Big) + 2(D^aD^b\alpha - \gamma^{ab}D^cD_c\alpha) \\ &\quad +16\pi\varepsilon_1\varepsilon^{cde}\gamma^{f(a}\gamma^{b)g}\Big(-2\alpha\theta M'_{eg}D_cL_{df} + D_c(\alpha\theta L_{df}M'_{eg}) \\ &\quad +D^h(\alpha\theta L_{df}\gamma_{cg}M'_{eh}) - D^h(\alpha\theta L_{dh}\gamma_{cf}M'_{eg})\Big) \\ &\quad +D_e(-\mu^{ea}D^b\alpha - \mu^{eb}D^a\alpha + \mu^{ab}D^e\alpha) \\ &\quad +D_e\big(-D^b(\alpha\mu^{ae}) - D^a(\alpha\mu^{be}) + D^e(\alpha\mu^{ab}) + \gamma^{ab}D_f(\alpha\mu^{ef})\big) \\ &\quad +4\pi\alpha\varepsilon_2\Big(\gamma^{ab}\Big[(\mathcal{L}_n\theta)^2 - (D^c\theta)(D_c\theta) - 2V\Big] + 2(D^a\theta)(D^b\theta)\Big) \\ &\quad +2\alpha L^{ab}\mu^{cd}L_{cd}\end{aligned} \tag{5.30}$$

Still lacking is an equation to evolve M_{ab}. It is expected that additional constraints will result from requiring that the primary constraints be preserved under evolution.

We now proceed by checking that the time derivatives of the constraints are zero. First, the constraint on μ^{ab},

$$\begin{aligned} 0 &= \partial_t(\mu^{ab} + 16\pi\varepsilon_1\theta\varepsilon^{cd(a}D_cL^{b)}{}_d) \\ &= \dot{\mu}^{ab} - \frac{\dot{\theta}}{\theta}\mu^{ab} + (-\alpha K + D_c\beta^c)\mu^{ab} \\ &\quad -16\pi\varepsilon_1\theta\varepsilon^{cd(a}\gamma^{b)e}\Big(-\dot{\gamma}_{ef}D_cL^f{}_d + D_c\dot{L}_{de} - \dot{\Gamma}^f_{ce}L_{df}\Big) \end{aligned} \tag{5.31}$$

With the evolution equations for γ_{ab}, L_{ab}, and μ^{ab} and some work, we can see that

$$\begin{aligned} 0 &= (\frac{1}{\theta}\mathcal{L}_n\theta - L)\mu^{ab} + \lambda^{ab} + 2L^{ab} - 2L\gamma^{ab} - 2\mu^{c(a}L^{b)}{}_c \\ &\quad +16\pi\varepsilon_1\theta\varepsilon^{cd(a}\gamma^{b)e}\Big[\frac{1}{\theta}M'_{de}D_c\theta - D_cR_{de} - L_{de}D_cL \\ &\quad -2L_{ef}D_cL^f{}_d - L^f{}_dD_cL_{ef}\Big] \end{aligned} \tag{5.32}$$

We have not yet checked that the time derivatives of the Hamiltonian and momentum constraints are zero.

In order to have a complete system of evolution equations, more information is needed about M_{ab}. Specifically, an evolution equation is needed for M_{ab}. The only sources of additional information at this stage are secondary constraints. In particular, we can see that (5.32) gives an expression for λ^{ab}. The time derivative of this equation will provide some additional information about $\dot{M}_{ab}$ at the expense of much additional work. However, $\dot{M}_{ab}$ can not be found uniquely using the time derivative of (5.32) alone.

5.3 Projections of the Cotton Tensor

A shortcut for deriving constraints and equations of motion for General Relativity is to project the Einstein equations,

$$G_{\alpha\beta} = 8\pi T_{\alpha\beta} \tag{5.33}$$

using n^{α} and $\gamma^{\alpha}{}_{\beta}$. All of the constraint and evolution equations can be obtained in such a way. That is,

$$G_{\alpha\beta} n^{\alpha} n^{\beta} = \frac{1}{2}(R + K^2 - K_{ab}K^{ab}), \tag{5.34}$$

$$G_{\alpha\beta} n^{\alpha} \gamma^{\beta}{}_{\mu} = D_{\mu}K - D^{\nu}K_{\mu\nu}, \tag{5.35}$$

and

$$\begin{aligned} &G_{\alpha\beta}(\gamma^{\alpha}{}_{\mu}\gamma^{\beta}{}_{\nu} - \frac{1}{2}\gamma_{\mu\nu}(\gamma^{\alpha\beta} - n^{\alpha}n^{\beta})) = \\ &R_{\mu\nu} + K_{\mu\nu}K - 2K^{\alpha}{}_{\mu}K_{\alpha\nu} - \frac{1}{\alpha}(\dot{K}_{\mu\nu} - \beta^{\alpha}D_{\alpha}K_{\mu\nu} - K_{\mu\alpha}D_{\nu}\beta^{\alpha} \\ &-K_{\alpha\nu}D_{\mu}\beta^{\alpha} + D_{\mu}D_{\nu}\alpha). \end{aligned} \tag{5.36}$$

In vacuum ($T_{\alpha\beta} = 0$), the projections of the Einstein equations are the previously derived ADM equations (2.27, 2.28, 2.29). Projecting the field equations to get a complete system of constraints and evolution equations will fail in Chern-Simons gravity. The reason is that the action depends on time derivatives of the extrinsic curvature K_{ab}. Because the action is higher order in time derivatives than the Einstein Hilbert action, there are additional degrees of freedom corresponding to the initial values of $\dot{K}_{ab}$. It is unclear from simply inspecting the Lagrangian

(5.12) how many degrees of freedom there are in the theory, since there may also be additional constraints. Still, the projections may contain useful information and are included below.

With the Chern-Simons term in the Lagrangian, the field equations take the form given in eq. (5.8). The normal-normal projection of the C-tensor is

$$\begin{aligned} C_{nn} &= n^\mu n^\nu C_{\mu\nu} \\ &= \varepsilon^{abc}\Big[(D_a\theta)\Big(-D_cD^dK_{bd}+K^d{}_c(R_{bd}-\mathcal{L}_nK_{bd}-\frac{1}{\alpha}D_bD_d\alpha)\Big) \\ &\quad +(D_aD_d\theta+(\mathcal{L}_n\theta)K_{ad})D_bK^d{}_c\Big]. \end{aligned} \tag{5.37}$$

The normal-normal projection of the stress energy $T^\theta_{\mu\nu}$ is simply

$$\begin{aligned} T_{nn} &= n^\mu n^\nu T^\theta_{\mu\nu} \\ &= \frac{1}{4}\varepsilon_2\Big((\mathcal{L}_n\theta)^2+(D_a\theta)(D^a\theta)+2V\Big). \end{aligned} \tag{5.38}$$

Hence, the normal-normal projection of the modified field equations is

$$\begin{aligned} 0 &= R+K^2-K_{ab}K^{ab}+16\pi\varepsilon_1\varepsilon^{abc}\Big[(D_a\theta)\Big(-D_cD^dK_{bd} \\ &\quad +K^d{}_c(R_{bd}-\mathcal{L}_nK_{bd}-\frac{1}{\alpha}D_bD_d\alpha)\Big)+(D_aD_d\theta+(\mathcal{L}_n\theta)K_{ad})D_bK^d{}_c\Big] \\ &\quad -4\pi\varepsilon_2\Big((\mathcal{L}_n\theta)^2+(D_a\theta)(D^a\theta)+2V\Big). \end{aligned} \tag{5.39}$$

This equation is equivalent to the Hamiltonian constraint (eq. 5.23), after using (5.29), (5.32), and (5.28) to substitute for μ^{ab}, λ^{ab}, and M'_{ab} respectively.

We perform the normal-spacial projection of the C-tensor in four parts, as it is significantly more complicated than the normal-normal projection.

$$
\begin{aligned}
(C_{n\gamma})_a &= n^\mu \gamma^\nu{}_a C_{\mu\nu} \qquad (5.40)\\
&= \underbrace{\frac{1}{2} n_\mu \gamma_{\alpha\nu} v_\sigma \varepsilon^{\sigma\beta\gamma\mu} \nabla_\gamma{}^{(4)} R^\nu{}_\beta}_{C^{(1)}_{n\gamma}} + \underbrace{\frac{1}{2} n_\mu \gamma_{\alpha\nu} v_\sigma \varepsilon^{\sigma\beta\gamma\nu} \nabla_\gamma{}^{(4)} R^\mu{}_\beta}_{C^{(2)}_{n\gamma}} \\
&\quad + \underbrace{\frac{1}{2} n_\mu \gamma_{\alpha\nu} v_{\sigma\tau}{}^{*(4)} R^{\tau\mu\nu\sigma}}_{C^{(3)}_{n\gamma}} + \underbrace{\frac{1}{2} n_\mu \gamma_{\alpha\nu} v_{\sigma\tau}{}^{*(4)} R^{\tau\nu\mu\sigma}}_{C^{(4)}_{n\gamma}}
\end{aligned}
$$

The first term is straightforward to compute,

$$
\begin{aligned}
C^{(1)}_{n\gamma} &= \frac{1}{2} \gamma^f{}_a (D_c \theta) \varepsilon^{cde} \Big[D_e (R_{fd} + K_{fd} K - 2K^g{}_f K_{dg} \qquad (5.41)\\
&\quad - \mathcal{L}_n K_{fg} - \frac{1}{\alpha} D_f D_d \alpha) - K_{ef} (D^g K_{dg} - D_d K) \Big].
\end{aligned}
$$

The second term is less straightforward, and we use the commutator

$$
\begin{aligned}
[\mathcal{L}_n, D_a] K_{bc} &= a_a (\mathcal{L}_n K_{bc} + 2K_{bd} K^d{}_c) + a_b K^d{}_a K_{cd} \qquad (5.42)\\
&\quad + a_c K^d{}_a K_{bd} - a^d (K_{ab} K_{cd} + K_{ac} K_{bd}) \\
&\quad + K^d{}_b (D_c K_{ad} + D_a K_{cd} - D_d K_{ac}) \\
&\quad + K^d{}_c (D_b K_{ad} + D_a K_{bd} - D_d K_{ab})
\end{aligned}
$$

to move covariant derivatives to the left of Lie derivatives. We use the notation $a_\alpha \equiv n^\beta \nabla_\beta n_\alpha$ to simplify expressions.

$$\begin{aligned} C^{(2)}_{n\gamma} &= \frac{1}{2}\varepsilon^{cde}\gamma_{ae}\Big\{(D_c\theta)\big[D_d(-\frac{1}{\alpha}D^f D_f\alpha + K^{gf}K_{gf}) \\ &\quad -2K^{gf}D_f K_{dg} - D^g \pounds_n K_{dg} - K^{gf}D_d K_{gf} - K_{df}D_g K^{gf} \\ &\quad +a^g(D_g a_d - R_{gd}) - a_d D^g a_g\big] + (\pounds_n\theta)\big[\\ &\quad -D_d D^f K_{cf} + K^g{}_d(R_{cg} - \pounds_n K_{cg} - \frac{1}{\alpha}D_c D_g\alpha)\big]\Big\} \end{aligned} \tag{5.43}$$

The third and fourth terms in the projection of the C-tensor are

$$\begin{aligned} C^{(3)}_{n\gamma} &= \frac{1}{2}\varepsilon^{cde}\gamma_{ae}\Big\{\big[D_g(\pounds_n\theta) + K^f{}_g D_f\theta\big]D_c K^g{}_d \\ &\quad +\big[K_{cg}(\pounds_n\theta) + D_c D_g\theta\big]\big(-\gamma^{gh}\pounds_n K_{dh} - \frac{1}{\alpha}D^g D_d\alpha - K^{gh}K_{dh}\big)\Big\} \end{aligned} \tag{5.44}$$

$$\begin{aligned} C^{(4)}_{n\gamma} &= \frac{1}{2}\varepsilon^{cde}\gamma_{fa}\Big\{\big[K_{cg}(\pounds_n\theta) + D_c D_g\theta\big]\big(-\frac{1}{2}R^{gf}{}_{de} - K^g{}_d K^f{}_e\big) \\ &\quad +\big[D_c(\pounds_n\theta) + K^h{}_c D_h\theta\big]D_d K^f{}_e\Big\} \end{aligned} \tag{5.45}$$

After combining all of the parts and simplifying, the result is

$$\begin{aligned} (C_{n\gamma})_a &= D^b\Big\{\gamma^f{}_{(a}\gamma_{b)e}\varepsilon^{cde}\Big[(D_d\theta)(\pounds_n K_{cf} + \frac{1}{\alpha}D_c D_f\alpha + K_{cf}K + R_{cf}) \\ &\quad +(\pounds_n\theta)D_c K_{df}\Big]\Big\} + \frac{1}{2}\varepsilon^{bcd}\Big\{D_g\Big[(D_f\theta)K^f{}_b K^g{}_c\gamma_{ad}\Big] \\ &\quad +(D_b\theta)\Big[D_f(K^f{}_d K_{ac}) + 2K_{af}D_c K^f{}_d - 2D_c R_{ad} + \gamma_{ad}D_f R^f{}_c\Big] \\ &\quad +(D_f\theta)D_b(K^f{}_c K_{ad})\Big\}. \end{aligned} \tag{5.46}$$

The normal-spacial projection of the stress energy is

$$\begin{aligned}(T_{n\gamma})_a &= n^\mu \gamma^\nu{}_a T^\theta_{\mu\nu} \\ &= \frac{1}{2}\varepsilon_2(\pounds_n\theta)D_a\theta.\end{aligned} \tag{5.47}$$

Together, the normal-spacial projection of the modified field equations is

$$\begin{aligned}0 = {} & D^b\Big\{\gamma_{ab}K - K_{ab} + 8\pi\varepsilon_1\gamma^f{}_{(a}\gamma_{b)e}\varepsilon^{cde}\Big[(D_d\theta)(\pounds_n K_{cf} \\ & + \frac{1}{\alpha}D_cD_f\alpha + K_{cf}K + R_{cf}) + (\pounds_n\theta)D_cK_{df}\Big]\Big\} \\ & + 4\pi\varepsilon_1\varepsilon^{bcd}\Big\{D_g\Big[(D_f\theta)K^f{}_bK^g{}_c\gamma_{ad}\Big] \\ & + (D_b\theta)\Big[D_f(K^f{}_dK_{ac}) + 2K_{af}D_cK^f{}_d - 2D_cR_{ad} + \gamma_{ad}D_fR^f{}_c\Big] \\ & + (D_f\theta)D_b(K^f{}_cK_{ad})\Big\} - 4\pi\varepsilon_2(\pounds_n\theta)D_a\theta.\end{aligned} \tag{5.48}$$

We have not yet checked whether the projection is equivalent to the momentum constraint (5.24) under the assumptions (5.29), (5.32), and (5.28). Both the modified Hamiltonian and momentum constraints offer little hope for general solutions in their present form. Additional simplifications might be possible. Also, there may be additional constraint equations which have not yet been found to which the Hamiltonian constraint and the momentum constraint will couple.

Finally, the spacial-spacial projection of the C-tensor is

$$
\begin{aligned}
(C_{\gamma\gamma})_{ab} \;=\; & \gamma_{c(a}\gamma^{d}{}_{b)}\varepsilon^{cef}\Big\{(\mathcal{L}_n\theta)\Big(D_e\Big(-R_{df}-K_{df}K+2K_{dg}K^{g}{}_{f} \\
& +\mathcal{L}_nK_{df}+\frac{1}{\alpha}D_dD_f\alpha\Big)+K_{de}(D^gK_{fg}-D_fK)\Big) \\
& +(D_e\theta)\Big(-D_dD_fK+D_fD^gK_{dg}+K_{df}(-\mathcal{L}_nK \\
& -\frac{1}{\alpha}D^gD_g\alpha+K^{gh}K_{gh})+a_f(D^gK_{dg}-D_dK) \\
& +a_d(D^gK_{fg}-D_fK) \\
& +\mathcal{L}_n\Big(R_{df}+K_{df}K-2K_{dg}K^{g}{}_{f}-\mathcal{L}_nK_{df}-\frac{1}{\alpha}D_dD_f\alpha\Big) \\
& +K^{g}{}_{d}\Big(R_{fg}+K_{fg}K-2K_{fh}K^{h}{}_{g}-\mathcal{L}_nK_{fg}-\frac{1}{\alpha}D_fD_g\alpha\Big)\Big) \\
& +(D^gD_f\theta+K^{g}{}_{f}\mathcal{L}_n\theta)(D_dK_{eg}-D_gK_{de}) \\
& +(D_f\mathcal{L}_n\theta+K^{g}{}_{f}D_g\theta)(R_{de}+K_{de}K+\mathcal{L}_nK_{de} \\
& +\frac{1}{\alpha}D_dD_e\alpha)+(\mathcal{L}_n\mathcal{L}_n\theta-a^iD_i\theta)D_eK_{df}\Big\}.
\end{aligned}
\tag{5.49}
$$

The result is very long and messy, and not very informative. The spacial spacial projection of the stress energy is

$$
(T_{\gamma\gamma})_{ab}=\frac{1}{2}\varepsilon_2\big((D_a\theta)(D_b\theta)+\frac{1}{2}\gamma_{ab}((\mathcal{L}_n\theta)^2-(D^c\theta)(D_c\theta)-2V)\big). \tag{5.50}
$$

The spacial-spacial projection of the modified field equations is

$$
\begin{aligned}
0 \;=\; & R_{ab}+K_{ab}K-2K_{ac}K^{c}{}_{b}-\mathcal{L}_nK_{ab}-\frac{1}{\alpha}D_aD_b\alpha \\
& +8\pi\varepsilon_1(C_{\gamma\gamma})_{ab}-4\pi\varepsilon_2(D_a\theta)(D_b\theta).
\end{aligned}
\tag{5.51}
$$

We encounter the same obstacle as for the Lagrangian formulation. That is, we can not solve for $\partial_t \mathcal{L}_n K_{ab}$.

All of the above projections were checked using Maple and the grtensor package. To check the projections for a specific spacetime metric, we calculate the C-tensor using (5.10) and project the result using the expressions for γ_{ab} and n^a. Then, we repeat the calculation using the expressions found in this section. For the test spacetimes, we used the Schwarzschild, Kerr, FRW, and slowly rotating solution to the CS modified field equations [64]. The two methods of computing the projections had the same results for each spacetime.

5.4 Summary

For this project we first rewrote the CS modified action in terms of the familiar spacial variables γ_{ab}, K_{ab}, α, β^a and additionally θ, $\mathcal{L}_n\theta$, and $\mathcal{L}_n K_{ab}$. Constraints were used to introduce additional variables so that the action depends only on the variables and their first time derivatives. We did this only for simplification. The resulting Lagrangian (5.14) was used to find the equations of motion, which we divided into constraints and evolution equations. The resulting set of evolution equations was incomplete in that no equation was found for $\partial_t(\mathcal{L}_n K_{ab})$. Additional work may be done in checking that the constraint equations are preserved under evolution. However, failure to find a complete set of evolution equations means that only one application of a time derivative can be applied to either (5.23), (5.24). Additional time derivatives will produce projections of the evolution equation for $\mathcal{L}_n K_{ab}$. More importantly, inability to solve for $\partial_t(\mathcal{L}_n K_{ab})$ indicates that variables in which the Lagrangian is expressed were chosen poorly.

Finally, projections of the C-tensor and the stress-energy of the scalar field θ were performed. The normal-normal projection of the modified field equations was found to be equivalent to the Hamiltonian constraint, while the normal-spacial projection resembles the momentum constraint. The spacial-spacial projection contains a projection of $\partial_t(\pounds_n K_{ab})$, which can not be inverted to solve for $\partial_t(\pounds_n K_{ab})$. This is the same problem encountered in the Lagrangian formulation of CS modified gravity.

Chapter 6

Summary

The recent progress in numerical relativity has made possible the simulation of very generic black hole merger scenarios. From these simulations are coming new and interesting predictions. Many of these predictions, including the waveforms to be used in matched template signal searches, depend on assumptions such as a choice of tetrad. Such an assumption needs to be checked. Checks currently taking place include comparing waveforms produced by different groups using different codes, and have shown very strong agreement between the waveforms. The first project in this dissertation is to investigate an additional method for checking the waveforms. The check can be performed on a single simulation by calculating gauge, tetrad, and background independent scalars during the simulation.

We find, using the speciality index and the BB scalar, that the fiducial tetrad is valid up to a spin boost transformation at times when $S \approx 1$ for the R1 solution. We found that the test was severely limited in where it could be applied due to the large difference between S and 1 for the simulations we performed. And, we show that this is due in part to ingoing radiation from grid boundaries.

While the check was inconclusive, it can be applied to very generic runs. The check has the power to catch errors in the technique used to compute gravitational radiation. Ideal runs for using the check will be those for which the extracted radiation is not contaminated by ingoing radiation from the grid boundaries. These runs should satisfy the condition that $S \approx 1$,

and will permit the use of the BB scalar check during the period when strong outgoing radiation is reaching the detectors. Thus, interesting additional work with the BB scalar check would be to use it on simulations for which the detectors are causally disconnected from the outer boundaries during the times strong outgoing radiation is reaching the detectors.

In the remainder of the dissertation, we attempt to derive an initial value formulation for Chern-Simons modified gravity. CS modified gravity is an extension of general relativity in which a parity violating term is added to the action. The term influences gravitational waves by suppressing or enhancing different polarizations. Thus, gravitational waves will play a strong role in testing the theory. To compute wave emitting solutions, numerical relativity will be required. And so, an initial value formulation is also needed.

We find that the Lagrangian can be simply expressed in terms of the familiar variables of the ADM equations plus additional variables representing the embedding field, its Lie derivative along the unit time-like normal, and the Lie derivative of the extrinsic curvature. We found the Euler-Lagrange equations of motion for the Lagrangian. We then showed that the equations do not represent a complete set of constraint and evolution equations. The missing equation, for the evolution of the Lie derivative of the extrinsic curvature, also can not be found from time derivatives of the constraint equations. Finally, we computed projections of the modified field equations.

Further work towards an initial value formulation of CS gravity must address the problem of finding a complete set of evolution equations. One solution may be to decompose M_{ab} into components for which we can find evolution equations, in a manner similar to the transverse traceless decomposition. Once a complete set of evolution and constraint equations is found for CS gravity, numerical CS gravity can embark down the long road numerical relativity has

traveled so successfully, in a hunt for stable evolution schemes, binary black hole mergers, and accurate gravitational waveforms.

Appendix A

Tetrad Rotations

Transformations of the tetrad which preserve the tetrad orthonormalization (3.12) can be divided into three subgroups [41]:

- Type I

$$\begin{aligned} l^{\alpha} &\rightarrow l^{\alpha} \\ m^{\alpha} &\rightarrow m^{\alpha} + d l^{\alpha} \\ n^{\alpha} &\rightarrow n^{\alpha} + d\bar{m}^{\alpha} + \bar{d} m^{\alpha} + d\bar{d} l^{\alpha} \end{aligned} \tag{A.1}$$

where d is a complex parameter. The NP scalars are also transformed,

$$\begin{aligned} \Psi_0 &\rightarrow \Psi_0 \\ \Psi_1 &\rightarrow \Psi_1 + \bar{d}\Psi_0 \\ \Psi_2 &\rightarrow \Psi_2 + 2\bar{d}\Psi_1 + \bar{d}^2\Psi_0 \\ \Psi_3 &\rightarrow \Psi_3 + 3\bar{d}\Psi_2 + 3\bar{d}^2\Psi_1 + \bar{d}^3\Psi_0 \\ \Psi_4 &\rightarrow \Psi_4 + 4\bar{d}\Psi_3 + 6\bar{d}^2\Psi_2 + 4\bar{d}^3\Psi_1 + \bar{d}^4\Psi_0. \end{aligned} \tag{A.2}$$

- Type II

$$\begin{aligned} l^\alpha &\rightarrow l^\alpha + e\bar{m}^\alpha + \bar{e}m^\alpha + e\bar{e}n^\alpha \\ m^\alpha &\rightarrow m^\alpha + en^\alpha \\ n^\alpha &\rightarrow n^\alpha \end{aligned} \tag{A.3}$$

for a complex parameter e means the NP scalars will transform as

$$\begin{aligned} \Psi_0 &\rightarrow \Psi_0 + 4\bar{e}\Psi_1 + 6\bar{e}^2\Psi_2 + 4\bar{e}^3\Psi_3 + \bar{e}^4\Psi_4 \\ \Psi_1 &\rightarrow \Psi_1 + 3\bar{e}\Psi_2 + 3\bar{e}^2\Psi_3 + \bar{e}^3\Psi_4 \\ \Psi_2 &\rightarrow \Psi_2 + 2\bar{e}\Psi_3 + \bar{e}^2\Psi_4 \\ \Psi_3 &\rightarrow \Psi_3 + \bar{e}\Psi_4 \\ \Psi_4 &\rightarrow \Psi_4. \end{aligned} \tag{A.4}$$

- Type III

$$\begin{aligned} l^\alpha &\rightarrow \Lambda l^\alpha \\ n^\alpha &\rightarrow \Lambda^{-1} n^\alpha \\ m^\alpha &\rightarrow e^{i\theta} m^\alpha \end{aligned} \tag{A.5}$$

for real parameters Λ and θ means will transform as

$$\begin{aligned} \Psi_0 &\rightarrow \Lambda^2 e^{2i\theta}\Psi_0 \\ \Psi_1 &\rightarrow \Lambda e^{i\theta}\Psi_1 \\ \Psi_2 &\rightarrow \Psi_2 \\ \Psi_3 &\rightarrow \Lambda^{-1} e^{-i\theta}\Psi_3 \\ \Psi_4 &\rightarrow \Lambda^{-2} e^{-2i\theta}\Psi_4 \end{aligned} \tag{A.6}$$

There is an additional freedom to exchange $l^\alpha \leftrightarrow n^\alpha$. The result on the NP scalars is that

$$\begin{aligned} \Psi_0 &\rightarrow \overline{\Psi}_4 \\ \Psi_1 &\rightarrow \overline{\Psi}_3 \\ \Psi_2 &\rightarrow \Psi_2 \\ \Psi_3 &\rightarrow \overline{\Psi}_1 \\ \Psi_4 &\rightarrow \overline{\Psi}_0 \end{aligned} \tag{A.7}$$

Appendix B

The quasi-Kinnersley frame for a Bowen-York spinning black hole

We perform all of the following computations using the approximation $L/M^2 \ll 1$, keeping terms up to order $O(L^4)$. The non-vanishing components of E_{ab} (3.44) for Bowen-York initial data for a spinning puncture (3.59-3.57) are

$$
\begin{aligned}
E_{rr} \;=\; & -\frac{8M}{r(M+2r)^2} \\
& -\frac{32}{5Mr(M+2r)^8}\left(M^4+8M^3r+14M^2r^2-80Mr^3-24r^4\right. \\
& \left.-18r^2(M^2+4r^2)\cos(2\theta)\right)L^2 \\
& -\frac{4}{825M^3r^4(M+2r)^{14}}\left(M^{11}+32M^{10}r+464M^9r^2+5360M^8r^3\right. \\
& +45776M^7r^4+230720M^6r^5+313664M^5r^6-1725352M^4r^7 \\
& -6314464M^3r^8-1278272M^2r^9-938880Mr^{10}-51840r^{11} \\
& +3(M^{11}+32M^{10}r+464M^9r^2+4048M^8r^3+23760M^7r^4 \\
& +80064M^6r^5+172864M^5r^6+387488M^4r^7+624000M^3r^8 \\
& -2066176M^2r^9-488960Mr^{10}-38400r^{11})\cos(2\theta) \\
& -24r^7(525M^4+19612M^3r+5992M^2r^2+78448Mr^3 \\
& \left.+8400r^4)\cos(4\theta)\right)L^4
\end{aligned}
\tag{B.1}
$$

$$
\begin{aligned}
E_{r\theta} &= -\frac{384(M-2r)r^2\sin(2\theta)}{5M(M+2r)^7}L^2 - \frac{4}{275M^3r^3(M+2r)^{13}}\big((M^{10} \\
&\quad +30M^9r+396M^8r^2+3080M^7r^3+15840M^6r^4+69824M^5r^5 \\
&\quad +209856M^4r^6+191040M^3r^7-569984M^2r^8-99072Mr^9 \\
&\quad -7680r^{10})\sin(2\theta)+96r^7(35M^3+1234M^2r \\
&\quad -2468Mr^2-280r^3)\sin(4\theta)\big)L^4
\end{aligned} \tag{B.2}
$$

$$
\begin{aligned}
E_{\theta\theta} &= \frac{4Mr}{(M+2r)^2}+\frac{16r\cos(2\theta)}{5M(M+2r)^8}(M^4+8M^3r+17M^2r^2+112Mr^3 \\
&\quad -12r^4-3r^2(7M^2+64Mr+28r^2))L^2-\frac{4}{825M^3r^2(M+2r)^{14}}\big(M^{11} \\
&\quad +23M^{10}r+236M^9r^2+752M^8r^3-5728M^7r^4-58384M^6r^5 \\
&\quad -430528M^5r^6-2131300M^4r^7-4648816M^3r^8+1019104M^2r^9 \\
&\quad +249408Mr^{10}+8640r^{11}-3(M^{11}+29M^{10}r+388M^9r^2 \\
&\quad +3168M^8r^3+17600M^7r^4+59024M^6r^5-4800M^5r^6-803408M^4r^7 \\
&\quad -2257088M^3r^8-21120M^2r^9-186112Mr^{10}-11520r^{11})\cos(2\theta) \\
&\quad +12r^7(735M^4+27844M^3r+227320M^2r^2+111376Mr^3 \\
&\quad +11760r^4)\cos(4\theta)\big)L^4
\end{aligned} \tag{B.3}
$$

$$
\begin{aligned}
E_{\phi\phi} &= \frac{4Mr\sin^2\theta^2}{(M+2r)^2} + \frac{16r\sin^2\theta}{5M(M+2r)^8}(M^4+8M^3r+11M^2r^2 \\
&\quad -272Mr^3-36r^4-3r^2(5M^2-64Mr+20r^2)\cos(2\theta))L^2 \\
&\quad +\frac{4\sin^2\theta}{825M^3r^2(M+2r)^{14}}(2M^{11}+55M^{10}r+700M^9r^2 \\
&\quad +6112M^8r^3+40048M^7r^4+172336M^6r^5-116864M^5r^6 \\
&\quad -3856652M^4r^7-10963280M^3r^8-259168M^2r^9 \\
&\quad -689472Mr^{10}-43200r^{11}+3r(3M^{10}+76M^9r+880M^8r^2 \\
&\quad +6160M^7r^3+21040M^6r^4+177664M^5r^5+1190896M^4r^6 \\
&\quad +2881088M^3r^7-2045056M^2r^8-302848Mr^9-26880r^{10})\cos(2\theta) \\
&\quad -12r^7(315M^4+11380M^3r-215336M^2r^2+45520Mr^3 \\
&\quad +5040r^4)\cos(4\theta))L^4
\end{aligned}
\tag{B.4}
$$

The non-vanishing components of the B_{ab} for Bowen-York spinning puncture initial data are

$$
\begin{aligned}
B_{rr} &= -\frac{96\cos\theta}{(M+2r)^4}L \\
&\quad -\frac{768\cos\theta}{5M(M+2r)^{10}}(M^3+8M^2r+20Mr^2-8r^3+24r^3\cos(2\theta))L^3
\end{aligned}
\tag{B.5}
$$

$$
\begin{aligned}
B_{r\theta} &= \frac{48(M-2r)r\sin\theta}{(M+2r)^5}L + \frac{384r\sin\theta}{5M(M+2r)^{11}}(M^4+4M^3r-16M^2r^2 \\
&\quad -140Mr^3+40r^4+60(M-2r)r^3\cos^2\theta)L^3
\end{aligned}
\tag{B.6}
$$

$$B_{\theta\theta} = \frac{48r^2\cos\theta}{(M+2r)^4}L + \frac{384r^2\cos\theta}{5M(M+2r)^{10}}(M^3+8M^2r+20Mr^2 \quad \text{(B.7)}$$
$$+4r^3+12r^3\cos(2\theta))L^3$$

$$B_{\phi\phi} = \frac{48r^2\cos\theta\sin^2\theta}{(M+2r)^4}L + \frac{384r^2\cos\theta\sin^2\theta}{5M(M+2r)^{10}}(M^3+8M^2r+20Mr^2 \quad \text{(B.8)}$$
$$-20r^3+36r^3\cos(2\theta))L^3$$

The non-zero components of the tensor $C^a{}_b$

$$C^r{}_r = -\frac{128Mr^3}{(M+2r)^6} - \frac{1536ir^4\cos\theta}{(M+2r)^8}L \quad \text{(B.9)}$$
$$-\frac{1536r^3}{5M(M+2r)^{12}}(M^4+8M^3r+18M^2r^2-24Mr^3$$
$$-8r^4-2r^2(3M^2-4Mr+12r^2)\cos(2\theta))L^2$$
$$-\frac{24576ir^4\cos\theta}{5M(M+2r)^{14}}(M^3+8M^2r+20Mr^2-2r^3+18r^3\cos(2\theta))L^3$$
$$-\frac{64}{825M^3(M+2r)^{18}}(M^{11}+24M^{10}r+288M^9r^2+9392M^8r^3$$
$$+129936M^7r^4+806592M^6r^5+1947200M^5r^6-756648M^4r^7$$
$$-9779232M^3r^8-2697536M^2r^9-2047104Mr^{10}-51840r^{11}$$
$$+3(M^{11}+24M^{10}r+288M^9r^2+2288M^8r^3+13200M^7r^4$$
$$+25152M^6r^5+4160M^5r^6+257952M^4r^7+850560M^3r^8$$
$$-3643136M^2r^9-889344Mr^{10}-38400r^{11})\cos(2\theta)$$
$$-72r^7(175M^4+9612M^3r-2696M^2r^2+38448Mr^3$$
$$+2800r^4)\cos(4\theta))L^4$$

$$C^{r}{}_{\theta} = \frac{768i(M-2r)r^5\sin(\theta)}{(M+2r)^9}L - \frac{6144(M-2r)r^6\sin(2\theta)}{5M(M+2r)^{11}}L^2 \tag{B.10}$$
$$+\frac{12288ir^5\sin\theta}{5M(M+2r)^{15}}(M^4+5M^3r-6M^2r^2-94Mr^3$$
$$+28r^4+42(M-2r)r^3\cos^2\theta)L^3 - \frac{64}{275M^3r(M+2r)^{17}}((M^{10}$$
$$+30M^9r+396M^8r^2+3080M^7r^3+15840M^6r^4+78272M^5r^5$$
$$+260544M^4r^6+224832M^3r^7-874112M^2r^8-166656Mr^9$$
$$-7680r^{10})\sin(2\theta)+96r^7(35M^3+1762M^2r-3524Mr^2$$
$$-280r^3)\sin(4\theta))L^4$$
$$= r^2C^{\theta}{}_{r} \tag{B.11}$$

$$C^{\theta}{}_{\theta} = \frac{64Mr^3}{(M+2r)^6}+\frac{768ir^4\cos\theta}{(M+2r)^8}L+\frac{768r^3}{5M(M+2r)^{12}}(M^4+8M^3r \tag{B.12}$$
$$+19M^2r^2+40Mr^3-4r^4-7r^2(M^2+8Mr+4r^2)\cos(2\theta))L^2$$
$$+\frac{12288ir^4\cos(\theta)}{5M(M+2r)^{14}}(M^3+8M^2r+20Mr^2+4r^3+12r^3\cos(2\theta))L^3$$
$$+\frac{64}{825M^3(M+2r)^{18}}(-M^{11}-27M^{10}r-324M^9r^2+1264M^8r^3$$
$$+47808M^7r^4+349488M^6r^5+1475392M^5r^6+4313700M^4r^7$$
$$+7066512M^3r^8-1880800M^2r^9-828864Mr^{10}-8640r^{11}$$
$$+3(M^{11}+25M^{10}r+300M^9r^2+2288M^8r^3+12320M^7r^4$$
$$+30512M^6r^5-165184M^5r^6-1434192M^4r^7-3520832M^3r^8$$
$$-353408M^2r^9-352512Mr^{10}-11520r^{11})\cos(2\theta)-36r^7(245M^4$$
$$+12884M^3r+104872M^2r^2+51536Mr^3+3920r^4)\cos(4\theta))L^4$$

$$
\begin{aligned}
C^{\phi}{}_{\phi} \;=\; & \frac{64Mr^3}{(M+2r)^6}+\frac{768ir^4\cos\theta}{(M+2r)^8}L+\frac{768r^3}{5M(M+2r)^{12}}(M^4+8M^3r \\
& +17M^2r^2-88Mr^3-12r^4-r^2(5M^2-72Mr+20r^2)\cos(2\theta))L^2 \\
& +\frac{12288ir^4\cos\theta}{5M(M+2r)^{14}}(M^3+8M^2r+20Mr^2-8r^3+24r^3\cos(2\theta))L^3 \\
& +\frac{64}{825M^3(M+2r)^{18}}(2M^{11}+51M^{10}r+612M^9r^2+8128M^8r^3 \\
& +82128M^7r^4+457104M^6r^5+471808M^5r^6-5070348M^4r^7 \\
& -16845744M^3r^8-816736M^2r^9-1218240Mr^{10}-43200r^{11} \\
& -3r(M^{10}+12M^9r-880M^7r^3+5360M^6r^4-169344M^5r^5 \\
& -1692144M^4r^6-4371392M^3r^7+3289728M^2r^8+536832Mr^9 \\
& +26880r^{10})\cos(2\theta)-36r^7(105M^4+6340M^3r \\
& -110264M^2r^2+25360Mr^3+1680r^4)\cos(4\theta))L^4
\end{aligned}
\tag{B.13}
$$

The desired eigenvector of $C^a{}_b$ is, to order L^4, is

$$\begin{aligned}
\hat{\sigma}^r &= -\frac{4r^2}{(M+2r)^2} - \frac{16r^2}{5M^2(M+2r)^8}(M^4+8M^3r+25M^2r^2 \\
&\quad -16Mr^3+20r^4-r^2(5M^2-32Mr+20r^2)\cos(2\theta))L^2 \\
&\quad +\frac{2816i(M-2r)^2r^5\cos\theta\sin^2\theta}{5M^3(M+2r))^{10}}L^3 \\
&\quad +\frac{8}{825M^4(M+2r)^{14}}(M^{10}+22M^9r-108M^8r^2-4184M^7r^3 \\
&\quad -36344M^6r^4-114432M^5r^5+39886M^4r^6+828040M^3r^7 \\
&\quad -3633168M^2r^8+1836576Mr^9+1223904r^{10}+3(M^{10}+22M^9r \\
&\quad +220M^8r^2+1320M^7r^3+6600M^6r^4+12288M^5r^5 \\
&\quad -31768M^4r^6-408480M^3r^7+1183424M^2r^8-901760Mr^9 \\
&\quad +190080r^{10})\cos(2\theta)-6r^6(18689M^4-35940M^3r \\
&\quad +264M^2r^2-143760Mr^3+299024r^4)\cos(4\theta))L^4
\end{aligned} \tag{B.14}$$

$$\begin{aligned}
\hat{\sigma}^\theta &= \frac{16i(M-2r)r^2\sin\theta}{M(M+2r)^5}L+\frac{352(M-2r)r^3\sin(2\theta)}{5M^2(M+2r)^7}L^2 \\
&\quad +\frac{128ir^2\sin\theta}{5M^3(M+2r)^{11}}(M^5+4M^4r-39M^3r^2-216M^2r^3+192Mr^4 \\
&\quad +184r^5+r^2(-31M^3+28M^2r-56Mr^2+248r^3)\cos(2\theta))L^3 \\
&\quad -\frac{8\sin\theta}{825M^4r^2(M+2r)^{13}}((M^{10}+30M^9r+396M^8r^2+3080M^7r^3 \\
&\quad +15840M^6r^4+22304M^5r^5-11904M^4r^6+1546608M^3r^7 \\
&\quad +7068256M^2r^8-6505152Mr^9-7304064r^{10})\cos(\theta) \\
&\quad +3312r^7(159M^3-490M^2r+980Mr^2-1272r^3)\cos(3\theta))L^4
\end{aligned} \tag{B.15}$$

$$\hat{\sigma}^{\phi} = 0 \tag{B.16}$$

The eigenvector defines the quasi-Kinnersley frame as outlined in equations (3.47-3.50). However, the resulting tetrad may still differ by a spin-boost transformation (A.5) from the Kinnersley tetrad. There are no known algebraic conditions on Λ and θ guaranteed to give the Kinnersley tetrad.

Appendix C

The BB scalar for boosted black hole initial data

In this chapter, we compute the NP scalars and the BB scalar for boosted black hole initial data. The aim is to demonstrate that the BB scalar gives us the ability to determine whether a given tetrad is in the qK frame without computing the qK frame itself. The utility of this knowledge is discussed elsewhere (Chapter 4).

The data are in spherical polar coordinates ($f_{ab} = \mathrm{diag}\{1, r^2, r^2 \sin^2\theta\}$) for a black hole with ADM linear momentum $P^a = P(\cos\theta, -\frac{1}{r} sin\theta, 0)$, ADM mass M, located at the origin. The Bowen-York solution for the traceless extrinsic curvature, then, is (2.46)

$$\bar{A}_{rr} = \frac{3P}{r^2}\cos\theta \tag{C.1}$$

$$= -2r^{-2}\bar{A}_{\theta\theta} = -2r^{-2}\sin^{-2}\theta\bar{A}_{\phi\phi} \tag{C.2}$$

$$\bar{A}_{r\theta} = -\frac{3P}{2r}\sin\theta. \tag{C.3}$$

The Hamiltonian constraint (2.50) will be a quasi-linear elliptic equation for ψ, which normally requires numerical methods for a solution. However, when $P/M \ll 1$, ψ can be expanded as a series in P/M. Then, at each order, the equation for ψ is a separable, linear equation. To fourth order in P/M, the solution for ψ is [29]

$$\psi = 1 + \frac{M}{2r} + \frac{P^2}{M^2}\left(1 + \frac{M}{2r}\right)^{-5}(H_{20}P_0(\cos\theta) + H_{22}P_2(\cos\theta)) \tag{C.4}$$
$$+P^4 F(r,\theta),$$

with

$$
\begin{aligned}
H_{20} &= -\frac{M^2}{512r^6}\Big(5M^4+48M^3r+180M^2r^2+320Mr^3+240r^4\Big) \qquad \text{(C.5)}\\
H_{22} &= \frac{M^2}{1280r^8}\Big(42M^5r+378M^4r^2+1316M^3r^3+2156M^2r^4\\
&\quad +1536Mr^5+240r^6+21M(M+2r)^5\ln\big(\frac{M}{M+2r}\big)\Big),
\end{aligned}
$$

and we keep the $O(P^4)$ dependence of the conformal factor in order to demonstrate later that the dependence is canceled out at $O(P^4)$ in $S(P)$ and $\xi(P)$.

Using the initial data above, the NP scalars are calculated using the fiducial tetrad (3.39). The calculations were performed using Maple, a computer algebra system, and grtensor, a package for Maple for performing tensor algebra calculations. We express the results in terms of the functions H_{20} and H_{22} in order to save space and simplify the results.

$$
\begin{aligned}
\Psi_0(P) &= -\frac{1536r^8\sin^2\theta(3M^2+2(M+2r)^2H_{22}))}{M^2(M+2r)^{12}}P^2 \qquad \text{(C.6)}\\
&\quad +\frac{147456r^{11}\cos\theta\sin^2\theta H_{22}}{M^2(M+2r)^{14}}P^3\\
&\quad +\frac{49152r^{14}\sin^2\theta}{M^4(M+2r)^{18}}\Big(4H_{20}\big(18M^2+5(M+2r)^2H_{22}\big)\\
&\quad +H_{22}\big(18M^2(1+3\cos(2\theta))+(M+2r)^2(23+33\cos(2\theta))H_{22}\big)\\
&\quad +\frac{M^4(M+2r)^{13}\big(\cot\theta\partial_\theta F(r,\theta)-\partial_\theta^2F(r,\theta)\big)}{1536r^{11}\sin^2\theta}\Big)P^4\\
&= \Psi_4(-P)
\end{aligned}
$$

The scalars $\Psi_0(P)$ and $\Psi_4(P)$ are equal except for the P^3 terms, which have opposite signs.

$$\begin{aligned}
\Psi_1(P) &= -\frac{768r^6\sin\theta}{(M+2r)^9}P - \frac{768r^8\sin(2\theta)}{M^2(M+2r)^{12}}\Big(3M^2 \qquad \text{(C.7)}\\
&\quad +2(7M^2+12Mr-4r^2)H_{22}+2r(M+2r)^2\partial_r H_{22}\Big)P^2\\
&\quad -\frac{6144r^{11}\sin\theta}{M^2(M+2r)^{15}}\Big(8(3M-8r)H_{20}-4(3M+13r+21r\cos(2\theta))H_{22}\\
&\quad +r(M+2r)\partial_r(4H_{20}+(1+3\cos(2\theta))H_{22})\Big)P^3\\
&\quad +\frac{12288r^{14}\sin(2\theta)}{M^4(M+2r)^{18}}\Big((53M^2+96Mr-20r^2)(2+6\cos(2\theta))H_{22}^2\\
&\quad +8H_{20}\big(18M^2+(53M^2+96Mr-20r^2)H_{22}+5r(M+2r)^2\partial_r H_{22}\big)\\
&\quad +4H_{22}\big(6r(M+2r)^2\partial_r H_{20}+(1+3\cos(2\theta))(9M^2\\
&\quad +4r(M+2r)^2\partial_r H_{22})\big)+\frac{M^4(M+2r)^{12}\csc(2\theta)}{384r^{11}}\big(2(M-r)\partial_\theta F(r,\theta)\\
&\quad +r(M+2r)\partial_r\partial_\theta F(r,\theta)\big)\Big)P^4\\
&= -\Psi_3(-P) \qquad \text{(C.8)}
\end{aligned}$$

$$
\begin{aligned}
\Psi_2(P) \;=\; & -\frac{64Mr^3}{(M+2r)^6} - \frac{256r^8}{M^2(M+2r)^{12}}\Big(9M^2(1+\cos(2\theta)) \\
& +16M(3M-10r)H_{20} + 2\big(9M^2-8Mr+12r^2\big)(1+3\cos(2\theta))H_{22} \\
& +2\big(M^2r-4r^3\big)(1+3\cos(2\theta))\partial_r H_{22} + (8M^2r-32r^3)\partial_r H_{20}\Big)P^2 \\
& +\frac{4096r^{14}}{M^4(M+2r)^{18}}\Big(64M(33M-40r)H_{20}^2 + \big(873M^2-292Mr \\
& +588r^2+12(81M^2-20Mr+60r^2)\cos(2\theta)+9(83M^2-12Mr \\
& +68r^2)\cos(4\theta)\big)H_{22}^2 + 8H_{20}(147M^2-100Mr \\
& +60r^2)(1+3\cos(2\theta))H_{22} + 2r^2(M+2r)^2(4\partial_r H_{20} \\
& +(1+3\cos(2\theta))\partial_r H_{22})^2 + (8H_{20} \\
& +2(1+3\cos(2\theta))H_{22})\big(108M^2\cos(2\theta) + r(17M^2+24Mr \\
& -20r^2)(4r\partial_r H_{20} + (1+3\cos(2\theta))\partial_r H_{22})\big) \\
& +\frac{M^4(M+2r)^{11}}{128r^{11}}\big((M+2r)^2(\cot\theta\partial_\theta F(r,\theta) + \partial_\theta^2 F(r,\theta)) \\
& -2r(M^2-4r^2)\partial_r F(r,\theta) - 2M(M-10r)F(r,\theta)\big)\Big)P^4
\end{aligned}
\tag{C.9}
$$

From the NP scalars, we can calculate I and J using (3.40) and (3.41). To order P^4, they are

$$
\begin{aligned}
I(P) \;=\; & \frac{12288M^2r^6}{(M+2r)^{12}} \\
& +\frac{98304r^{11}}{M(M+2r)^{18}}\big(9M^2-12Mr+9M^2\cos(2\theta)+12Mr\cos(2\theta) \\
& +16M(3M-10r)H_{20}+2(9M^2-8Mr+12r^2)(1+3\cos(2\theta))H_{22} \\
& +(2M^2r-8r^3)\partial_r(4H_{20}+(1+3\cos(2\theta))H_{22})\big)P^2 \\
& +\frac{786432r^{16}}{M^4(M+2r)^{24}}\Big(3\sin^4(\theta)(3M^2+2(M+2r)^2H_{22})^2+(9M^2\cos^2(\theta) \\
& +8M(3M-10r)H_{20}+(9M^2-8Mr+12r^2)(1+3\cos(2\theta))H_{22} \\
& +r(M^2-4r^2)(4\partial_rH_{20}+(1+3\cos(2\theta))\partial_rH_{22}))^2 \\
& -3(-\sin^2(2\theta)(3M^2+2(M+2r)((7M-2r)H_{22}+r(M+2r)\partial_rH_{22}))^2 \\
& +16M^2r\sin^2(\theta)(8(3M-8r)H_{20}-4(3M+13r+21r\cos(2\theta))H_{22} \\
& +r(M+2r)(4\partial_rH_{20}+(1+3\cos(2\theta))\partial_rH_{22}))) \\
& -2Mr(64M(33M-40r)H_{20}^2+(873M^2-292Mr+588r^2+12(81M^2 \\
& -20Mr+60r^2)\cos(2\theta)+9(83M^2-12Mr+68r^2)\cos(4\theta))H_{22}^2 \\
& +2r^2(M+2r)^2(4\partial_rH_{20}+(1+3\cos(2\theta))\partial_rH_{22})^2 \\
& +2(1+3\cos(2\theta))H_{22}(108M^2\cos^2(\theta)+(17M-10r)r(M+2r)(4\partial_rH_{20} \\
& +(1+3\cos(2\theta))\partial_rH_{22}))+8H_{20}(108M^2\cos^2(\theta) \\
& +(147M^2-100Mr+60r^2)(1+3\cos(2\theta))H_{22} \\
& +(17M-10r)r(M+2r)(4\partial_rH_{20}+(1+3\cos(2\theta))\partial_rH_{22}))) \\
& +\frac{M^5(M+2r)^{11}}{64r^{10}}\big(2M(M-10r)-(M+2r)^2\cot\theta\partial_\theta F(r,\theta) \\
& -(M+2r)^2\partial_\theta^2F(r,\theta)-2r(4r^2-M^2)\partial_rF(r,\theta))\Big)P^4
\end{aligned}
\tag{C.10}
$$

$$
\begin{aligned}
J(P) \;=\; & \frac{262144M^3r^9}{(M+2r)^{18}} + \frac{6291456r^{14}}{(M+2r)^{24}}\Big((4r(M^2-4r^2)\partial_r H_{20} \\
& +24M^2H_{20}-80MrH_{20}) + (1+3\cos(2\theta))(r(M^2-4r^2)\partial_r H_{22} \\
& +(9M^2-8Mr+12r^2)H_{22}) + M(9M\cos^2(\theta)-12r\sin^2(\theta))\Big)P^2 \\
& + \frac{12582912r^{19}}{M^3(M+2r)^{30}}\Big(144Mr\sin^4(\theta)(3M^2+2(M+2r)^2H_{22}) \\
& -12\sin^4(\theta)(3M^2+2(M+2r)^2H_{22})^2 - 48Mr\sin^2(\theta)(4r(M^2 \\
& -4r^2)\partial_r H_{20} + r(M^2-4r^2)(1+3\cos(2\theta))\partial_r H_{22} + M(9M\cos^2(\theta) \\
& +24MH_{20}-80rH_{20}) + (9M^2-8Mr+12r^2)(1+3\cos(2\theta))H_{22}) \\
& +4(4r(M^2-4r^2)\partial_r H_{20} + r(M^2-4r^2)(1+3\cos(2\theta))\partial_r H_{22} \\
& +M(9M\cos^2(\theta)+24MH_{20}-80rH_{20}) + (9M^2-8Mr+12r^2)(1 \\
& +3\cos(2\theta))H_{22})^2 - 4Mr(2r^2(M+2r)^2(4\partial_r H_{20}+\partial_r H_{22} \\
& +3\cos(2\theta)\partial_r H_{22})^2 + 64M(33M-40r)H_{20}^2 + 2(1+3\cos(2\theta)) \\
& \times(108M^2\cos^2(\theta) + (17M-10r)r(M+2r)(4\partial_r H_{20}+\partial_r H_{22} \\
& +3\cos(2\theta)\partial_r H_{22}))H_{22} + (873M^2-292Mr+588r^2+12(81M^2 \\
& -20Mr+60r^2)\cos(2\theta)+9(83M^2-12Mr+68r^2)\cos(4\theta))H_{22}^2 \\
& +8H_{20}(108M^2\cos^2(\theta)+(17M-10r)r(M+2r)(4\partial_r H_{20}+\partial_r H_{22} \\
& +3\cos(2\theta)\partial_r H_{22}) + (147M^2-100Mr+60r^2)(1+3\cos(2\theta))H_{22})) \\
& -6(16M^2r\sin^2(\theta)(r(M+2r)(4\partial_r H_{20}+\partial_r H_{22}+3\cos(2\theta)\partial_r H_{22}) \\
& +8(3M-8r)H_{20} - 4(3M+13r+21r\cos(2\theta))H_{22}) - \sin(2\theta)^2(3M^2 \\
& +2(M+2r)(r(M+2r)\partial_r H_{22} + (7M-2r)H_{22}))^2) \\
& + \frac{M^5(M+2r)^{11}}{32r^{10}}\big(2M(M-10r)F(r,\theta) - (M+2r)^2\cot\theta\partial_\theta F(r,\theta) \\
& -(M+2r)^2\partial_\theta^2 F(r,\theta) - 2r(4r^2-M^2)\partial_r F(r,\theta)\big)\Big)P^4
\end{aligned}
\tag{C.11}
$$

From $I(P)$ and $J(P)$, we can calculate the speciality index $S(P)$ (3.42).

$$\begin{aligned} S(P) &= 1-\frac{1728r^{10}\sin^4\theta}{M^6(M+2r)^{12}}\Big(M(3M-4r)+2(M+2r)^2H_{22}\Big)^2P^4 \qquad \text{(C.12)} \\ &= 1-\frac{27\sin^4\theta}{6400M^4r^6(M+2r)^{12}}\Big(2r(21M^8+273M^7r+1498M^6r^2 \\ &\quad +4466M^5r^3+7712M^4r^4+7504M^3r^5+3552M^2r^6+1440Mr^7 \\ &\quad -1280r^8)+21M^2(M+2r)^7\ln\left(\frac{M}{M+2r}\right)\Big)^2P^4 \end{aligned}$$

Note that S is independent of $F(r,\theta)$ to order P^4. Then, the BB scalar is, to lowest order in P [25] ,

$$\begin{aligned} \xi(P) &= -\frac{I}{9}(S-1) \qquad \text{(C.13)} \\ &= \frac{2359296r^{16}\sin^4\theta}{M^4(M+2r)^{24}}\Big(M(3M-4r)+2(M+2r)^2H_{22}\Big)^2P^4. \end{aligned}$$

References

[1] Cactus computational tookit. http://www.cactuscode.org.

[2] Carpet mesh refinement. http://www.carpetcode.org.

[3] Miguel Alcubierre, Gabrielle Allen, Bernd Bruegmann, Edward Seidel, and Wai-Mo Suen. Towards an understanding of the stability properties of the 3+1 evolution equations in general relativity. *Phys. Rev.*, D62:124011, 2000.

[4] Miguel Alcubierre et al. Gauge conditions for long-term numerical black hole evolutions without excision. *Phys. Rev.*, D67:084023, 2003.

[5] Stephon Alexander and Nicolas Yunes. A new PPN parameter to test Chern-Simons gravity. *Phys. Rev. Lett.*, 99:241101, 2007.

[6] Stephon Alexander and Nicolas Yunes. Chern-Simons Modified General Relativity. 2009.

[7] Marcus Ansorg, Bernd Bruegmann, and Wolfgang Tichy. A single-domain spectral method for black hole puncture data. *Phys. Rev.*, D70:064011, 2004.

[8] Arnowitt, R., Deser, S., and Misner, C.W. *Gravitation: An Introduction to Current Research*. Wiley, New York, 1962.

[9] John G. Baker and Manuela Campanelli. Making use of geometrical invariants in black hole collisions. *Phys. Rev.*, D62:127501, 2000.

[10] John G. Baker, Manuela Campanelli, C. O. Lousto, and R. Takahashi. Modeling gravitational radiation from coalescing binary black holes. *Phys. Rev.*, D65:124012, 2002.

[11] John G. Baker, Manuela Campanelli, and Carlos O. Lousto. The lazarus project: A pragmatic approach to binary black hole evolutions. *Phys. Rev.*, D65:044001, 2002.

[12] John G. Baker, Joan Centrella, Dae-Il Choi, Michael Koppitz, and James van Meter. Binary black hole merger dynamics and waveforms. *Phys. Rev.*, D73:104002, 2006.

[13] John G. Baker, Joan Centrella, Dae-Il Choi, Michael Koppitz, and James van Meter. Gravitational wave extraction from an inspiraling configuration of merging black holes. *Phys. Rev. Lett.*, 96:111102, 2006.

[14] Thomas W. Baumgarte and Stuart L. Shapiro. On the numerical integration of Einstein's field equations. *Phys. Rev.*, D59:024007, 1999.

[15] Thomas W. Baumgarte and Stuart L. Shapiro. Numerical relativity and compact binaries. *Phys. Rept.*, 376:41–131, 2003.

[16] Christopher Beetle, Marco Bruni, Lior M. Burko, and Andrea Nerozzi. Towards wave extraction in numerical relativity: Foundations and initial-value formulation. *Phys. Rev.*, D72:024013, 2005.

[17] Christopher Beetle and Lior M. Burko. A radiation scalar for numerical relativity. *Phys. Rev. Lett.*, 89:271101, 2002.

[18] Tanja Bode. *The Robustness of Binary of Binary Black Hole Mergers and Waveforms*. PhD thesis, 2009. Pennsylvania State University.

[19] Carles Bona, Joan Masso, Edward Seidel, and Joan Stela. A New formalism for numerical relativity. *Phys. Rev. Lett.*, 75:600–603, 1995.

[20] J. M. Bowen. General solution for flat-space longitudinal momentum. *General Relativity and Gravitation*, 14:1183–1191, December 1982.

[21] Jeffrey M. Bowen and James W. York. Time-asymmetric initial data for black holes and black-hole collisions. *Phys. Rev. D*, 21(8):2047–2056, Apr 1980.

[22] Steven Brandt and Bernd Bruegmann. A Simple construction of initial data for multiple black holes. *Phys. Rev. Lett.*, 78:3606–3609, 1997.

[23] David Brown, Peter Diener, Olivier Sarbach, Erik Schnetter, and Manuel Tiglio. Turducken-ening black holes: an analytical and computational study. 2008.

[24] Lior M. Burko. Towards a wave-extraction method for numerical relativity. V. Extracting the Weyl scalars in the quasi-Kinnersley tetrad from spatial data. *Phys. Rev.*, D75:084039, 2007.

[25] Lior M. Burko, Thomas W. Baumgarte, and Christopher Beetle. Towards a novel wave–extraction method for numerical relativity: Iii. analytical examples for the beetle–burko radiation scalar. *Phys. Rev.*, D73:024002, 2006.

[26] Manuela Campanelli, Bernard J. Kelly, and Carlos O. Lousto. The lazarus project ii: Space-like extraction with the quasi-kinnersley tetrad. *Phys. Rev.*, D73:064005, 2006.

[27] Manuela Campanelli, C. O. Lousto, P. Marronetti, and Y. Zlochower. Accurate Evolutions of Orbiting Black-Hole Binaries Without Excision. *Phys. Rev. Lett.*, 96:111101, 2006.

[28] S. Chandrasekhar. The mathematical theory of black holes. Oxford, UK: Clarendon (1992) 646 p.

[29] Kenneth A. Dennison, Thomas W. Baumgarte, and Harald P. Pfeiffer. Approximate initial data for binary black holes. *Phys. Rev.*, D74:064016, 2006.

[30] David R. Fiske, John G. Baker, James R. van Meter, Dae-Il Choi, and Joan M. Centrella. Wave zone extraction of gravitational radiation in three- dimensional numerical relativity. *Phys. Rev.*, D71:104036, 2005.

[31] J. N. Goldberg, A. J. Macfarlane, E. T. Newman, F. Rohrlich, and E. C. G. Sudarshan. Spin-s spherical harmonics and [small eth, icelandic]. *Journal of Mathematical Physics*, 8(11):2155–2161, 1967.

[32] Michael B. Green and John H. Schwarz. Anomaly Cancellation in Supersymmetric D=10 Gauge Theory and Superstring Theory. *Phys. Lett.*, B149:117–122, 1984.

[33] Daniel Grumiller and Nicolas Yunes. How do Black Holes Spin in Chern-Simons Modified Gravity? *Phys. Rev.*, D77:044015, 2008.

[34] David Guarrera and A. J. Hariton. Papapetrou energy-momentum tensor for Chern-Simons modified gravity. *Phys. Rev.*, D76:044011, 2007.

[35] Carsten Gundlach and Jose M. Martin-Garcia. Hyperbolicity of second-order in space systems of evolution equations. *Class. Quant. Grav.*, 23:S387–S404, 2006.

[36] Laurens Gunnarsen, Hisa-Aki Shinkai, and Kei-Ichi Maeda. Finding principal null directions for numerical relativists. 1994.

[37] Mark Hannam et al. The Samurai Project: verifying the consistency of black- hole-binary waveforms for gravitational-wave detection. 2009.

[38] Sascha Husa, Ian Hinder, and Christiane Lechner. Kranc: a Mathematica application to generate numerical codes for tensorial evolution equations. 2004.

[39] R. A. Isaacson. Gravitational Radiation in the Limit of High Frequency. II. Nonlinear Terms and the Effective Stress Tensor. *Physical Review*, 166:1272–1279, February 1968.

[40] R. Jackiw and S. Y. Pi. Chern-simons modification of general relativity. *Phys. Rev.*, D68:104012, 2003.

[41] A. I. Janis and E. T. Newman. Structure of Gravitational Sources. *Journal of Mathematical Physics*, 6:902–914, June 1965.

[42] William Kinnersley. Type D Vacuum Metrics. *J. Math. Phys.*, 10:1195–1203, 1969.

[43] Simone Mercuri and Victor Taveras. Interaction of the Barbero–Immirzi Field with Matter and Pseudo-Scalar Perturbations. 2009.

[44] Andrea Nerozzi, Christopher Beetle, Marco Bruni, Lior M. Burko, and Denis Pollney. Towards wave extraction in numerical relativity: The quasi- kinnersley frame. *Phys. Rev.*, D72:024014, 2005.

[45] Andrea Nerozzi, Marco Bruni, Lior M. Burko, and Virginia Re. Towards a novel wave-extraction method for numerical relativity. 2006.

[46] Andrea Nerozzi, Marco Bruni, Virginia Re, and Lior M. Burko. Towards a wave-extraction method for numerical relativity. iv: Testing the quasi-kinnersley method in the bondi-sachs framework. *Phys. Rev.*, D73:044020, 2006.

[47] Andrea Nerozzi and Oliver Elbracht. Using curvature invariants for wave extraction in numerical relativity. 2008.

[48] E. T. Newman and R. Penrose. Note on the bondi-metzner-sachs group. *Journal of Mathematical Physics*, 7(5):863–870, 1966.

[49] Ezra Newman and Roger Penrose. An approach to gravitational radiation by a method of spin coefficients. *J. Math. Phys.*, 3:566–578, 1962.

[50] Niall O Murchadha and James W. York. Gravitational energy. *Phys. Rev.*, D10:2345–2357, 1974.

[51] R. Penrose and W Rindler. *Spinors and Space-time*, volume 1 and 2. Cambridge University Press, 1984, 1986.

[52] A. Z. Petrov. The classification of spaces defining gravitational fields. *Scientific Proceedings of Kazan State University, 114, (8) 55-69 (1954)). Jubilee (1804-1954) Collection.*, 114:55–69, 1954.

[53] C. Reisswig, N. T. Bishop, D. Pollney, and B. Szilagyi. Unambiguous determination of gravitational waveforms from binary black hole mergers. 2009.

[54] Oscar A. Reula. Strongly hyperbolic systems in General Relativity. 2004.

[55] Olivier Sarbach, Gioel Calabrese, Jorge Pullin, and Manuel Tiglio. Hyperbolicity of the BSSN system of Einstein evolution equations. *Phys. Rev.*, D66:064002, 2002.

[56] M. Shibata and T. Nakamura. Evolution of three-dimensional gravitational waves: Harmonic slicing case. *Phys. Rev.*, D52:5428–5444, 1995.

[57] Hisa-aki Shinkai and Gen Yoneda. Constraint propagation in (N+1)-dimensional spacetime. *Gen. Rel. Grav.*, 36:1931–1937, 2004.

[58] P. Szekeres. The gravitational compass. *Journal of Mathematical Physics*, 6(9):1387–1391, 1965.

[59] Saul A. Teukolsky. Perturbations of a rotating black hole. 1. fundamental equations for gravitational electromagnetic, and neutrino field perturbations. *Astrophys. J.*, 185:635–647, 1973.

[60] K. S. Thorne. Multipole expansions of gravitational radiation. *Reviews of Modern Physics*, 52:299–340, April 1980.

[61] Gen Yoneda and Hisa-aki Shinkai. Advantages of modified ADM formulation: constraint propagation analysis of Baumgarte-Shapiro-Shibata-Nakamura system. *Phys. Rev.*, D66:124003, 2002.

[62] J. W. York, Jr. *Essays in General Relativity*. Academic, New York, 1980.

[63] J. W. York, Jr. *Initial data for collisions of black holes and other gravitational miscellany.*, pages 89–109. 1989.

[64] Nicolas Yunes and Frans Pretorius. Dynamical Chern-Simons Modified Gravity I: Spinning Black Holes in the Slow-Rotation Approximation. 2009.

Vita

Shaun Wood was born in DeLand, Florida on September 15, 1980. He attended the College of Charleston from 1999 to 2003, where he graduated *magna cum laude*, receiving a B. S. in Physics and Pure Math, with a minor in Computer Science. From 2003 to 2009 he attended the Pennsylvania State University, finding a home in the Numerical Relativity group in 2006. His honors include receiving the University Graduate Fellowship and Roberts and Miller Fellowship during the 2003 academic year. He is a member of the Golden Key International Honour Society and the Sigma Alpha Pi Honor Society.